
Synthesis and Upconversion Properties of NaYF₄:Er
Nanocrystals

Xianjia Luo

February 2013

Synthesis and Upconversion Properties of NaYF₄:Er
Nanocrystals

Xianjia Luo

Doctoral Program in Applied Physics

Submitted to the Graduate School of
Pure and Applied Sciences
in Partial Fulfillment of the Requirements
for the Degree of Doctor of Philosophy in
Engineering
at the
University of Tsukuba

Abstract

Recently, upconversion (UC) materials have attracted significant attentions, due to their potential applications to solar cells, telecommunications, biolabeling, temperature sensing and three dimensional displays. For the application to solar cells, UC materials could enhance the response in the infrared spectral region, which decreases the transmission loss of the sub-bandgap light. One of the promising UC materials is hexagonal (β)-phase NaYF_4 doped with rare earth (Re^{3+}), due to the low phonon energy of the host, which suppresses non-radiative relaxation. Bulk β -phase $\text{NaYF}_4:\text{Re}^{3+}$ has high UC efficiency than nano-size one; however nanocrystals (NCs) materials have high potentiality to improve UC efficiency. Since the synthesis method generally used is relatively complex, sensitive to its condition and discharges toxic gas such as COF_2 , it is significant to develop an environment-friendly and facile synthesis method for $\text{NaYF}_4:\text{Re}^{3+}$ NCs with phase controllability. It has been reported that the β -phase $\text{NaYF}_4:\text{Er}^{3+}$ was used as a converter to improve the efficiencies of solar cells under laser excitation about 1520 nm. However, UC materials should be applied to harvesting solar energy over a wide spectral range to effectively utilize the solar spectrum. Recently, the higher UC efficiencies have been reported under the broad spectrum illumination. However, the mechanism of higher UC efficiencies is not clear. By understanding the mechanism of these higher efficiencies, UC materials could be better applied to improving the efficiency of solar cells under broad spectrum illumination.

In this thesis, a user-friendly and facile synthesis method was developed for pure β -phase NaErF_4 , NaYF_4 and $\text{NaYF}_4:10\%\text{Er}/\text{NaYF}_4$ core/shell NCs. The phase control of $\text{NaYF}_4:\text{Er}^{3+}$ NCs could be achieved by controlling the temperature and the molar ratio of OA/ODE during synthesis. The UC emission spectra of β -phase NaErF_4 , $\text{NaYF}_4:\text{Er}^{3+}$ and core/shell NCs were observed with emission peaks at about 980 nm, 800 nm, 660 nm and 540 nm under 1550 nm excitation. 3 times UC enhancement was achieved by coating the core with NaYF_4 shell, compared to $\text{NaYF}_4:10\%\text{Er}^{3+}$ core NCs. The values of the slope n in pump-power dependence of UC emission intensity confirmed that 980 nm, 800 nm emission were 2-step UC, and 660 nm, 540 nm emission were 3-step UC. The results showed that the optimum Er^{3+} concentration for 2-step and 3-step UC was around 10% ~ 30%.

Additionally, in order to understand the reason of higher UC efficiencies under broad spectrum illumination, we have studied the UC mechanisms not only under resonant (1550 nm) excitation, but also under off-resonant (1620 nm) excitation, whose energy is smaller than the lowest energy level of Er^{3+} ($^4\text{I}_{15/2} \rightarrow ^4\text{I}_{13/2}$). The UC spectrum for $\text{NaYF}_4:10\%\text{Er}^{3+}/\text{NaYF}_4$ NCs under off-resonant excitation mainly had five peaks, including 1540, 980, 800, 660 and 540 nm. The absorption and Raman spectra showed that the off resonant absorption was the phonon-assisted absorption. The two orders enhancement of 980 nm emission was observed under 1620 nm excitation at the temperature from 80 to 360 K, while fourfold increase under 1550 nm excitation was found. The strong temperature dependence under 1620 nm excitation also showed the UC processes of phonon-assisted excitation. The power dependence confirmed these UC processes. These results

showed that the UC materials could be applied to harvesting the off resonant solar spectrum through phonon-assisted absorption.

In addition, we studied the UC mechanisms for NaYF₄:10%Er³⁺/NaYF₄ NCs under resonant and off-resonant excitation simultaneously (1550 and 1620 nm), which are part of the AM1.5 spectrum and not absorbed by the silicon solar cells. This two-color excitation may be a simple model to examine the mechanism of UC under the AM1.5 spectrum illumination. 1.14 times UC enhancement was obtained under resonant and off-resonant excitation at the same power (160 Wm⁻²) and no obvious UC emission was obtained only under off-resonant excitation. Temperature dependence showed that UC enhancement hardly depend on temperature and the process of UC enhancement is the ground state absorption of 1550 nm photon following excited state absorption of 1620 nm photon. This result confirmed that the higher UC efficiencies under the broad spectrum illumination was attributed to the ground state absorption of resonant (1480~1580 nm) photon following excited state absorption of off-resonant photon, such as 1600~1640 nm one. The 2.9 times UC enhancement was observed under resonant (8 Wm⁻²) and off resonant (160 Wm⁻²) excitation at different power. This UC enhancement depended on temperature. This result showed including another optical process for UC enhancement, ground state absorption of 1620 nm photon and following ⁴I_{13/2}→⁴I_{9/2} transition resulting from absorption of 1550 nm photon. Thus, there were two optical processes for UC enhancement under both resonant and off-resonant excitation.

Contents

Chapter 1. Introduction.....	1
1.1 Energy loss mechanisms of solar cells	1
1.2 Photon conversion	2
1.3 Upconversion materials	4
1.3.1 Dopant.....	4
1.3.2 Host	6
1.3.3 NaYF ₄ :Er ³⁺	8
1.3.4 Nanocrystals.....	9
1.4 Recent synthesis method for β -phase NaYF ₄ :Re ³⁺ nanocrystals	11
1.5 Application of upconversion materials to solar cells.....	12
1.6 Research motivations.....	15
1.7 Chapter 1 References.....	16
Chapter 2.Upconversion mechanisms of rare earths	18
2.1 Spontaneous radiative and non-radiative decay	18
2.2 Dominant upconversion mechanisms	22
2.3 Power dependence of upconversion	24
2.4 summary	26
2.5 Chapter 2 References.....	27
Chapter 3. Experimental method.....	28
3.1 X-ray diffraction (XRD)	28
3.2 Transmission electron microscope (TEM).....	30
3.3 Spectroscopy.....	33
3.3.1 Absorption Spectrum	33
3.3.2 Raman and photoluminescence spectrum.....	33
3.3.3 Upconversion spectrum	34
3.3.4 Power and temperature dependence Spectrum	34
3.4 Chapter 3 references	35
Chapter 4. A user-friendly and facile synthesis for β -phase NaYF ₄ :Er ³⁺ and NaYF ₄ :Er ³⁺ /NaYF ₄ NCs	36
4.1. Introduction	36
4.2. Experimental	36
4.3. Results and discussions	37
4.3.1. Crystal structure	37
4.3.2. Morphology.....	41
4.3.3. Photoluminescence (PL) spectrum.....	43
4.3.4. UC emission spectrum	45
4.3.5. Core/shell NaYF ₄ :Er ³⁺ /NaYF ₄ NCs.....	51
4.4. Summary	53
4.5. Chapter 4 references	54
Chapter 5.UC properties in β -phase NaYF ₄ :Er ³⁺ /NaYF ₄ NCs by off-resonant excitation	55
5.1. Introduction	55
5.2. Experimental	55
5.3. Results and discussions	55

5.3.1.	UC emission spectrum	55
5.3.2.	Absorption and Raman spectrum	56
5.3.3.	UC Temperature dependence	58
5.3.4.	UC power dependence and optical process	60
5.4.	Summary	62
5.5.	Chapter 5 references	63
Chapter 6.	UC properties under both off-resonant and resonant excitation	64
6.1.	Introduction	64
6.2.	Experimental	64
6.3.	Results and discussions	65
6.3.1.	UC emission under both off-resonant and resonant excitation at the same power	65
6.3.2.	UC emission under both off-resonant and resonant excitation at different power	70
6.4.	Summary	75
6.5.	Chapter 6 references	76
Chapter 7.	Final conclusions	77
Acknowledgements	78
Publication list	79

Chapter 1. Introduction

1.1 Energy loss mechanisms of solar cells

Due to the decline of conventional source of energy, increasing pollution and global warming, the fossil fuel based energy structure is being replaced by renewable energy based structure. Photovoltaics, the direct conversion of sunlight to electricity using solar cells, is recognized as one of the most promising options for the future of renewable energy, since sunlight is abundant source of energy. Most present photovoltaic sales are bulk silicon solar cells, but bulk silicon productions encounter the challenges of reducing cost and improving the efficiency.

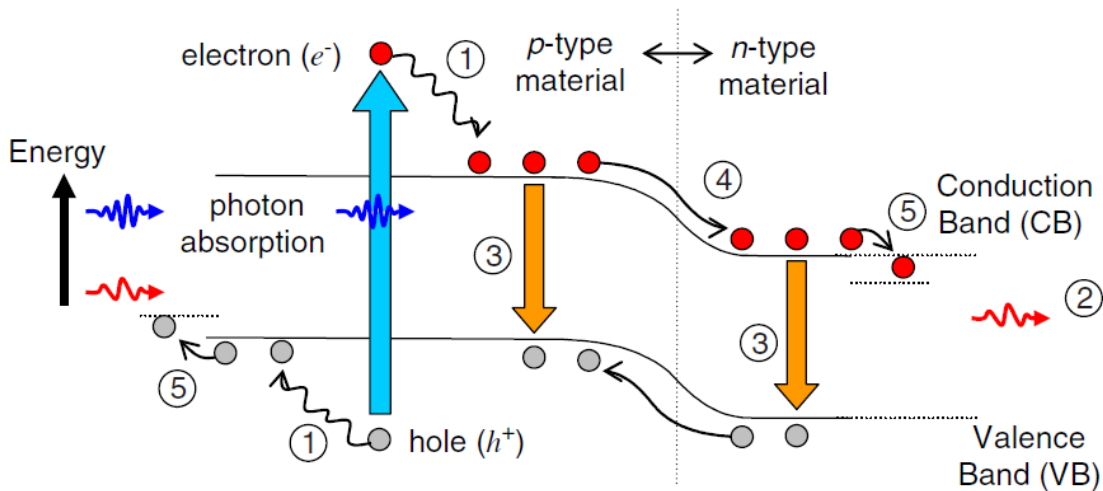


Fig. 1-1 Energy loss processes in a standard solar cell: ① lattice thermalisation loss; ② transparency loss; ③ recombination loss; ④ junction loss; ⑤ contact voltage loss.[1-1][1-2]

The semiconductor solar cell including silicon solar cell, is a p-n junction, as shown in fig. 1-1[1-2]. The incident photons, which have higher energy than the bandgap of semiconductor, can be absorbed to excite electrons e^- into the conduction band with a hole h^+ in the valence band. The $e^- - h^+$ pairs formed near the p-n junction can be separated by the strong internal electric field at the junction and collected from the p and n type regions respectively. If a wire is attached to the cathode (n-type) and the anode (p-type), an electrical current will flow through the wire.

As shown in fig. 1-1, there are five primary energy losses in semiconductor solar cells with single p-n junction, including ① lattice thermalisation loss resulting from the absorption of high energy photon; ② transparency loss of sub-bandgap photon; ③ recombination loss; ④ junction loss; ⑤ contact voltage loss. The technological improvement in material and processing techniques can decrease the ③-⑤ energy losses.

Since ① thermalisation loss and ② transparency loss are attributed to the intrinsic properties of the semiconductor materials, however, these losses limit for the efficiency of a single-junction solar cell [1-3].

1.2 Photon conversion

Due to the thermalisation and transparency losses, the solar cell only utilizes a small fraction of the solar spectrum, as shown in fig. 1-2 [1-2]. The blue spectral regions from 300 to 1150 nm denote the thermalisation loss and those from 1150 to 2500 nm indicate the transparency loss. The thermalisation and transparency losses amount to around 50% loss of the incident solar energy in silicon solar cell [1-4].

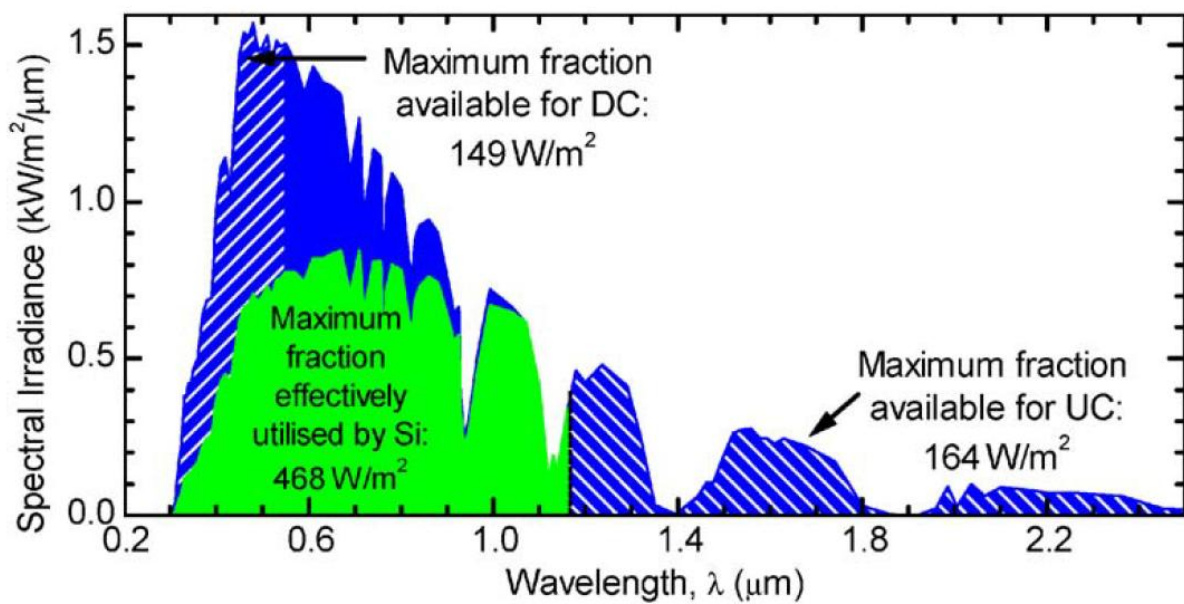


Fig. 1-2 AM 1.5G spectrum showing the fraction (highlighted in green) absorbed by a typical silicon based PV cell and the spectral regions that can be utilized through down conversion and upconversion processes (highlighted in white oblique line) [1-2].

One of methods to improve the response of solar cells in the broad solar spectrum is photon conversion. The photon conversion includes photoluminescence, down conversion (DC) and upconversion (UC) [1-5]. Photoluminescence, whereby high energy photons are shifted to low energy regions, could minimize surface recombination loss, since high energy photons absorbed in the surface tend to be affected, leading to a weak spectrum response in high energy regions, as shown in fig. 1-2. DC, whereby a photon with twice energy of the band gap is converted into two photons absorbed by solar cells, could decrease the thermalisation loss. UC, whereby, two or more low energy photons are converted to a single photon with higher energy than the band gap, could reduce the transparency losses. The left blue solar spectrum highlighted in white oblique line in fig. 1-2, indicates maximum fraction available for DC, around 149W/m², 33% of maximum fraction effectively utilized by Si. The right blue solar spectrum highlighted in white oblique line, shows maximum fraction available for UC, around 164W/m², 35% of maximum fraction effectively utilized by Si. Based on a de

tailed balance mode, Trupke et al. predicted that the upper limit of the energy conversion efficiency is 37% with an ideal upconverter on the rear side of a bifacial single-junction solar cell for nonconcentrated sunlight (30% without upconverter in the bandgap of 1.32 eV) and 40.2% on the basis of AM1.5G spectrum instead of black body radiation, as shown in table 1-1 [1-6][1-7][1-8].

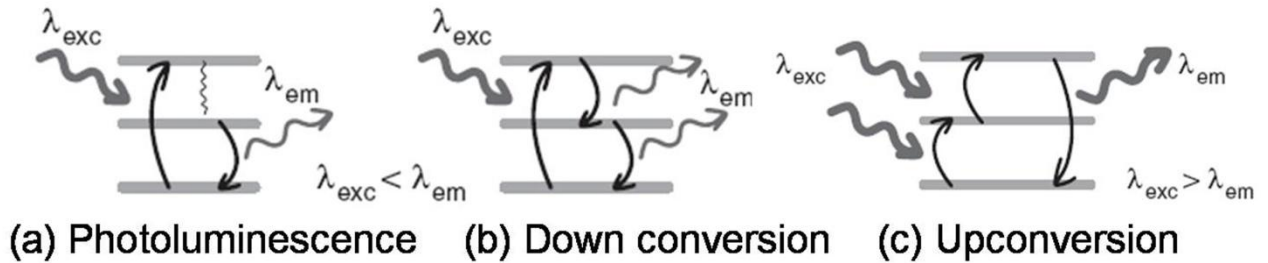


Fig. 1-3 Photon conversion: (a) photoluminescence; (b) Down conversion; (c) Upconversion [1-5]

Conc.	Band gap	Shockley - Queisser Black body	Trupke - with up-converter	
			No relaxation Black body	Relaxation allowed Black body AM1.5G
no	opt.	30% [1-7] $E_G = 1.32 \text{ eV}$		47.6% [1-6] 50.7% [1-8] $E_G = 2 \text{ eV}$ $E_G = 2 \text{ eV}$ $E_{g4} = 0.9393 \text{ eV}$ $E_{g4} = 0.94 \text{ eV}$ $E_{g3} = 1.3906 \text{ eV}$ $E_{g3} = 1.4 \text{ eV}$ $E_{relax} = 0.33 \text{ eV}$ $E_{relax} = 0.34 \text{ eV}$
	1.1 eV			37% [1-6] 40.2% [1-8]
maximum conc.	opt.	40.7% [1-7] $E_G = 1.1 \text{ eV}$	61.40% [1-6] $E_G = 1.86 \text{ eV}$ $E_{g4} = 0.667 \text{ eV}$	62.18% [1-6] $E_G = 1.9 \text{ eV}$ $E_{g4} = 0.7206 \text{ eV}$ $E_{g3} = 1.2294 \text{ eV}$ $E_{relax} = 0.50 \text{ eV}$
	1.1 eV	40.7% [1-7]		
minimum emission	opt.		63.17% [1-6] $E_G = 1.95 \text{ eV}$ $E_{g4} = 0.713 \text{ eV}$	
	1.1 eV			

Table 1-1 Efficiency limits without upconverter (Shockley-Queisser-limit) and with upconverter (calculated by Trupke) for different concentration conditions, photon selectivity properties (relaxation not allowed or allowed) and illuminating spectra [1-5].

1.3 Upconversion materials

UC materials could absorb two or more infrared photons and emit one higher energy photon which could be absorbed by solar cells. Thus, they need an intermediate excited state, via which the electron in ground state moves up to high energy state by absorbing two infrared photons. Generally, the available materials for UC are inorganic host materials, mainly doped with rare earth ions or transition metal ions. Due to the filled outer shell, the energetic levels in rare earth ions like those in free rare earth ions, while the energetic levels in transition metal ions are strongly influenced by the crystal field of host. Thus, the inorganic hosts doped rare earth ions are ideal UC materials. The rare earth will be discussed in this thesis.

1.3.1 Dopant

Rare earth, also referred to as lanthanides, has an electronic configuration of $[\text{Xe}]4f^n5s^25p^6$, in which n corresponds to the ions Ce^{3+} ($n=1$) to Yb^{3+} ($n=13$). Due to the filled outer shell, the optical properties of rare earth resulting from 4f-4f transitions are weakly affected by the crystal field of host.

A common energy level diagram for rare earth ions doped into the crystal LaCl_3 is shown in fig. 1-4 [1-9][1-10]. The energy levels are denoted as $^{2S+1}L_J$. The red frame shows that the ions' energy levels are lower than around 9000 cm^{-1} , which could not be absorbed by silicon based solar cells. Thus, intermediate excited states for UC are within these regions. From the energy level diagram for rare earth ions, it is found that erbium (Er) is a promising UC ion for solar cells, since its lowest absorption is at about 1550 nm and the second low energy level is within the absorption of silicon based solar cells. In addition, its ladder of nearly equally spaced energy levels are multiples of the $^4I_{15/2} \rightarrow ^4I_{13/2}$ ($\sim 1550 \text{ nm}$) transition, which is suitable to single wavelength laser excitation, as shown in fig. 1-5.

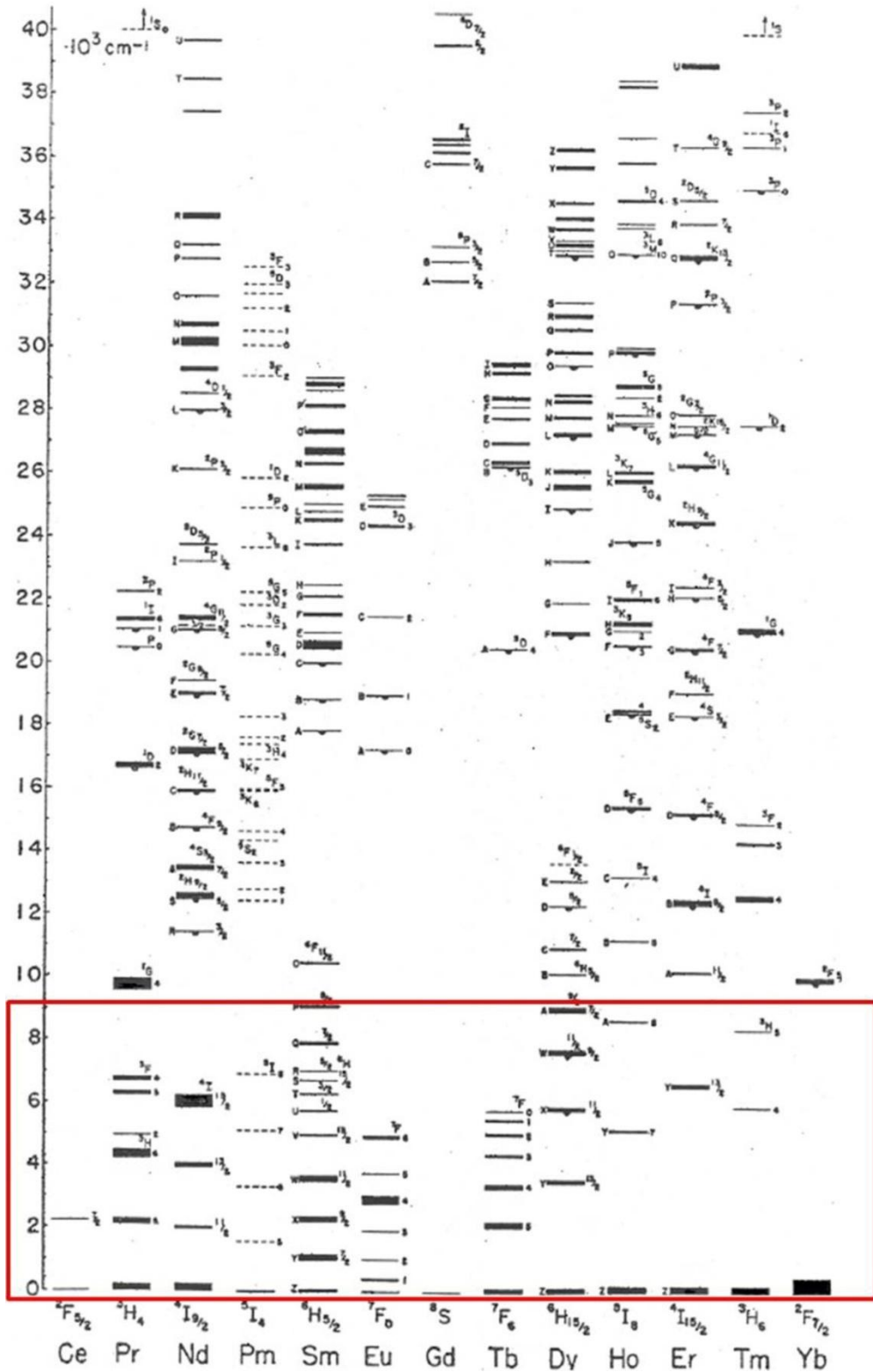


Fig. 1-4 Energy level diagram for Rare earth ions doped into the crystal LaCl_3 [1-9][1-10]. The red frame shows that the ions' energy levels are lower than around 9000 cm^{-1} , which could not be absorbed by silicon based solar cells.

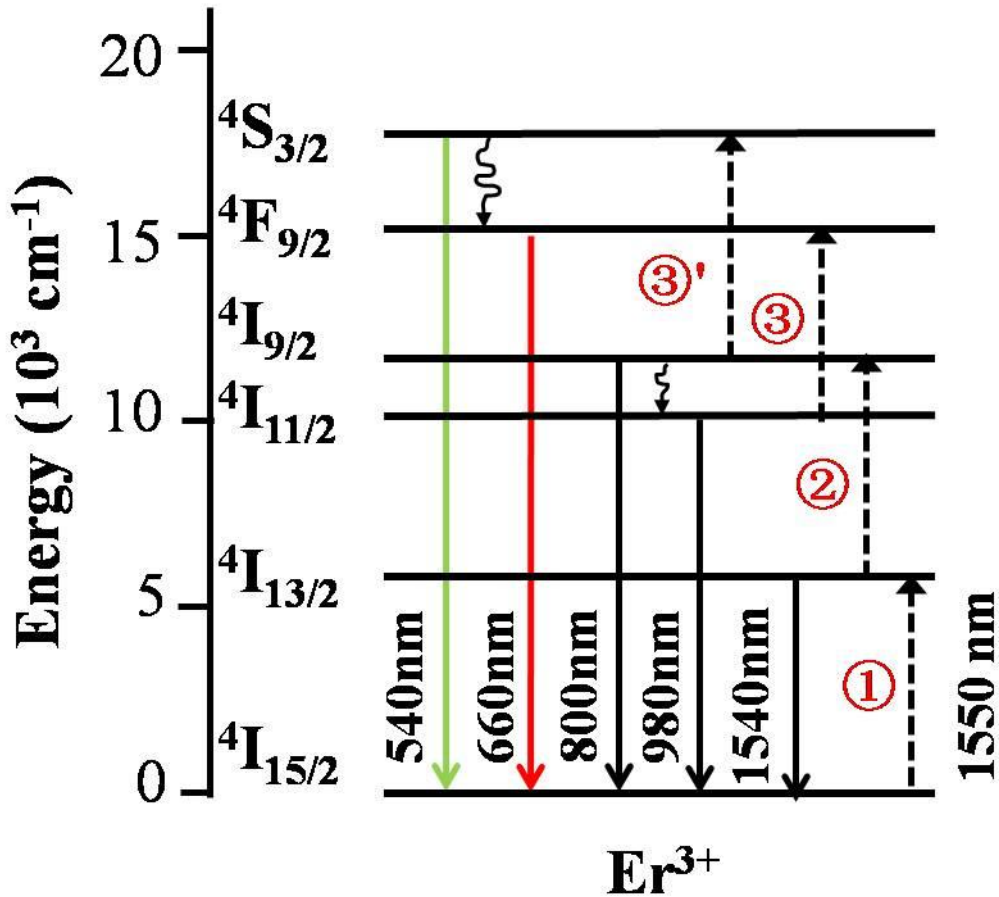


Fig. 1-5 Three-step UC process for Er^{3+} ions using single laser excitation at 1550 nm.

1.3.2 Host

Although the energetic levels in rare earth ions like those in free rare earth ions, the host materials could affect the $^{2S+1}\text{L}_J$ state in two ways [1-5]:

- (1) Phonon energy: The host materials should have the relatively low phonon energy, which suppresses non-radiative relaxation, since UC needs intermediate excited state, via which the electron in ground state moves up to high energy state. Thus, the UC efficiency is determined by the phonon energy. Fig. 1-6 shows the highest phonons' energies for each halide and oxide hosts, and the phonon energies generally increase with decreasing atomic number of halides [1-11][1-3]. Fig. 1-7 shows how the phonon energies influence the non-radiative relaxation [1-11]. Due to low phonon energies, it is easier for electrons of chlorides, bromides and iodides (Cl, Br, I) move up to high energy state ($4\text{H}_{9/2}$), compared to fluorides and oxides (F, O), in which phonon relaxations easily take place [1-12].

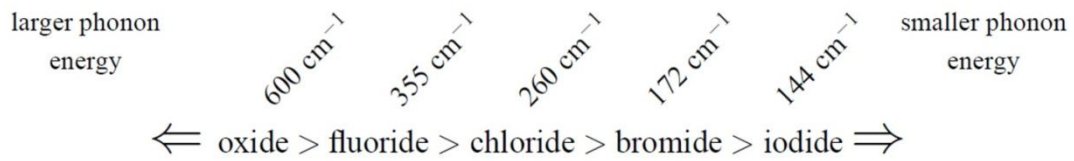


Fig. 1-6 Typical highest phonons' energies for each halide and oxide hosts [1-11][1-3]

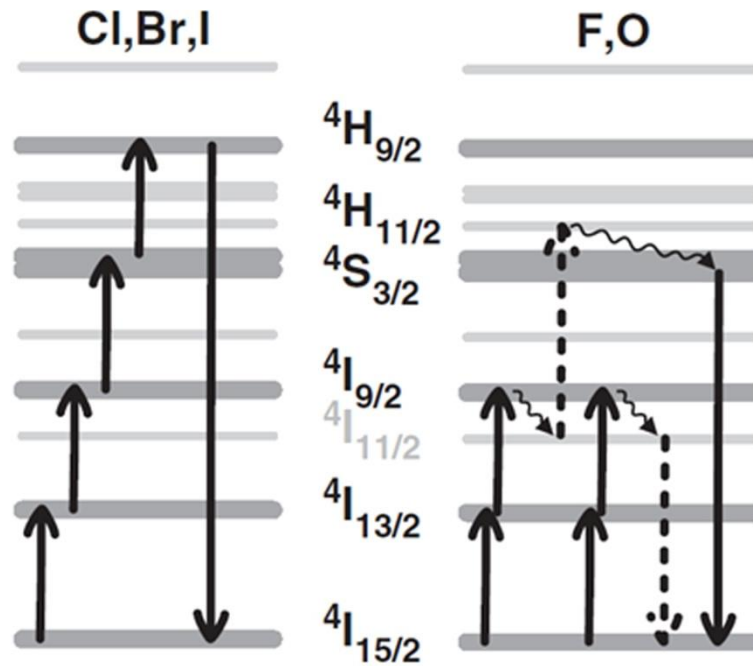


Fig. 1-7 Influence of the higher phonon energies on the UC properties [1-11]

- (2) Energy levels' splitting: The crystal field of host leads to additional level splitting (stark levels), which is much smaller than the spin-orbit splitting (due to atomic forces) [1-3]. Thus, although the absorption and emission properties of rare earth ions are almost the same as those in free Rare earth ions, the shape of the absorption and emission spectrum depends on the stark splitting. The splitting increases with decreasing the ionic radius, which causes broader excitation range. Fig. 1-8 shows excitation spectra of fluoride, chloride, bromide and iodide [1-13]. The fluoride has a broad excitation range, while the chloride, bromide and iodide have narrow excitation range.

In addition, the chloride, bromide and iodide are hygroscopic and are limited to application. Thus, generally used host materials for UC are fluorides, due to their low phonon energies, broad excitation range and chemical stability.

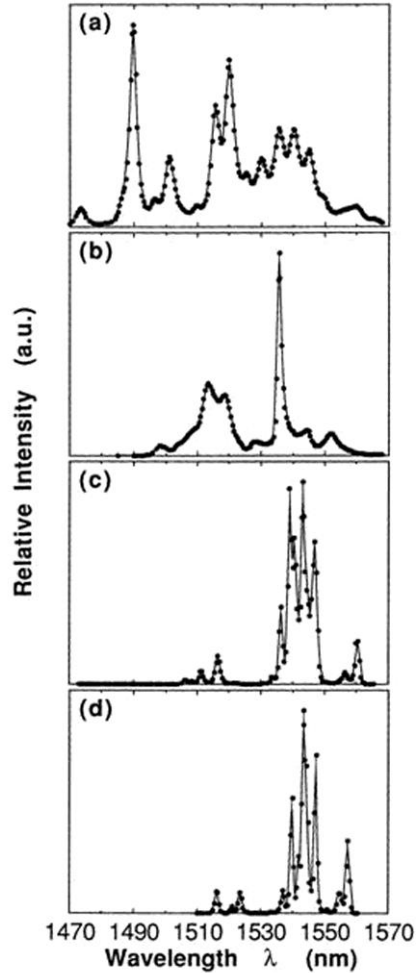
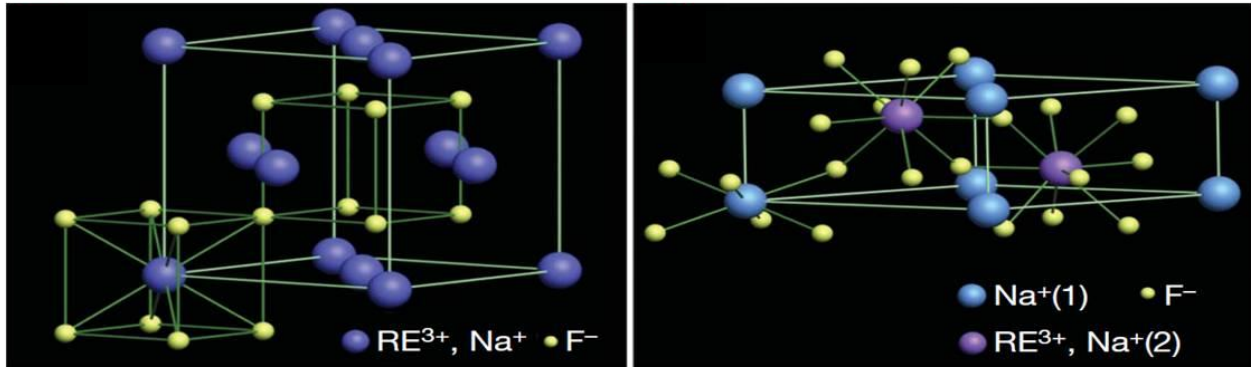


Fig. 1-8 Excitation spectra of (a) fluoride ($\text{YF}_3:20\%\text{Er}^{3+}$), (b) chloride ($\text{BaCl}_2:28\%\text{Er}^{3+}$), (c) bromide ($\text{YBr}_3:20\%\text{Er}^{3+}$) and (d) iodide ($\text{YI}_3:40\%\text{Er}^{3+}$) [1-13]. ($\lambda_{\text{EM}}=550 \text{ nm}$)

1.3.3 $\text{NaYF}_4:\text{Er}^{3+}$

Selection of specific fluoride host materials doped with Er^{3+} for UC needs consider close lattice matches to dopant ion. Since all trivalent lanthanide ions have similar ionic size and chemical properties, their inorganic compounds are considered as ideal host materials doped with Er^{3+} for UC [1-14]. It is found that NaYF_4 host is the most efficient host doped with Re^{3+} for UC, since it has lower phonon energies (418 cm^{-1}) than that of LiYF_4 (570 cm^{-1}) [1-15] [1-16]. NaYF_4 host has two phases: one is cubic (α) phase and the other is hexagonal (β) phase, as shown in fig. 1-9 [1-17]. The β -phase NaYF_4 has low symmetry compared to α -phase one. Since low symmetry host materials have higher f-f transition probabilities of the rare earth ions than that of high symmetry, the β -phase $\text{NaYF}_4:\text{Er}^{3+}$ is an ideal UC material for silicon-based solar cells.



Cubic (α)-phase NaYF_4

Hexagonal (β)-phase NaYF_4

Fig. 1-9 Cubic- and hexagonal-phase NaYF_4 doped with rare earth ions (Re^{3+}) [1-17].

1.3.4 Nanocrystals

Bulk β -phase NaYF_4 doped with rare earth ions has high UC efficiency than nano-size counterparts, as shown in table 1-2 [1-18]. The quantum yield (QY) for green emission of bulk β -phase $\text{NaYF}_4:2\% \text{Er}^{3+}$, $20\% \text{Yb}^{3+}$ is 3 %, while the QYs in the range of 0.005% to 0.3% have been measured with particle sizes from 10 to 100 nm. A 3-times QY enhancement of $\text{NaYF}_4:2\% \text{Er}^{3+}$, $20\% \text{Yb}^{3+}/\text{NaYF}_4$ core/shell sample has been observed compared to the core sample, which may be ascribed to the NaYF_4 shell which can reduce the fluorescence quenching on NCs surface resulting from the organic surfactant [1-19].

However, NCs have high potentiality to improve UC efficiency. Enhancements in UC emissions for NCs have been achieved through plasmonic coupling of Au NCs [1-20]. Fig. 1-19 (a) and (b) show TEM image of $\text{NaYF}_4:\text{Yb}^{3+}$, Tm^{3+}/Au NCs and dependence of the enhancement factor on 980 nm excitation power for the UC intensities. The 109-times enhancement for 5-phonon UC emissions has been observed. This enhancement can be interpreted as that the plasmon field enhancement directly increases the pumping power density of 980 nm excitation around Au NCs, resulting in the increase of excited Yb^{3+} ions. The author has calculated the amplitude distribution of pump light when a single Au sphere is attached on the surface of a spherical $\text{NaYF}_4:\text{Yb}^{3+}$, Tm^{3+} NCs. It is found that the enhancement of pump light is bigger than one in the 10 nm region under the surface of $\text{NaYF}_4:\text{Yb}^{3+}$, Tm^{3+} NCs. This indicates that the enhancement factor by plasmon field enhancement depends on the distance between Au NCs and NaYF_4 NCs. The enhancement factor increases with decreasing the distance. Thus, the nano-size NaYF_4 has higher enhancement factor than bulk one through plasmon field enhancement.

Sample #	Average particle size/nm	Power density/ W cm ⁻²	QY (%)
ErYb1	≫ 100	20	3.0 ± 0.3
ErYb2 (1 wt%)	100	150	0.30 ± 0.10
ErYb3 (1 wt%)	30	150	0.10 ± 0.05
ErYb4 (1 wt%)	8–10	150	0.005 ± 0.005
ErYb5 core shell (1 wt%)	30	150	0.30 ± 0.10

Table 1-2 Quantum yield for green emission (18000-19500 cm⁻¹) of β-phase NaYF₄:2%Er³⁺, 20%Yb³⁺ samples with different particle sizes excited with a 980 nm laser diode. Sample ErYb1 is the micro-sized powder (bulk) and 1 wt% means the colloidal solution in hexanes with 1% NaYF₄:2%Er³⁺, 20%Yb³⁺ samples [1-18].

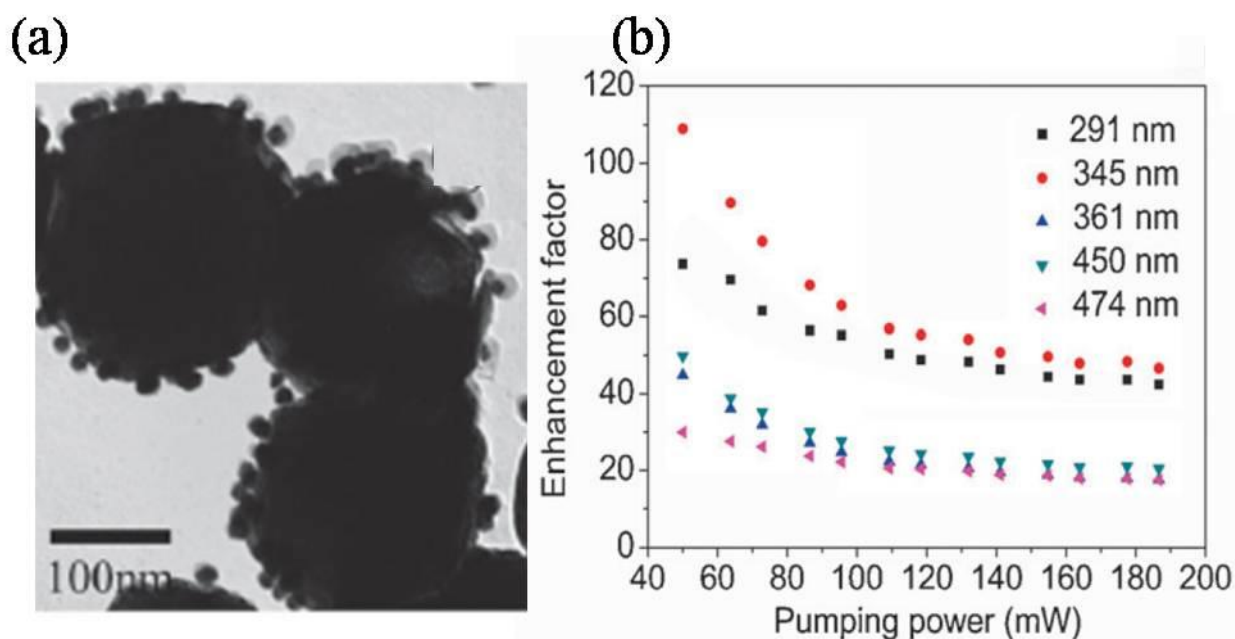


Fig. 1-10 (a) TEM image of NaYF₄:Yb³⁺, Tm³⁺/Au NCs and (b) dependence of the enhancement factor on 980 nm excitation power for the UC intensities of different peaks from both NaYF₄:Yb³⁺, Tm³⁺ and NaYF₄:Yb³⁺, Tm³⁺/Au NCs [1-20].

Another NCs' example for highly improving UC efficiency is exploiting organic dyes with large absorption cross-sections as antenna to absorb broad spectrum and transmit the energy to the Yb³⁺ ion, as shown in fig. 1-11 (a) [1-21]. Fig. 1-11 (b) shows that the UC action peak in the range 740-850 nm results from the absorption of organic dye, IR-806 and the tiny action peak in the range 900-990 nm (fig. 1-11 (b) inset) cor-

responds to the absorption of β -phase $\text{NaYF}_4:\text{Er}^{3+}, \text{Yb}^{3+}$ NCs. The spectral response ratio of dye-coated to non-sensitized NCs at peaks is around 1000:1 and the integrated spectral response ratio in 720-1000 nm is about 3300:1.

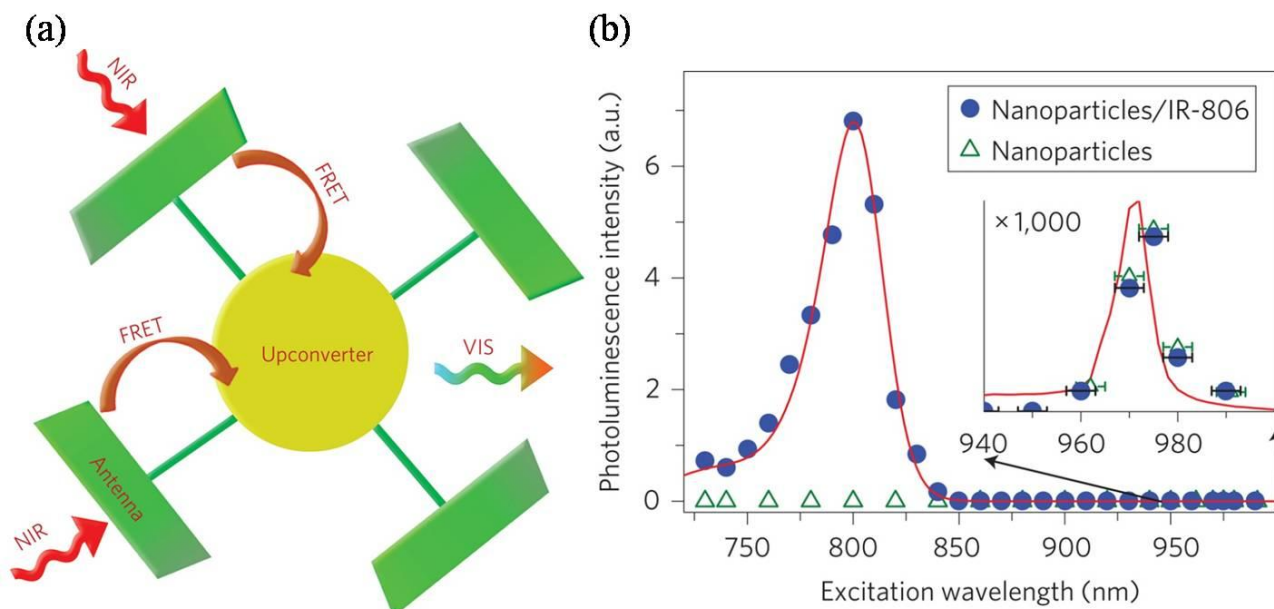


Fig. 1-11 (a) Principal concept of the dye-sensitized NCs and (b) experimental upconversion spectra of β -phase $\text{NaYF}_4:\text{Er}^{3+}, \text{Yb}^{3+}$ NCs/IR-806 and β -phase $\text{NaYF}_4:\text{Er}^{3+}, \text{Yb}^{3+}$ NCs, both dissolved in CHCl_3 (The emission intensity is integrated in the 500-685 nm range with excitation from a 2 mW c.w. laser) [1-21].

1.4 Recent synthesis method for β -phase $\text{NaYF}_4:\text{Re}^{3+}$ nanocrystals

The β -phase $\text{NaYF}_4:\text{Re}^{3+}$ NCs can be synthesized through hydro(solvo)thermal synthesis. The advantages of hydro(solvo)thermal synthesis method consist of highly crystalline phase, while the disadvantages of it include potential safety concerns caused by high pressure and the impossibility of observing the growth process of NCs [1-14]. In recent years, the generally used synthesis for high quality β -phase $\text{NaYF}_4:\text{Re}^{3+}$ NCs is thermal decomposition method. Mai and co-workers have reported the synthesis of NaReF_4 via thermal decomposition ($\text{CF}_3\text{COO-Na}$ or $-\text{Re}$) in the presence of oleic acid (OA), 1-octadecene (ODE) and oleylamine (OM), as shown in fig. 1-12 [1-22]. OA was used as a ligand, which prevents the NCs from agglomeration, and ODE as a solvent, because of its high boiling point (315 °C). OM was used as both ligand and solvent. The disadvantages of the thermal decomposition method are relatively complex, sensitive to its condition and discharges toxic gas such as COF_2 . It is important to develop an environment-friendly and facile synthesis method for β -phase NaYF_4 . Schafer and co-workers have reported an environment-friendly and facile method for β -phase $\text{NaYF}_4:\text{Re}^{3+}$ NCs in the presence of OA and OM with $\text{Y}_2(\text{CO}_3)_3 \cdot x\text{H}_2\text{O}$, $\text{Er}_2(\text{CO}_3)_3 \cdot x\text{H}_2\text{O}$, Na_2CO_3 and NH_4F as precursors [1-23]. However, the obtained NCs required post-annealing and the production included α and β -phase $\text{NaYF}_4:\text{Re}^{3+}$ and NaF .

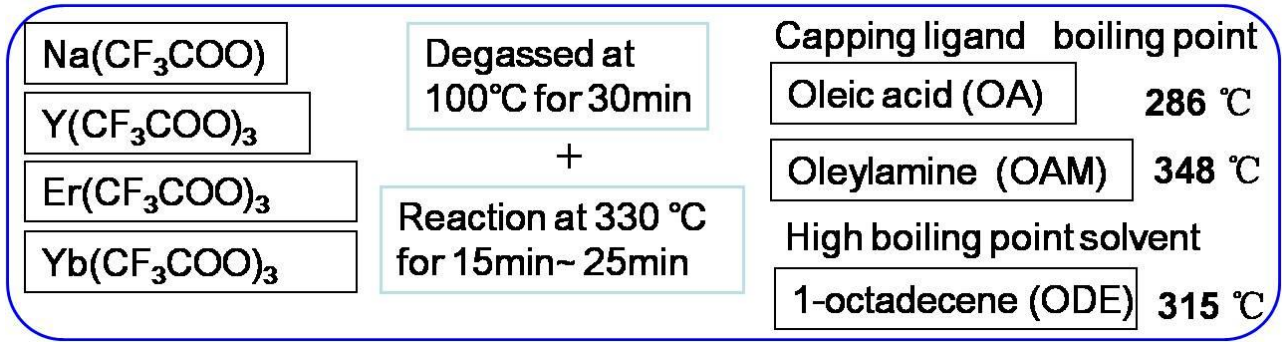


Fig. 1-12 The synthesis of β -phase NaYF₄:Er³⁺, Yb³⁺ via thermal decomposition method [1-22].

1.5 Application of upconversion materials to solar cells

For the application of UC materials to solar cells, the upconverter can be placed at the rear side of a solar cell with an insulator to electrically isolate each other. A reflector is placed behind the upconverter, as shown in Fig. 1-13 [1-6]. This structure ensures that the solar spectrum with energy higher than the bandgap is absorbed by solar cell, the low energy light is transmitted to the upconverter and the upconverted light is reflected into cell. Shalav et al. firstly showed an application of UC materials, NaYF₄:20%Er³⁺, to solar cell in 2005 [1-24]. An external quantum efficiency of 2.5% was observed under 5.1 mW excitation at 1523 nm. This report regarded the UC properties of NaYF₄:Er³⁺ for solar-cell applications under the excitation energy corresponded to the energy of the lowest f-f transition of Er³⁺ (⁴I_{15/2}→⁴I_{13/2}).

However, in order to effectively utilize the solar spectrum, UC materials should be applied to harvesting solar energy over a wide spectral range. Recently, the higher UC efficiencies have been reported under the broad spectrum illumination, compared to that under 1523 nm excitation at comparable irradiance [1-25]. Fig. 1-14 shows the power dependence of external quantum efficiency (EQE) for a silicon solar cell with upconverter. From the inset of fig. 1-14, it is found that excitation wavelength response of highest EQE is in 1523 nm. The schematic of the setup for the system of concentrated light is shown in fig. 1-15. The infrared light of a Xe-lamp can be concentrated by lenses and transmitted to the upconverter from Si wafer and solar cell. Then after the light is upconverted by UC material, it is reflected back to Si solar cell and the IV response can be observed. Table 1-3 shows the summary of the UC solar cell response under concentrated broad spectrum and monochromatic illumination (1523 nm). The active photon fluxes of upconverter from 1460 and 1600 nm have been calculated and compared to the same region photon fluxes in the AM1.5G to obtain effective concentration levels. When the UC EQE under concentrated broad spectrum illumination was compared to that under monochromatic laser excitation at same irradiance, both two EQE values under broad spectrum illumination were higher than those for monochromatic illumination, as shown in table 1-3. However, the mechanism of higher UC efficiencies under broad spectrum illumination is not clear.

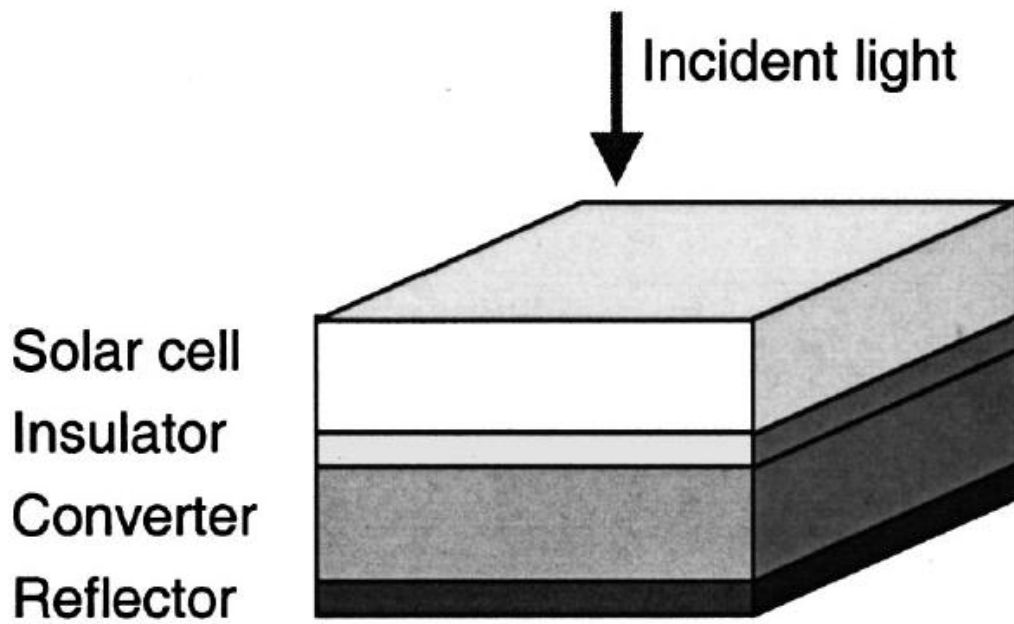


Fig. 1-13 Schematic diagram of a solar cell with insulator, upconverter and reflector [1-6].

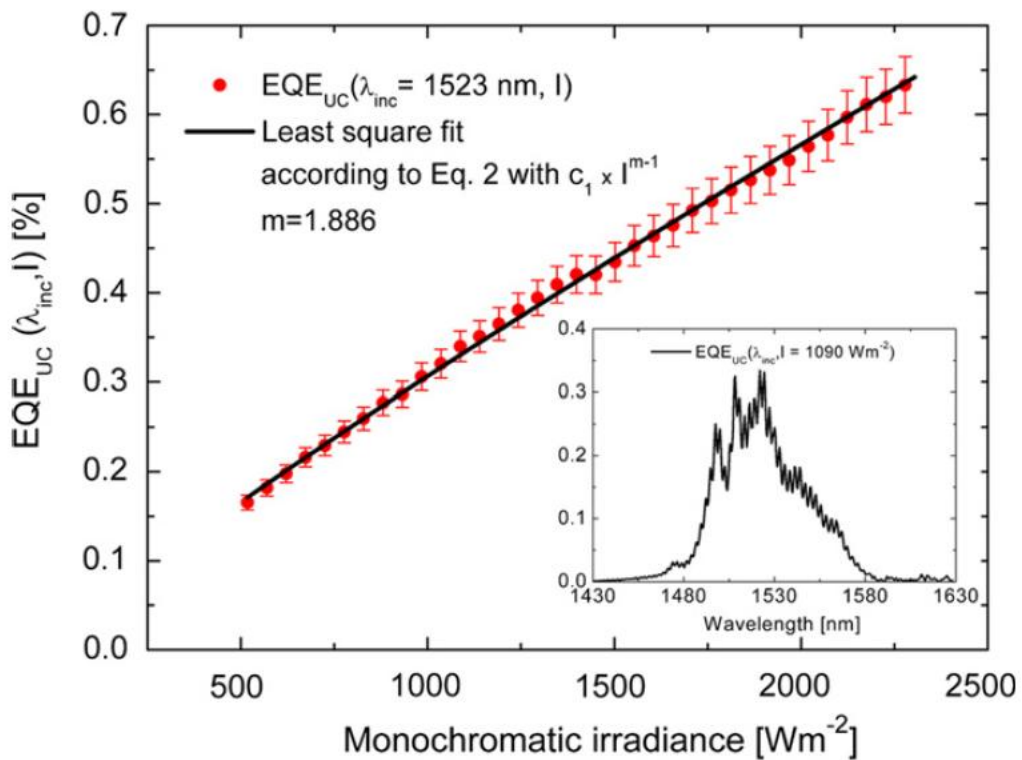


Fig. 1-14 Power dependence of external quantum efficiency (EQE) for a silicon solar cell with upconverter at an excitation wavelength of 1523 nm. The inset shows the EQE for different excitation wavelengths under the excitation density of 1090 Wm^{-2} [1-25].

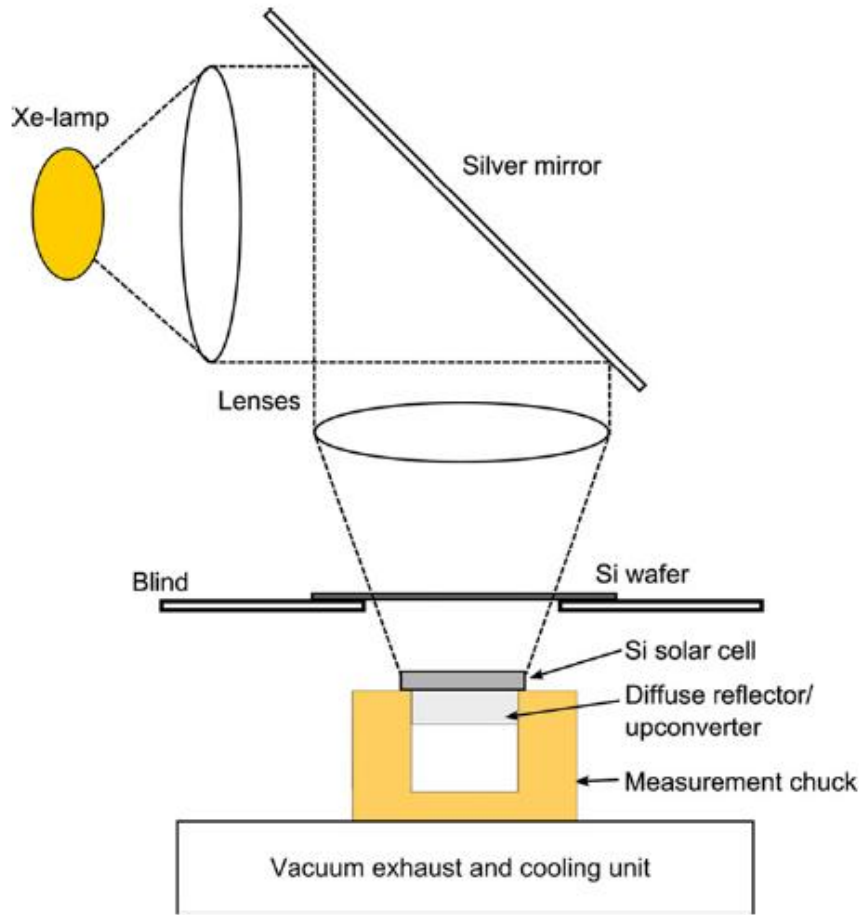


Fig. 1-15 Schematic of the setup for the IV-measurements of solar cells under concentrated light of a Xe-lamp [1-25]. A polished Si wafer serves as a pass filter.

Concentration onto the solar cell upconverter device [suns]	458 ± 5	732 ± 17
$I_{SC,PTFE}$ [mA]	1.67 ± 0.02	3.26 ± 0.08
$I_{SC,Zap}$ [mA]	1.99 ± 0.02	3.95 ± 0.04
$I_{SC,UC}$ [mA]	0.33 ± 0.03	0.69 ± 0.08
Photon flux $\Phi_{cell,UCrange}$ [s ⁻¹] in the active upconverter range of 1460–1600 nm	$(2.53 \pm 0.03) \times 10^{17}$	$(4.04 \pm 0.09) \times 10^{17}$
$EQE_{UC,int}(\Phi_{cell,UCrange})$ [%]	0.81 ± 0.07	1.07 ± 0.13
$EQE_{UC}(\lambda_{inc}=1523\text{ nm}, I)$ [%] for monochromatic measurements	0.47 ± 0.01	0.71 ± 0.02

Table 1-3 Summary of the UC solar cell response under concentrated broad spectrum and monochromatic illumination [1-25].

1.6 Research motivations

As mentioned above, the β -phase $\text{NaYF}_4:\text{Er}^{3+}$ NCs have high potentiality to improve UC efficiency. However, the synthesis method generally used is relatively complex, sensitive to its condition and discharges toxic gas such as COF_2 . It is important to develop an environment-friendly and facile synthesis method for the β -phase $\text{NaYF}_4:\text{Er}^{3+}$ NCs. In addition, the higher UC efficiencies have been reported under the broad spectrum illumination, compared to that under 1523 nm excitation at comparable irradiance, although the reason for this is as yet unknown. To resolve this issue, it is necessary to form a clear understanding of the UC optical process during off-resonant excitation.

Considering these issues, we have set our research motivations as follows:

- 1) Developing a user-friendly and facile synthesis method for β -phase $\text{NaYF}_4:\text{Er}^{3+}$ NCs.
- 2) Studying the UC optical process in β -phase $\text{NaYF}_4:\text{Er}^{3+}/\text{NaYF}_4$ NCs using off-resonant excitation at 1620 nm, whose energy is smaller than that corresponding to the lowest f-f transition of Er^{3+} (${}^4\text{I}_{15/2} \rightarrow {}^4\text{I}_{13/2}$).
- 3) Studying the UC mechanisms for β -phase $\text{NaYF}_4:\text{Er}^{3+}/\text{NaYF}_4$ NCs under resonant and off-resonant excitation simultaneously (1550 and 1620 nm), which are part of the AM1.5 spectrum and not absorbed by the silicon solar cells, in order to better apply UC materials to improving the efficiency of solar cells under broad spectrum excitation.

1.7 Chapter 1 References

- [1-1] M. Green, "Third generation photovoltaics: Ultra-high conversion efficiency at low cost," *Progress in Photovoltaics: Research and Applications* 9 (2001) 123–135.
- [1-2] B. S. Richards, *Sol. Energy Mater. Sol. Cells.* 90 (2006) 2329–2337.
- [1-3] Avi Shalav, Thesis: Rare-earth Doped Up-converting Phosphors for an Enhanced Silicon Solar Cell Response, University of New South Wales, (2006).
- [1-4] Xiaoyong Huang, Sanyang Han, Wei Huang and Xiaogang Liu. *Chem. Soc. Rev.* 42 (2013) 173-201.
- [1-5] C. Strumpel, M. McCann, G. Beaucarne, V. Arkhipov, A. Slaoui, V. Svrcek, C. del Canizo, I. Tobias, Modifying the solar spectrum to enhance silicon solar cell efficiency—An overview of available materials. *Solar Energy Materials and solar cells* 91 (2007) 238-249.
- [1-6] T. Trupke, M. Green, P. Würfel, *J. Appl. Phys.* 92 (7) (2002) 4117.
- [1-7] W. Shockley, H. Queisser, Detailed balance limit of efficiency of p-n junction solar cells, *J. Appl. Phys.* 32 (3) (1961) 510.
- [1-8] T. Trupke, A. Shalav, B. Richards, P. Würfel, M. Green, Efficiency Enhancement of solar cells by luminescent up-conversion of sun-light, *Sol. Energy Mater. Sol. Cells* 90 (2006) 3327.
- [1-9] G. Dieke, *Spectra and Energy Levels of Rare Earth Ions in Crystals*, Inter science Publishers, New York, (1968).
- [1-10] G. Dieke and H. Crosswhite, "The spectra of the doubly and triply ionized rare earth," *Applied Optics* 2 (1963) 675–686.
- [1-11] D. R. Gamelin and H. U. Gudel, "Upconversion processes in transition metal and rare earth metal systems" *Top. Curr. Chem.* 214, (2001) 1-56.
- [1-12] Claudia Strumpel, Thesis: Application of Erbium-Doped Up-Converters to Silicon Solar Cells, University Konstanz, (2007).
- [1-13] J. Ohwaki and Y. Wang, "Efficient 1.5µm to visible upconversion in Er³⁺-doped halide phosphors," *Japanese Journal of Applied Physics* 33(3A) (1994) L334–L337.
- [1-14] F. Wang, X. Liu, *Chem. Soc. Rev.* 38 (2009) 976.
- [1-15] J.F. Suyver, J. Grimm, M.K.V. Veen, D. Biner, K.W. Kramer, H.U. Gudel, *J. Lumin.* 117 (2006) 1.
- [1-16] S. Miller, H. Rast and H. Caspers, "Lattice vibrations of LiYF₄," *The Journal of Chemical Physics* 52(8) (1970) 4172–4175.
- [1-17] F. Wang, Y. Han, C.S. Lim, Y.H. Lu, J. Wang, J. Xu, H.Y. Chen, C. Zhang, M.H. Hong, X.G. Li, *Nature* 463 (2010) 1061.
- [1-18] J.C. Boyer, F.C.J.M van Veggel; Absolute Quantum Yield Measurements of Colloidal NaYF₄:Er³⁺, Yb³⁺ Upconverting Nanoparticles, *Nanoscale* 2 (2010) 1417.
- [1-19] Y.G. Shun and G.M. Chow, *Chem. Mater.* 19 (3) (2007) 341–343.
- [1-20] N. Liu, W.P. Qin, G.S. Qin, T. Jiang, D. Zhao, *Chem. Commun.* 47 (2011) 7671-7673.
- [1-21] W.Q. Zou, C. Visser, J.A. Maduro, M.S. Pshenichnikov, J.C. Hummelen, *Nature photonics* 6 (2012) 560-564.
- [1-22] H.X. Mai, Y.W. Zhang, R. Si, Z.G. Yan, L.D. Sun, L.P. You, C.H. Yan, *J. Am. Chem. Soc.* 128 (2006) 6426.
- [1-23] H. Schafer, P. Ptacek, H. Eickmeier, M. Haase, *Adv. Funct. Mater.* 19 (2009) 3091.
- [1-24] A. Shalav, B. S. Richards, T. Trupke, K. W. Kramer, H. U. Gudel. Application of NaYF₄:Er

up-converting phosphors for enhanced near-infrared silicon solar cell response. *Applied Physics Letters* 86 (2005) 013505.

[1-25] J. C. Goldschmidt, S. Fischer, P. Loper, K. W. Kramer, D. Biner, M. Hermle, and S. W. Glunz, Experimental analysis of upconversion with both coherent monochromatic irradiation and broad spectrum illumination. *Solar Energy Materials and solar cells* 95 (2011) 1960-1963.

Chapter 2. Upconversion mechanisms of rare earths

2.1 Spontaneous radiative and non-radiative decay

Generally, the change of population N in the excited state can be given by

$$\frac{dN}{dt} = -A^T N = -(A^{rad} + A^{nr})N \quad (2.1)$$

Where A^T is the total decay rate, consisting of radiative decay rate A^{rad} and non-radiative decay rate A^{nr} . Equation 2.1 shows that the population in excited state decreases exponentially with the total decay rate A^T . The total decay lifetime τ is given by

$$\frac{1}{\tau} = A^{rad} + A^{nr} = \frac{1}{\tau_{rad}} + A^{nr} \quad (2.2)$$

where the radiative lifetime τ_{rad} is inversely proportional to the radiative decay rate. The radiative quantum efficiency (QE) is given by

$$QE = \frac{A^{rad}}{A^{rad} + A^{nr}} \quad (2.3)$$

Rate of spontaneous emission

The probability of spontaneous radiative transition can be described by Fermi's golden rule and given by [2-1]

$$A_{ij}^{rad} = \frac{\omega^3 n |\mu_{ij}|^2}{3\pi\epsilon_0 \hbar c_0^3} \quad (2.4)$$

where μ_{ij} is the transition dipole moment from the initial state i to final state j , n is the refraction index,

ω is the emission frequency, ϵ_0 is the vacuum permittivity, \hbar is the reduced Planck constant and c_0 is the vacuum speed of light.

Non-radiative decay rate

The non-radiative decay rate in rare earth ions results from the multi-phonon emission and can be given by

$$A^{nr} = A^{nr}(0)e\left(-\alpha \frac{\Delta E}{\hbar\omega_{\max}}\right) \quad (2.5)$$

where $A^{nr}(0)$ and α are empirical constants, which depend on the host material and not on the rare earth ions, ΔE is the energy gap between the excited state and the next lower-lying state of a rare earth ion and $\hbar\omega_{\max}$ is the highest phonon energies of the host. Equation 2.5 is exclusively applied to rare earth ions, because of the energetic levels in rare earth ions weakly affected by the crystal field of host [2-2].

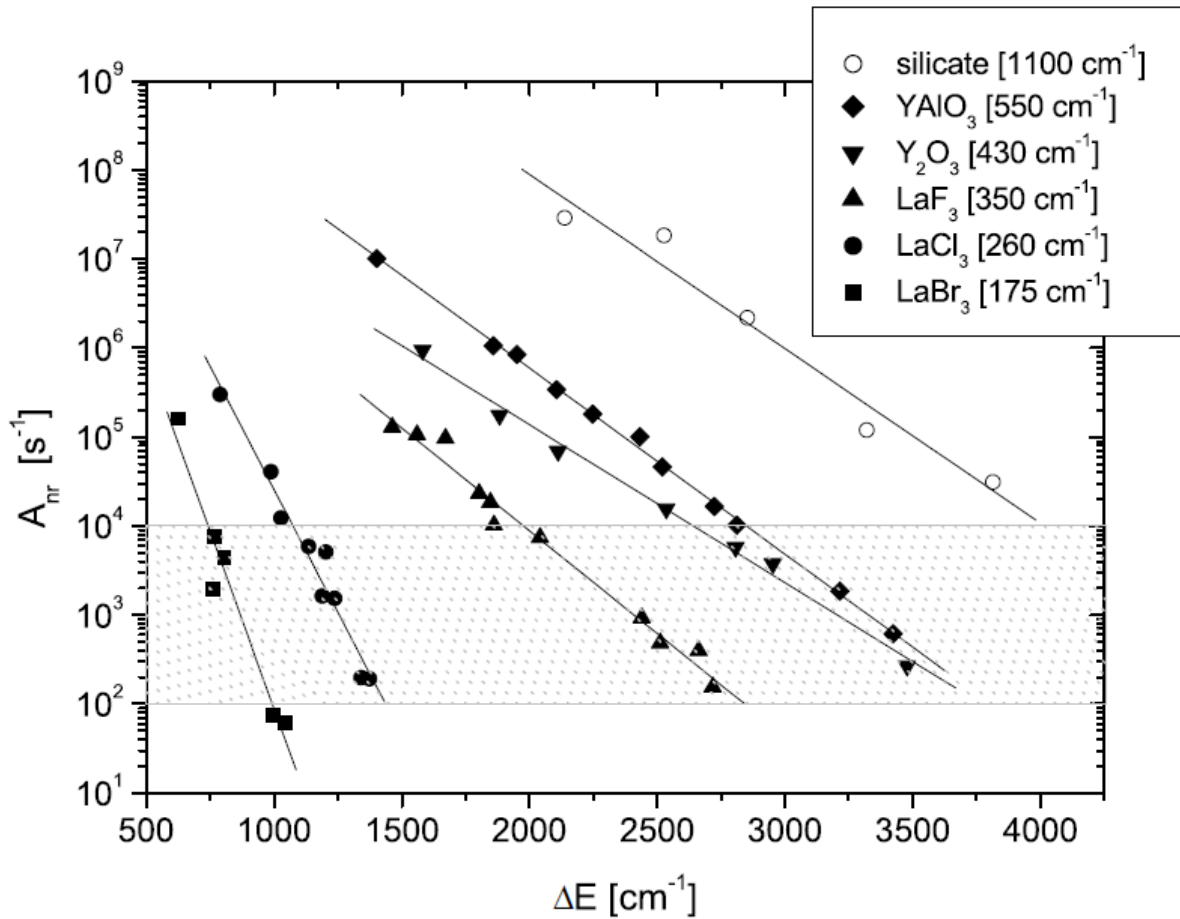


Fig. 2-1 Non-radiative rates as a function of ΔE in different hosts. The shaded area indicates the usual radiative rates. The wave number in brackets indicates the highest phonon energy of the hosts [2-3][2-4].

Host	Max. phonon E [cm ⁻¹]	α	$A_{nr}(0)$
Silicate glass	1100	0.0045±0.0005	7.3×10 ¹¹
YAlO ₃	550	0.00481±0.00007	9.0×10 ⁹
Y ₂ O ₃	430	0.0041±0.0002	4.9×10 ⁸
LaF ₃	350	0.0053±0.0002	3.7×10 ⁸
LaCl ₃	260	0.0012±0.001	8.7×10 ⁹
LaBr ₃	175	0.0018±0.002	9.7×10 ⁹

Table 2-1 Calculated $A^{nr}(0)$ and α constants for different hosts [2-4].

Fig. 2-1 shows the experimental data of non-radiative rates A^{nr} as a function of the energy gap ΔE in different hosts on a log-log scale, which shows a linear relationship between A^{nr} and ΔE [2-3]. The shaded area indicates the usual radiative rates reported by J. Sole et al. [2-2]. The A^{nr} decreases exponentially with the energy gap ΔE . The radiative decay dominates, when the energy gap ΔE is enough large, generally more than 5 phonons energy. Thus, in the same energy gap ΔE , the radiative decay dominates in low phonon energy host compared to high one. Table 2-1 shows the calculated $A^{nr}(0)$ and α constants for different hosts [2-4].

Shalav et al. have reported the calculated radiative and non-radiative rates for different Er³⁺ doped hosts based on the rate equations introduced in Chapter 2.3, as shown Fig. 2-2 [2-4]. The radiative rate A of LiYF₄:Er³⁺ is used as an approximate value for NaYF₄:Er³⁺, due to no reports about the parameters of transition dipole moment for NaYF₄:Er³⁺. In addition, the parameters of non-radiative rate A^{nr} for the NaYF₄ host have not been reported in the literature, so A^{nr} of LaF₃ is used as an approximate value for NaYF₄:Er³⁺. Furthermore, the parameters of transition dipole moment for the ${}^4I_{9/2} \rightarrow {}^4I_{11/2}$ have not been reported in the literature. From the results in Fig. 2-2, transitions ${}^4I_{15/2} \rightarrow {}^4I_{13/2} \rightarrow {}^4I_{9/2}$ take place by absorbing two 1550 nm photons and most of electrons at ${}^4I_{9/2}$ would be non-radiatively relaxed to ${}^4I_{11/2}$ in the hosts with the phonon energies larger than 350 cm⁻¹ (LaF₃). Fig. 2-3 shows calculated radiative and non-radiative rates from the ${}^4I_{11/2}$ level for different Er³⁺ doped hosts. It is found that the radiative rate for the transition ${}^4I_{11/2} \rightarrow {}^4I_{15/2}$ is an order of magnitude higher than that for the transition ${}^4I_{11/2} \rightarrow {}^4I_{13/2}$. For low phonon energy host (350 cm⁻¹ LaF₃), the non-radiative rate for transition ${}^4I_{11/2} \rightarrow {}^4I_{13/2}$ is less than the radiative rate for the transitions ${}^4I_{11/2} \rightarrow {}^4I_{15/2}$ and ${}^4I_{11/2} \rightarrow {}^4I_{13/2}$, so the radiative emission for ${}^4I_{11/2} \rightarrow {}^4I_{15/2}$ is dominant, whose energy is higher than the bandgap of silicon. For high phonon energy hosts, such as YAlO₃ (550 cm⁻¹) and Y₂O₃ (430 cm⁻¹), the non-radiative rate for transition ${}^4I_{11/2} \rightarrow {}^4I_{13/2}$ is dominant, compared to radiative rates for the transitions ${}^4I_{11/2} \rightarrow {}^4I_{15/2}$ and ${}^4I_{11/2} \rightarrow {}^4I_{13/2}$. This shows that low phonon energy hosts have crucial effect on UC emission.

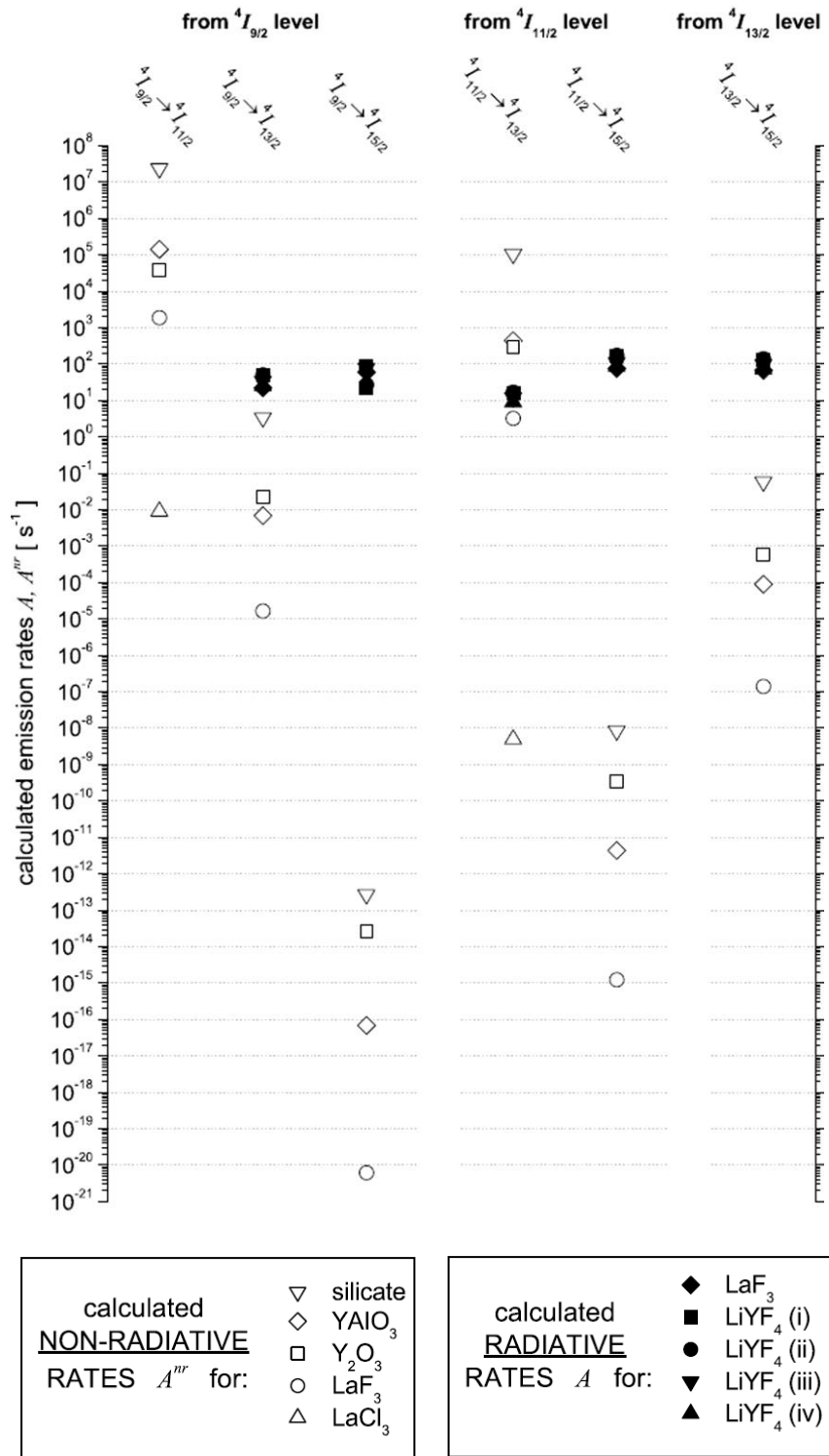


Fig. 2-2 Calculated radiative and non-radiative rates for different Er^{3+} doped hosts [2-4]

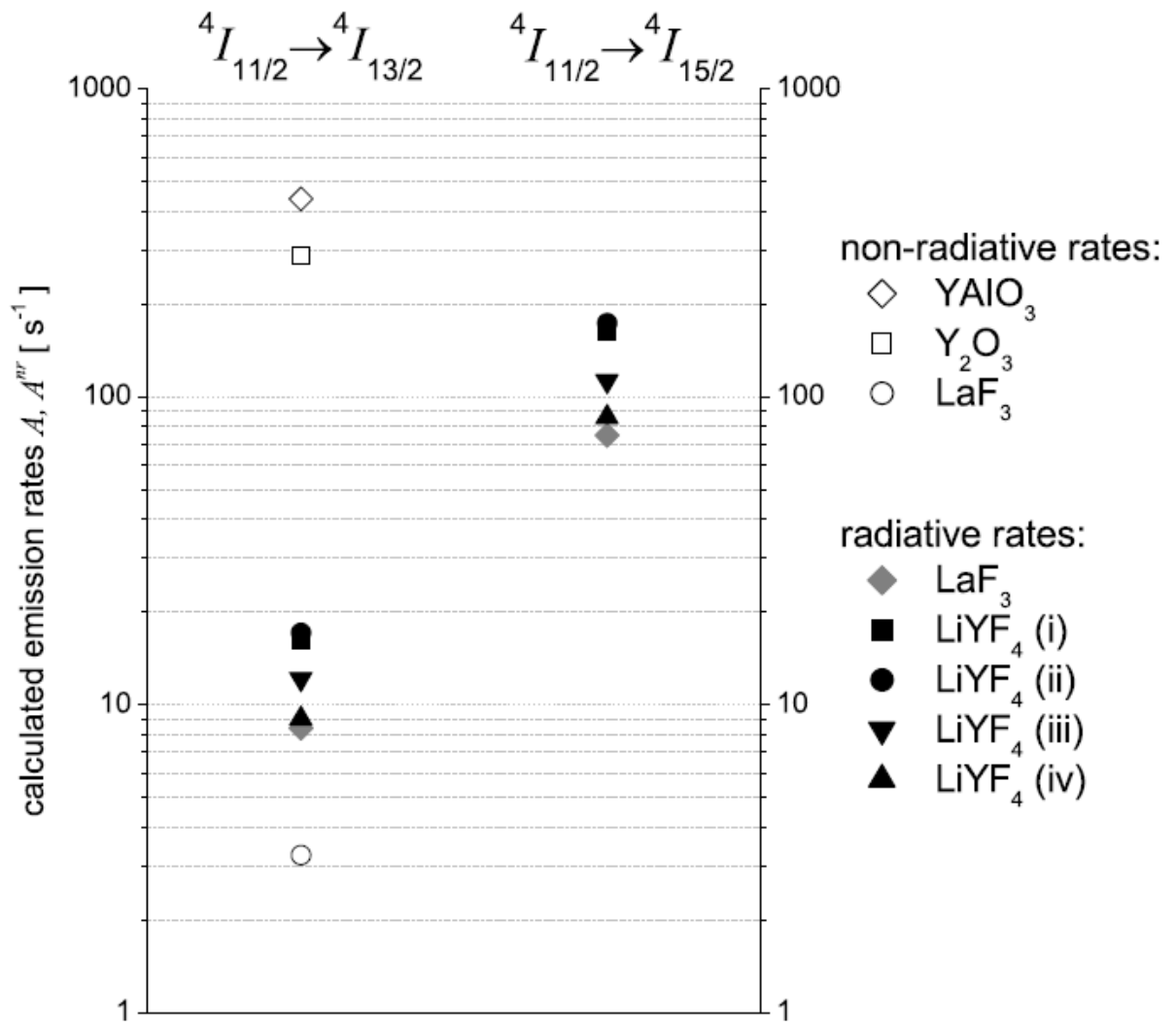


Fig. 2-3 Calculated radiative and non-radiative rates from the ${}^4I_{11/2}$ level for different Er^{3+} doped hosts [2-4]

2.2 Dominant upconversion mechanisms

There are two main UC mechanisms, ground state absorption followed by excited state absorption (GSA/ESA) and energy transfer up-conversion (ETU) [2-5]. Fig. 2-4 shows the UC processes of GSA/ESA under 1550 nm excitation in Er^{3+} ion. By an excitation at 1550 nm, the ground state of Er^{3+} (${}^4I_{15/2}$) would be excited to ${}^4I_{13/2}$, and the emission at 1540 nm ($\text{Er}^{3+}: {}^4I_{13/2} \rightarrow {}^4I_{15/2}$) occurs. By the subsequent excitation, the transition from ${}^4I_{13/2}$ to ${}^4I_{9/2}$ would take place by ESA processes. Then the light emission at 800 nm occurs, originating from ${}^4I_{9/2} \rightarrow {}^4I_{15/2}$ transition. Some of electrons at ${}^4I_{9/2}$ would be non-radiatively relaxed to ${}^4I_{11/2}$, resulting in the generation of 980 nm emission corresponding to ${}^4I_{11/2} \rightarrow {}^4I_{15/2}$ transition. The green emission at 540 nm ($\text{Er}^{3+}: {}^4S_{3/2} \rightarrow {}^4I_{15/2}$) arises from another ESA processes corresponding to ${}^4I_{9/2} \rightarrow {}^4S_{3/2}$ transition. The red emission at 660 nm ($\text{Er}^{3+}: {}^4F_{9/2} \rightarrow {}^4I_{15/2}$) occurs through the ${}^4S_{3/2} \rightarrow {}^4F_{9/2}$ relaxation or ${}^4I_{11/2} \rightarrow {}^4F_{9/2}$ transition,

which shows two optical passes to form ${}^4F_{9/2}$ excited state.

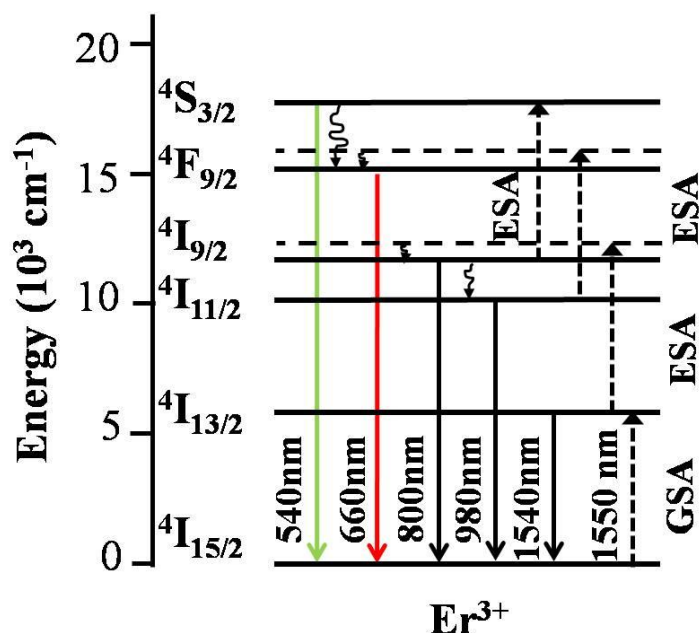


Fig. 2-4 Energy level diagram for Er^{3+} showing the UC processes of GSA/ESA under 1550 nm excitation. (Excitation photons, radiative and multi-phonon relaxation processes are depicted in dotted, full and curly lines, respectively.)

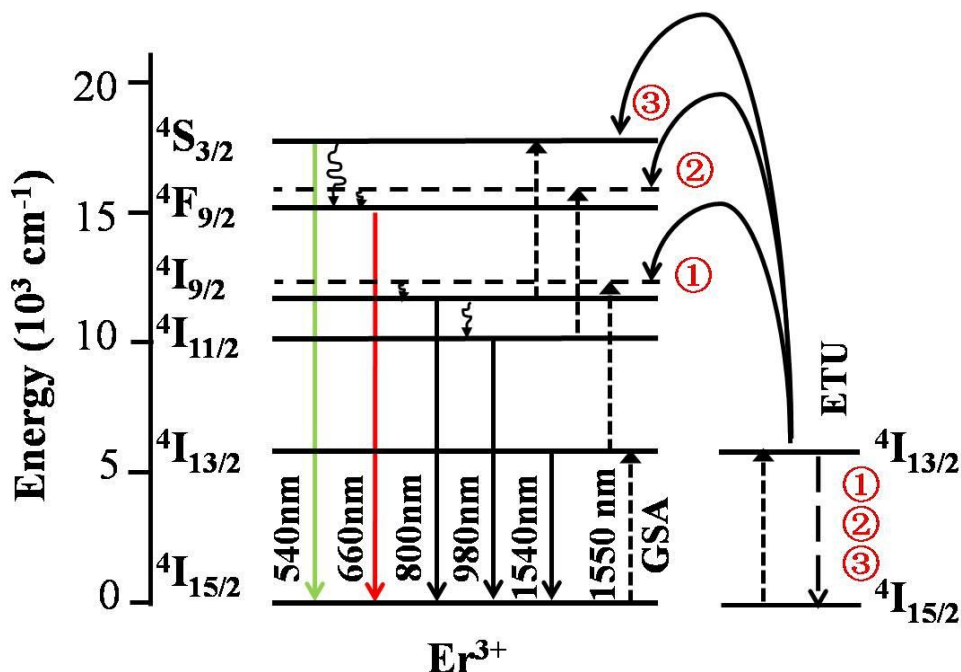


Fig. 2-5 Energy level diagram for Er^{3+} showing the UC processes of GSA/ETU under 1550 nm excitation. (Excitation photons, energy transfers, radiative and multi-phonon relaxation processes are depicted in dotted, dashed, full and curly lines, respectively.)

Fig. 2-5 shows the UC processes of GSA/ETU under 1550 nm excitation in Er^{3+} ion. After absorption of a photon of 1550 nm, the ground state of Er^{3+} ($^4\text{I}_{15/2}$) would be excited to $^4\text{I}_{13/2}$. Via the energy transfer from the neighboring ion, the transition from $^4\text{I}_{13/2}$ to $^4\text{I}_{9/2}$ would take place. Then the $^4\text{I}_{11/2} \rightarrow ^4\text{F}_{9/2}$ transition and $^4\text{I}_{9/2} \rightarrow ^4\text{S}_{3/2}$ transition occur, arising from another ETU processes. The GSA/ESA process occurs within a single ion, while GSA/ETU process takes place within two or more ions. Thus, GSA/ETU process depends on the concentration of the ions, however, GSA/ESA process not on it.

2.3 Power dependence of upconversion

UC is a non-linear optical process, in which the emitted intensity I_{em} non-linearly depends on the intensity of the incident pump power P . For a three-level system (ground state, intermediate state, upconverter state) in fig. 2-6, the population density of ground, intermediate and upconverter state are N_0 , N_1 and N_2 respectively, constants of decay rate is A , absorption coefficients are α_0 and α_1 for ground state and intermediate state absorption, a corresponding parameter of ETU is W_1 and the corresponding parameter of power is ρ [2-6].

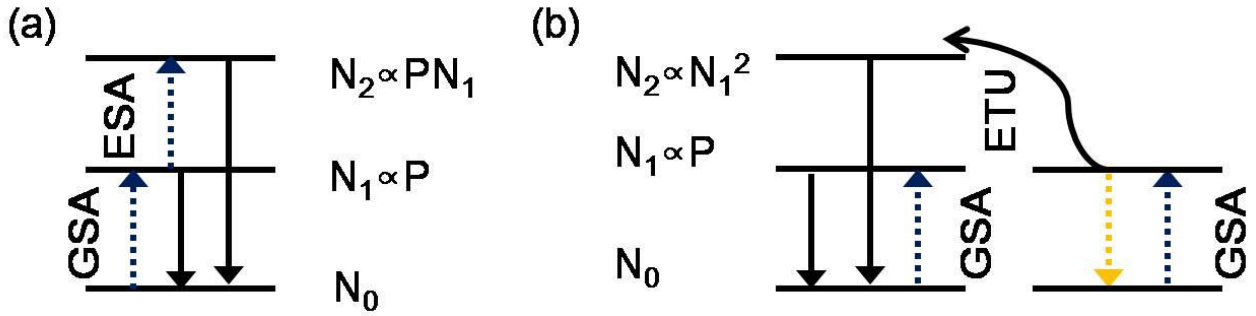


Fig. 2-6 Three-level upconversion scheme. (a) GSA/ESA, (b) GSA/ETU. (Excitation photons, energy transfers, radiative processes are depicted in dotted, dashed and full, respectively.) [2-6]

Assuming that the UC mechanism is GSA/ESA, the rate equations is given by

$$\frac{dN_1}{dt} = \rho\alpha_0 N_0 P - \rho\alpha_1 N_1 P - A_1 N_1 \quad (2.6)$$

$$\frac{dN_2}{dt} = \rho\alpha_1 N_1 P - A_2 N_2 \quad (2.7)$$

Under steady-state excitation, it follows from equation (2.7) and (2.6) that

$$A_2 N_2 = \rho\alpha_1 N_1 P \quad (2.8)$$

$$\rho\alpha_0 N_0 P = \rho\alpha_1 N_1 P + A_1 N_1 \quad (2.9)$$

If linear decay is the dominant depletion mechanism, it follows from equation (2.9) that

$$\rho\alpha_0 N_0 P = A_1 N_1 \quad (2.10)$$

We obtain that $N_1 \propto P$, considering the population density of ground state N_0 is constant. Form equation (2.8), we find that

$$N_2 \propto P^2 \quad (2.11)$$

Assuming that the UC mechanism is GSA/ETU, the rate equations is given by

$$\frac{dN_1}{dt} = \rho\alpha_0 N_0 P - 2W_1 N_1^2 - A_1 N_1 \quad (2.12)$$

$$\frac{dN_2}{dt} = W_1 N_1^2 - A_2 N_2 \quad (2.13)$$

Under steady-state excitation, it follows from equation (2.13) and (2.12) that

$$A_2 N_2 = W_1 N_1^2 \quad (2.14)$$

$$\rho\alpha_0 N_0 P = 2W_1 N_1^2 + A_1 N_1 \quad (2.15)$$

If linear decay is the dominant depletion mechanism, it follows from equation (2.15) that

$$\rho\alpha_0 N_0 P = A_1 N_1 \quad (2.16)$$

We obtain that $N_1 \propto P$, considering the population density of ground state N_0 is constant. Form equation (2.14), we find that

$$N_2 \propto P^2 \quad (2.17)$$

For more than three-level system if linear decay is the dominant depletion mechanism, we generally obtain that from the rate equations

$$I_{em} \propto P^n \quad (2.18)$$

where the exponent n represents the effective number of photons required to produce one UC emission photon. This is ideal case of the power dependence, without regard to other linear decaying mechanisms. In high pump power, a saturation effect takes place, leading to a reduction of the slope n on a log-log depiction of emitted intensity versus pump power.

2.4 summary

The spontaneous radiative and non-radiative decay have been summarized in this chapter. Dominant upconversion mechanisms, including GSA/ESA and GSA/ETU, have been discussed. Via rate equations, the emitted intensity depends on the pump power with a power law have been determined, as indicated in equation 2.18.

2.5 Chapter 2 References

- [2-1] B. Henderson and G. Imbusch, *Optical Spectroscopy of Inorganic Solids*, Clarendon Press, Oxford, UK, (1989).
- [2-2] J. Sole, L. Bausa, D. Jaque, *An Introduction to the Optical Spectroscopy of Inorganic Solids*, John Wiley & Sons, Ltd, (2005).
- [2-3] M. Weber, "Rare earth lasers," in *Handbook on the Physics and Chemistry of Rare Earths* (K. Gschneidner and L. Eyring, eds.), North Holland publishing, Amsterdam, vol. 4 (1979) ch: 35.
- [2-4] Avi Shalav, *Thesis: Rare-earth Doped Up-converting Phosphors for an Enhanced Silicon Solar Cell Response*, University of New South Wales, (2006).
- [2-5] F. Auzel, *Chem. Rev.* 104 (2004) 139
- [2-6] M. Pollnau, D.R. Gamelin, S.R. Luthi, H.U. Gudel, M.P. Hehlen, *Phys. Rev. B.* 61 (2000) 3337.

Chapter 3. Experimental method

3.1 X-ray diffraction (XRD)

X-ray diffraction is an analytical technique which can obtain the information of the crystal structure and chemical composition etc. The X-ray diffraction (XRD) of prepared NCs powders were characterized by using Panalytical X'Pert diffractometer.

Bragg's law

Bragg's law has been used to clarify the interference pattern of X-ray scattered by the crystal structure, as shown in fig. 3-1. The incident angle, θ , is denoted as an angle between the incident beam and the sample surface. The diffracted angle, 2θ , is denoted as an angle between the incident beam and the diffracted beam. For the wavelength of the X-ray, λ , and the space distance, d_{hkl} between the planes, constructive interference takes place through the Bragg's law [3-1], which is given by

$$n\lambda = 2d_{hkl} \sin \theta, \quad n = 1, 2, 3, \dots \quad (3.1)$$

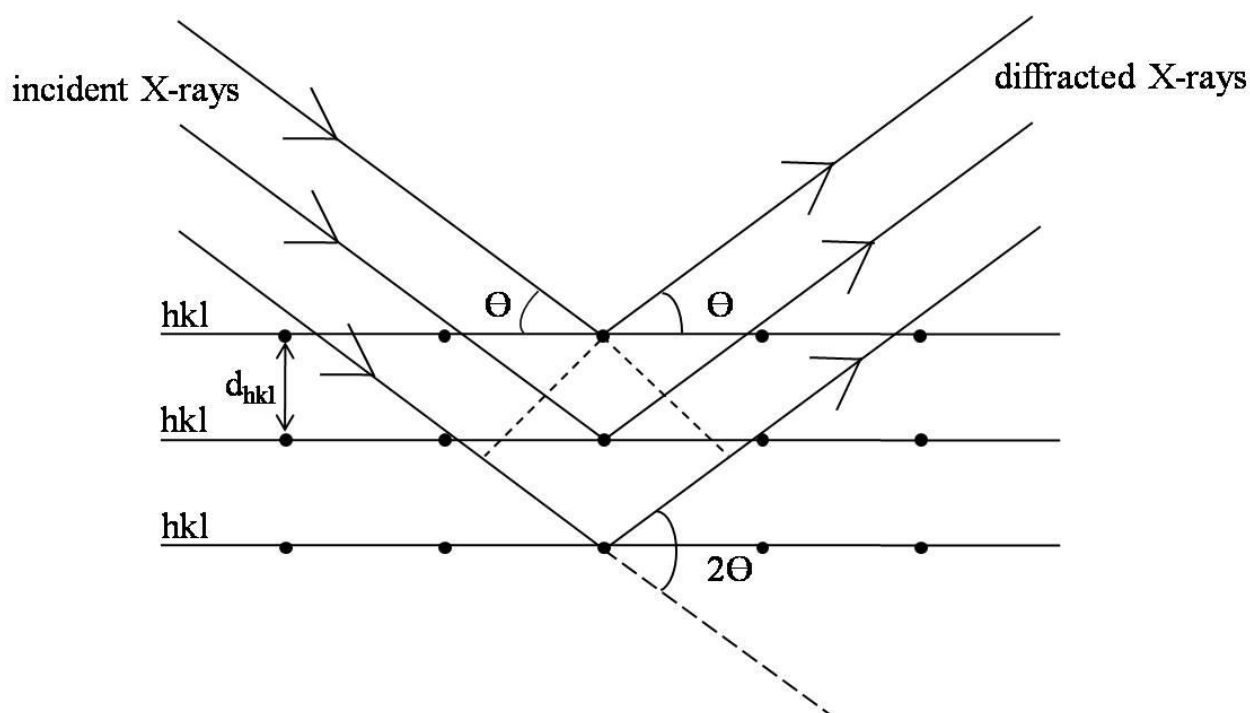


Fig. 3-1 Bragg's law

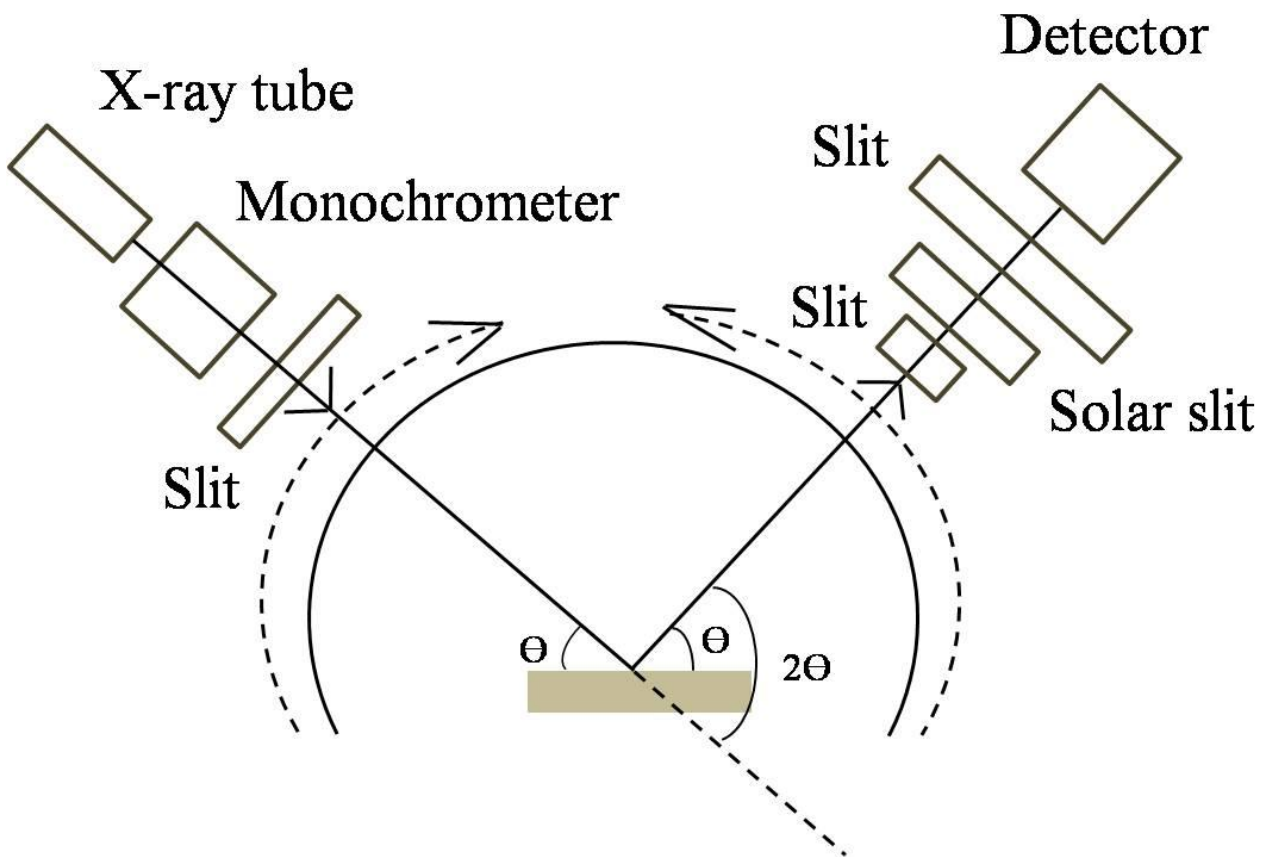


Fig. 3-2 Schematic of the setup for X-ray diffractometer

Fig. 3-2 shows the schematic of the setup for X-ray diffractometer.

Scherrer's equation

The crystal size from the XRD can be calculated by the Scherrer's equation,

$$D = \frac{K\lambda}{\beta \cos \theta} \quad (3.2)$$

where D is the mean size of the crystal, K is the shape factor, λ is the X-ray wavelength, β is the line broadening at half the maximum intensity in radians and θ is the Bragg angle [3-2][3-3].

3.2 Transmission electron microscope (TEM)

TEM is an available microscopy technique and important analysis method for physical, chemical and biological sciences. TEM's imaging is higher resolution than the light microscope, due to the small de Broglie wavelength of electrons. The high-resolution image is obtained via the interaction of the electrons transmitted through the specimen. Fig. 3-3 and 3-4 show the essential column parts [3-4]. The electrons emitted from the electron gun are focused by electromagnetic lenses into a very thin beam under vacuum in the column of the microscope. The electron beam transmits through the specimen and arrives at the fluorescent screen, which yields a shadow image. The shadow image can be recorded by photographic film or detected by a CCD camera.

Transmission electron microscopy (TEM) of NCs was carried out using a JEOL 2010 transmission electron microscope with an acceleration voltage of 200 kV in this study.

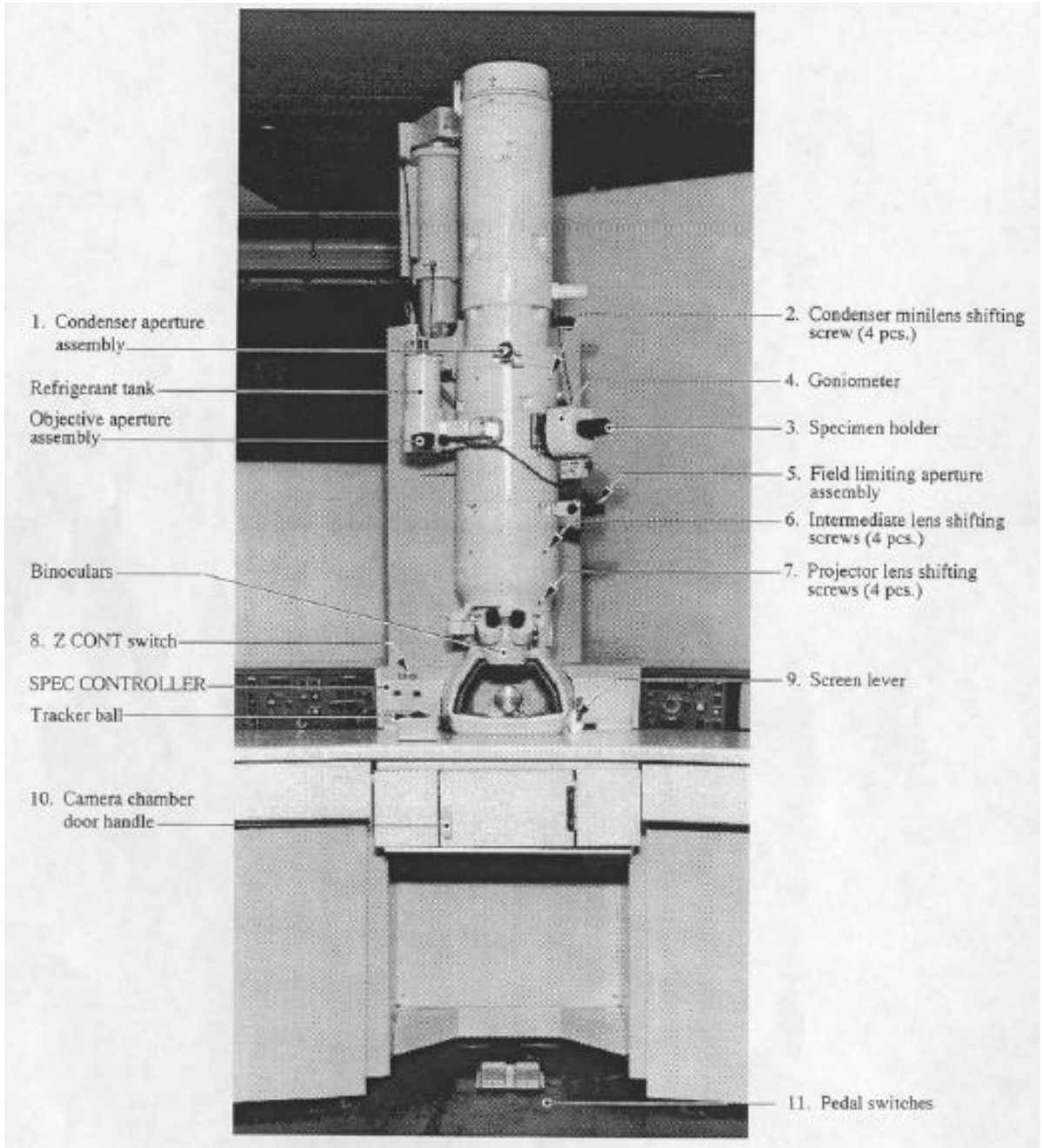


Fig. 3-3 External view of column [3-4]

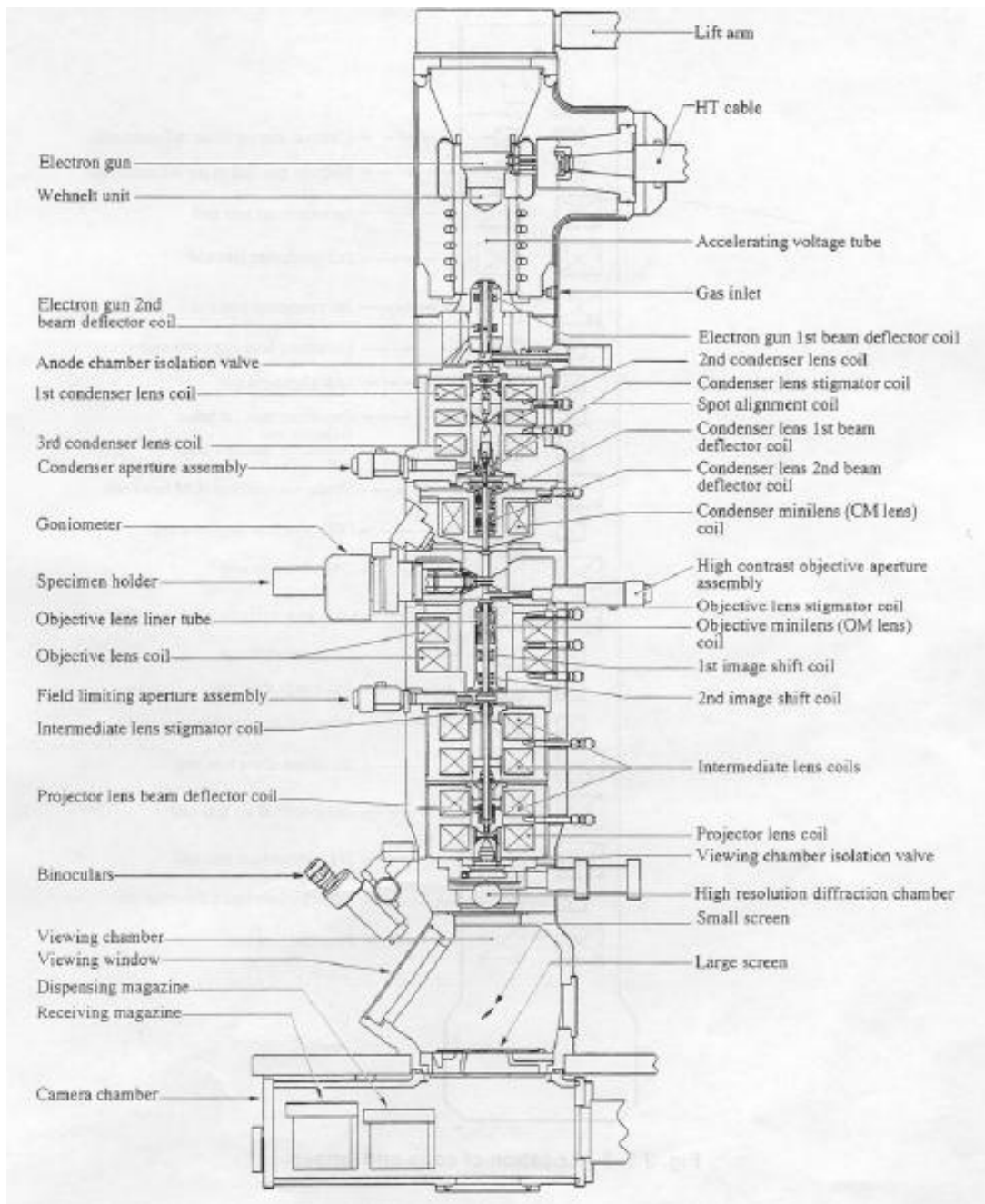


Fig. 2-4 Cross-section of microscope column [3-4]

3.3 Spectroscopy

3.3.1 Absorption Spectrum

The absorption spectra were collected using Jasco V-670 spectrometer. A PMT detector and a Peltier-cooled PbS detector are employed for the UV/VIS and NIR region, respectively. The detector is automatically exchanged in the range of 800 to 900 nm. The detective wavelength can be selected from 190 to 2700 nm.

3.3.2 Raman and photoluminescence spectrum

To measure the Raman and photoluminescence spectrum, the emission signals were detected using the Nanofinder 30 microscopy system, with a laser excitation at 532 nm. Fig. 3-5 shows the setup of Nanofinder 30 microscopy system.

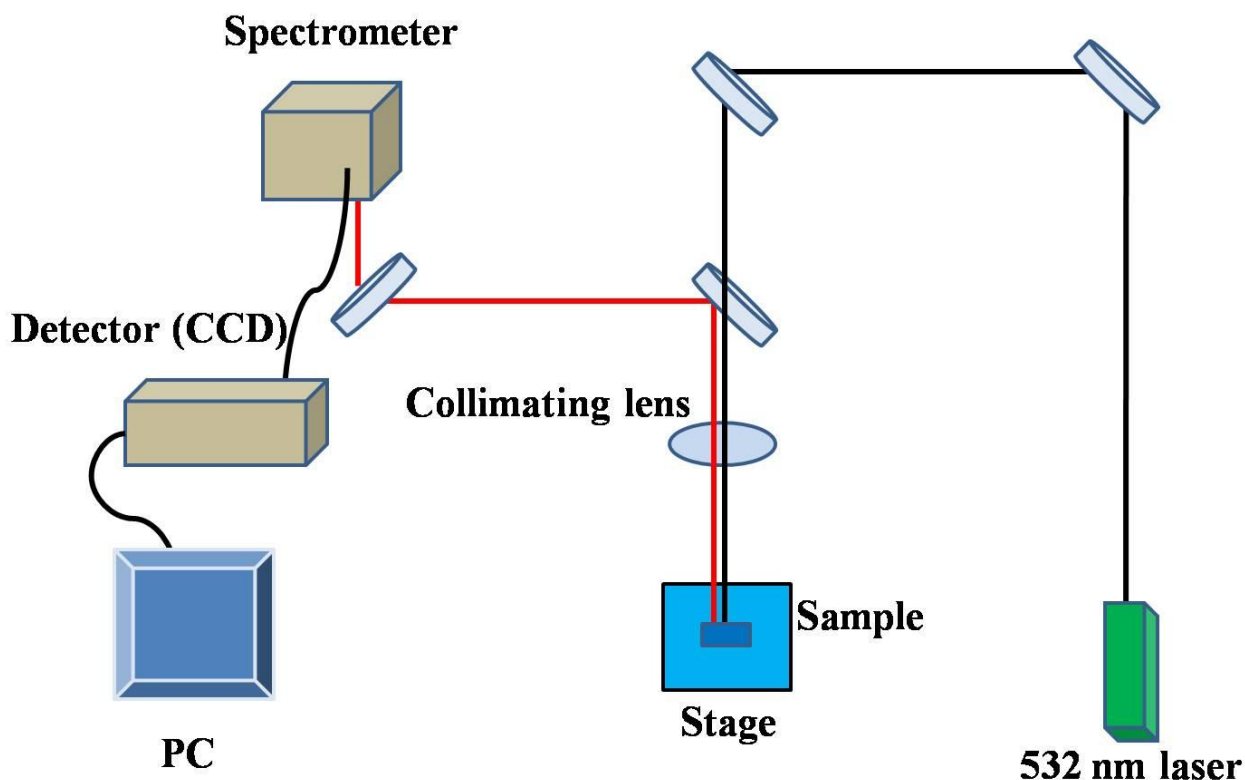


Fig. 3-5 Schematic of the setup for Nanofinder 30 microscopy system with a laser excitation at 532 nm

3.3.3 Upconversion spectrum

UC emission spectrum was measured using a Seki Technotron spectrometer under lasers excitation at 1550 or 1620 nm.

3.3.4 Power and temperature dependence Spectrum

The power and temperature dependence of UC emission spectra were measured by using the Nanofinder 30 microscopy system, under lasers excitation at 1550 and 1620 nm. Fig. 3-6 shows the setup of Nanofinder 30 microscopy system. The temperature controlling system consists of temperature controller and liquid nitrogen tank. Two lasers at 1550 and 1620 nm are introduced into the microscopy system, and focused on the sample holder. The emission signals are introduced into spectrometer and are detected by the detector PMT or CCD. The detecting ranges of CCD and PMT are 650-1100nm and 950-1700 nm, respectively.

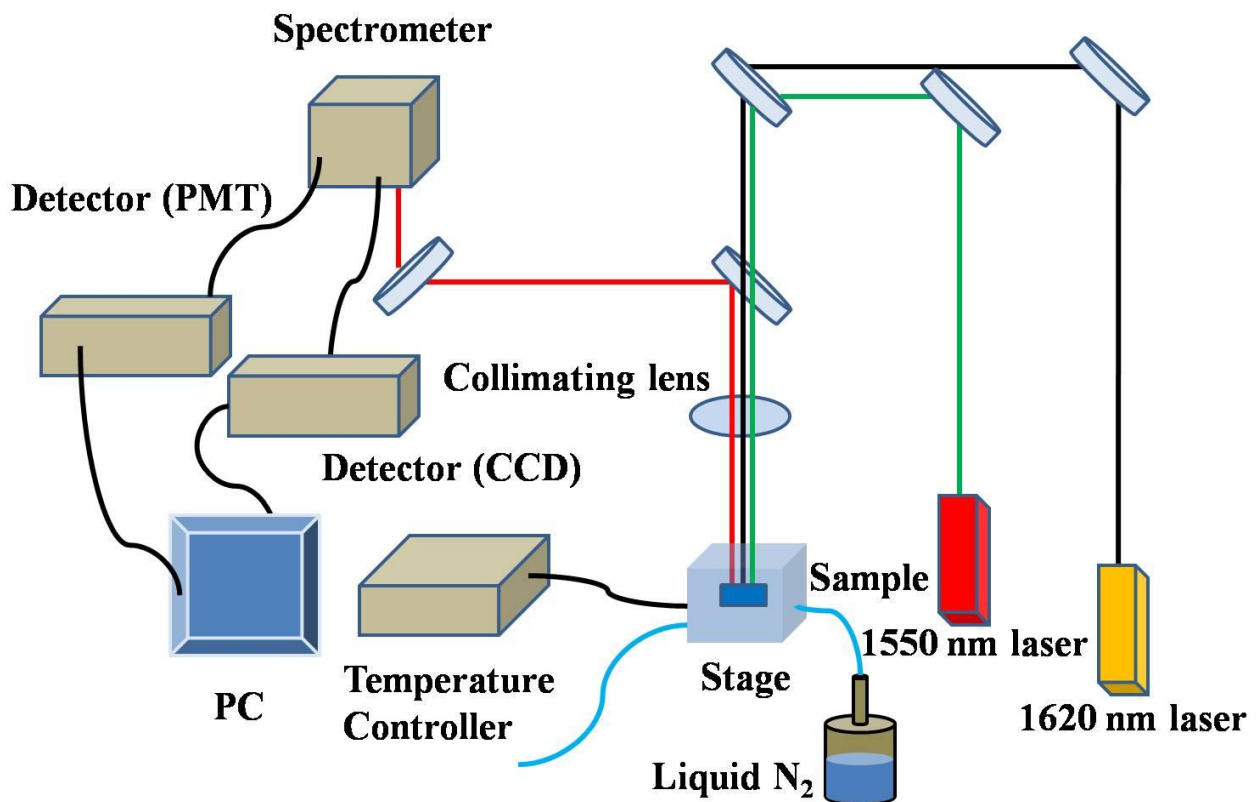


Fig. 3- 6 Schematic of the setup for Nanofinder 30 microscopy system with lasers excitation at 1550 and 1620 nm

3.4 Chapter 3 references

- [3-1] Charles Kittel, Introduction to solid state physics, chapter2, John Wiley & Sons, New York (2003)
- [3-2] P. Scherrer, Gottinger Nachrichten Gesell Vol. 2 (1918) 98.
- [3-3] A. Patterson, "The Scherrer Formula for X-Ray Particle Size Determination". Phys. Rev. 56(10) (1939) 978–982
- [3-4] JEOL JEM 2010 training transmission electron microscope, user manual, version 5.1

Chapter 4. A user-friendly and facile synthesis for β -phase $\text{NaYF}_4:\text{Er}^{3+}$ and $\text{NaYF}_4:\text{Er}^{3+}/\text{NaYF}_4$ NCs

4.1. Introduction

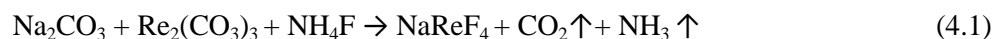
UC NCs have recently attracted significant attentions, due to their potential applications to solar cells [4-1][4-2], telecommunications [4-3], biolabeling [4-4][4-5], 3-dimensional displays [4-6][4-7] and temperature sensing [4-8][4-9]. One of the promising UC materials is NaYF_4 doped with rare earth, since the phonon energy of the host is relatively low which suppresses non-radiative relaxation [4-10]. The phase control and rare earth concentration in NaYF_4 are very important to get high conversion efficiency, as the UC emission properties are strongly dependent on them [4-7] [4-11]. The synthesis method generally used is relatively complex, sensitive to its condition and discharges toxic gas such as COF_2 [4-12]. It is important to develop an environment-friendly and facile synthesis method for NaYF_4 with phase controllability [4-13][4-14]. In order to improve the UC intensity, one of the methods is synthesizing the NCs with an undoped NaYF_4 shell [4-15].

In this work, a user-friendly and facile method was developed to produce the high quality β -phase $\text{NaYF}_4:\text{Er}^{3+}$ and $\text{NaYF}_4:\text{Er}^{3+}/\text{NaYF}_4$ core/shell NCs. The $\text{NaYF}_4:\text{Er}^{3+}$ and $\text{NaYF}_4:\text{Er}^{3+}/\text{NaYF}_4$ NCs were synthesized in oleic acid (OA) and 1-octadecene (ODE) with $\text{Y}_2(\text{CO}_3)_3 \cdot x\text{H}_2\text{O}$, $\text{Er}_2(\text{CO}_3)_3 \cdot x\text{H}_2\text{O}$, Na_2CO_3 and NH_4F as precursors. This proposed method is simple and less toxic compared with generally used method so far.

4.2. Experimental

The typical synthesis method of $\text{NaYF}_4:10\%\text{Er}^{3+}$ NCs was as follows: $\text{Y}_2(\text{CO}_3)_3 \cdot x\text{H}_2\text{O}$ (1.35 mmol), $\text{Er}_2(\text{CO}_3)_3 \cdot x\text{H}_2\text{O}$ (0.15 mmol), Na_2CO_3 (1.5 mmol) and NH_4F (12 mmol) were mixed with oleic acid (OA, 30 mmol) and octadecene (ODE, 90 mmol), which were used as a ligand and solvent, respectively. The mixed solution was degassed at 100 °C for 0.5 h. The temperature was then increased to around 310 °C for 0.5 h and 330 °C for 0.5 h. Following cooling to room temperature, the $\text{NaYF}_4:10\%\text{Er}^{3+}$ NCs were collected by centrifugation and washed three times with ethanol. The products were then dried at 80 °C for 3 h. To produce $\text{NaYF}_4:10\%\text{Er}^{3+}/\text{NaYF}_4$ core/shell NCs, the $\text{NaYF}_4:10\%\text{Er}^{3+}$ (1 mmol) NCs were mixed with $\text{Y}_2(\text{CO}_3)_3 \cdot x\text{H}_2\text{O}$ (0.5 mmol), Na_2CO_3 (0.5 mmol), NH_4F (4 mmol), OA (10 mmol) and ODE (30 mmol). The synthesis method was the same as that described above for $\text{NaYF}_4:10\%\text{Er}^{3+}$.

The chemical reaction can be expressed as below:



In fact, Na_2CO_3 and rare earth carbonates were mixed with NH_4F in OA and ODE, and the reaction tempera-

ture was increased to 100 °C, resulting in occurrence of ammonia gas and the formation of nanoscale α -phase NaErF_4 .

4.3. Results and discussions

4.3.1. Crystal structure

Fig. 4-1 shows XRD profiles of the NaErF_4 NCs prepared at 280 °C with various OA/oleylamine(OM) ratios. In all various OA/OM ratios, the cubic-phase NaErF_4 NCs were dominant.

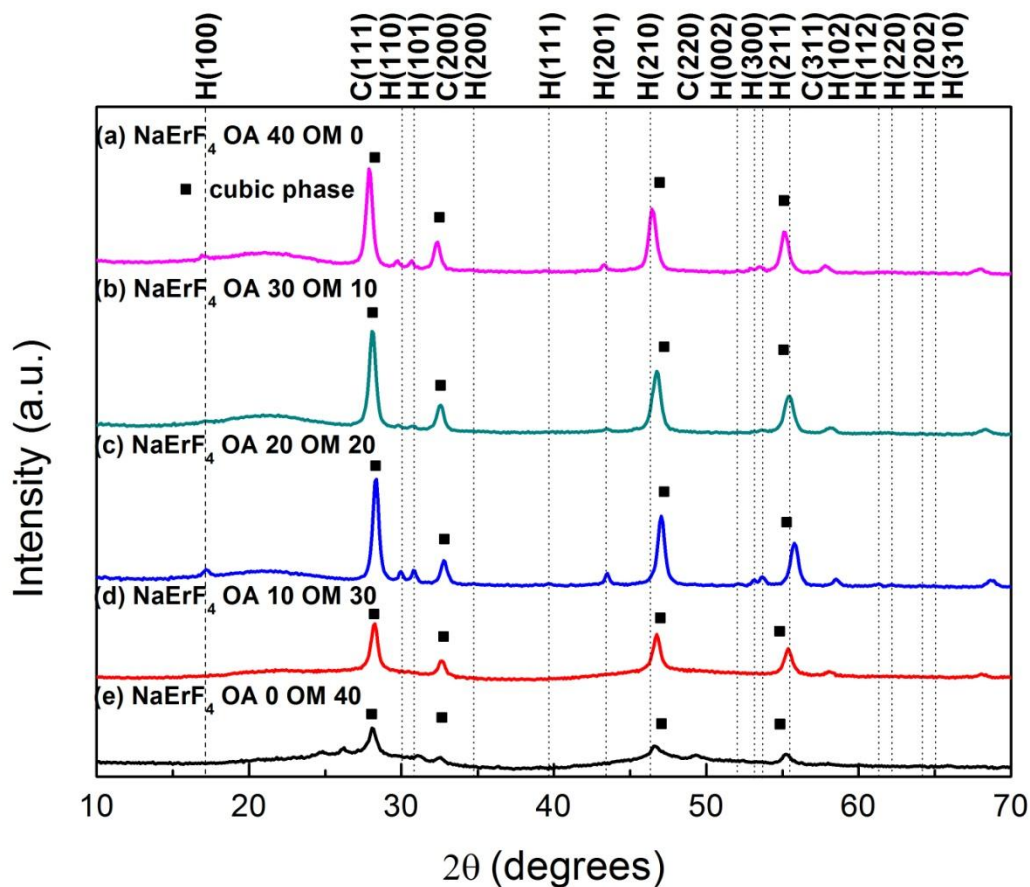


Fig. 4-1 XRD profiles of NaErF_4 NCs obtained at 280 °C with various OA/OM ratios. H(100) and C(111) are hexagonal-phase (100) peak and cubic-phase (111) peak, respectively.

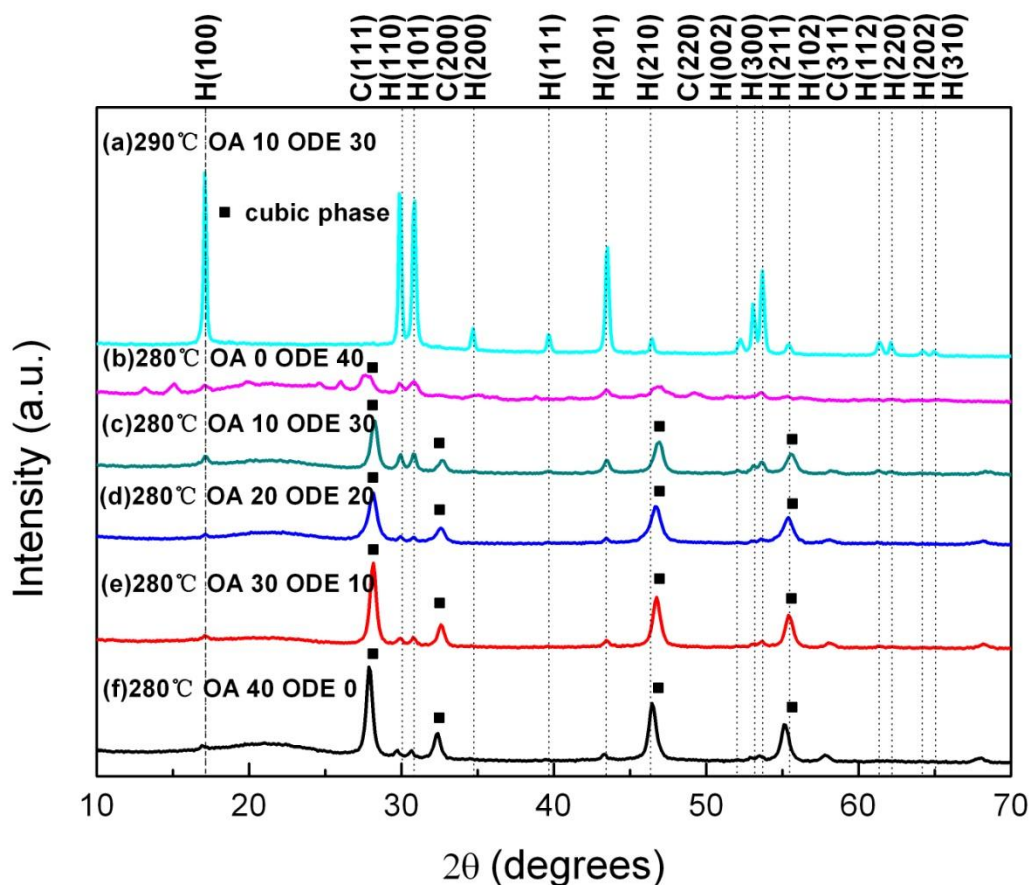


Fig. 4-2 XRD profiles of NaErF_4 NCs obtained at $280\text{ }^\circ\text{C}$ with various OA/ODE ratios and $290\text{ }^\circ\text{C}$ with OA/ODE=10/30. H(100) and C(111) are hexagonal-phase (100) peak and cubic-phase (111) peak, respectively.

Fig. 4-2 shows XRD profiles of the NaErF_4 NCs prepared at $280\text{ }^\circ\text{C}$ with various OA/ODE ratios. As shown in the figure, the peak intensities of β -phase NaErF_4 were highest at the OA/ODE ratio of 10/30 (mmol) than other OA/ODE ratio. Pure β -phase NaErF_4 NCs were obtained at $290\text{ }^\circ\text{C}$ with OA/ODE=10/30 as shown in fig. 4-2(a).

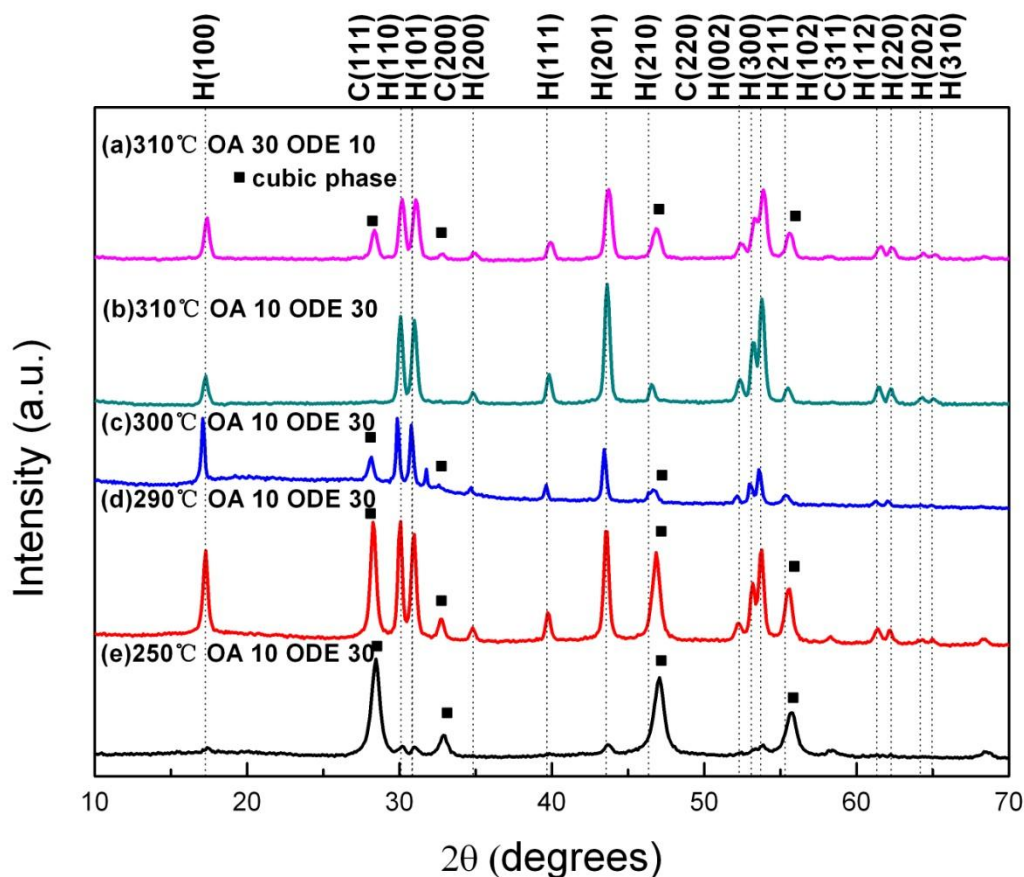


Fig. 4-3 XRD profiles of $\text{NaYF}_4:20\%\text{Er}$ NCs obtained under the OA/ODE=10/30 (mmol) with various temperatures. For reference, The NCs obtained at 310 °C under OA/ODE=30/10. H(100) and C(111) are hexagonal-phase (100) peak and cubic-phase (111) peak, respectively.

Fig. 4-3 shows XRD profiles of the $\text{NaYF}_4:20\%\text{Er}^{3+}$ NCs prepared with the OA/ODE ratio of 10/30 with various temperatures. With increasing temperature, β -phase $\text{NaYF}_4:20\%\text{Er}^{3+}$ became dominant and pure β -phase was obtained at 310 °C. XRD profile of the $\text{NaYF}_4:20\%\text{Er}^{3+}$ prepared at 310 °C with the OA/ODE ratio of 30/10 demonstrated the mixed phase, as shown in fig. 4-3(a).

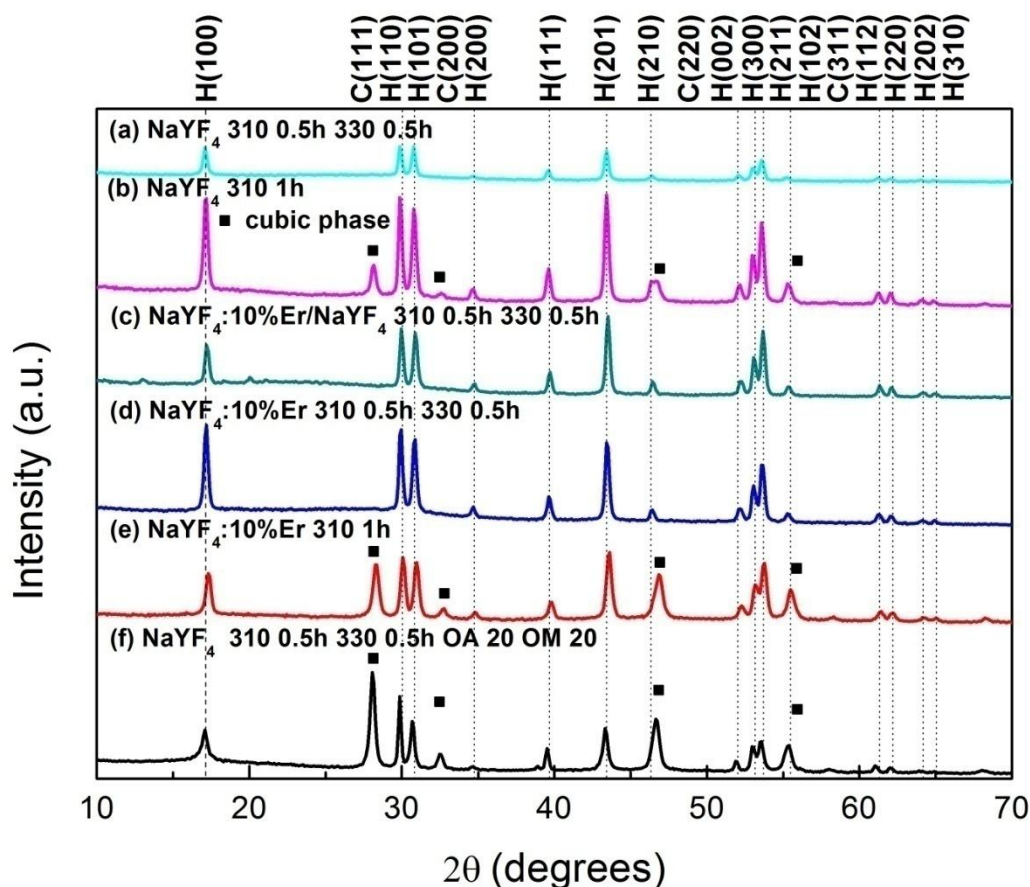


Fig. 4-4 XRD profiles of NaYF₄, NaYF₄:10%Er³⁺ and NaYF₄:10%Er³⁺/NaYF₄ NCs obtained under the OA/ODE=10/30 (mmol) with various temperatures. (f) Both α - and β - phase NaYF₄ was obtained with OA/OM=20/20 for reference. H(100) and C(111) are hexagonal-phase (100) peak and cubic-phase (111) peak, respectively.

Fig. 4-4(a), (d), (c) indicates that pure β -phase NaYF₄, NaYF₄:10%Er³⁺ and NaYF₄:10%Er³⁺/NaYF₄ have been obtained at 310 °C for 0.5 h following at 330 °C for 0.5 h with the OA/ODE ratio of 10/30. When the synthesis temperature was lower than 330 °C, corresponding β -phase NCs could not be obtained. From these results, the high temperature and the OA/ODE ratio (10/30) are key factors for the formation of pure β -phase NaYF₄ and NaYF₄:Er³⁺ NCs. Both α - and β - phase NaYF₄ was observed at 310 °C for 0.5 h following at 330 °C for 0.5 h with OA/OM=20/20.

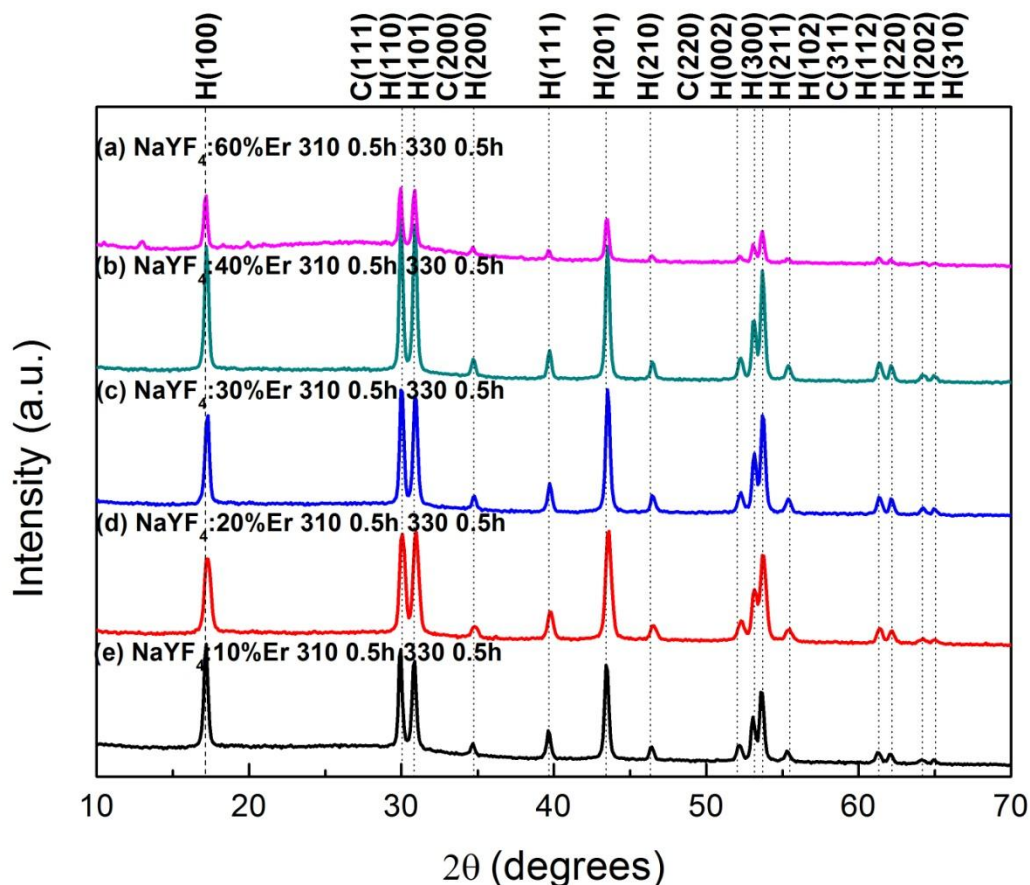


Fig. 4-5 XRD patterns of the NaYF₄:10%, 20%, 30%, 40%, 60% Er³⁺ NCs obtained after heating at 310 °C for 0.5 h following 330 °C for 0.5 h with the OA/ODE ratio of 10/30. H(100) and C(111) are hexagonal-phase (100) peak and cubic-phase (111) peak, respectively.

Fig. 4-5 shows the XRD pattern of NaYF₄ NCs doped with 10%, 20%, 30%, 40% and 60% Er³⁺, prepared at 310 °C for 0.5 h following 330 °C for 0.5 h with the OA/ODE ratio of 10/30. The XRD data demonstrated that the pure β -phase NaYF₄ NCs doped with 10~60% were obtained.

4.3.2. Morphology

The TEM image of NaYF₄: 20%Er³⁺ NCs prepared at 250 and 310 °C with OA/ODE=10/30 is shown in Fig. 4-6 (a) and (b). The XRD in fig. 4-3 (b) shows that the NaYF₄: 20%Er³⁺ NCs prepared at 310 °C was pure β -phase. Thus, β -phase NaYF₄: 20%Er³⁺ NCs had hexagonal shape with the side length of ranging from 47 to 58 nm. While α - phase NaYF₄: 20%Er³⁺ NCs had smaller size than that of β -phase. A size distribution of pure β -phase NaYF₄: 20%Er³⁺ obtained from the 200 pieces of NCs in TEM image, is demonstrated in Fig. 4-7. The dispersion of the crystal size was from 43 to 63 nm with the peak position of 52 nm. The mean size of pure β -phase NaYF₄: 20%Er³⁺ NCs calculated by XRD shown in fig. 4-3(b), using Scherrer's equation (3.2), was about 30 nm, which was roughly consistent with the result shown in fig. 4-7, considering the height of hexagonal nano-plate to be about 20 nm.

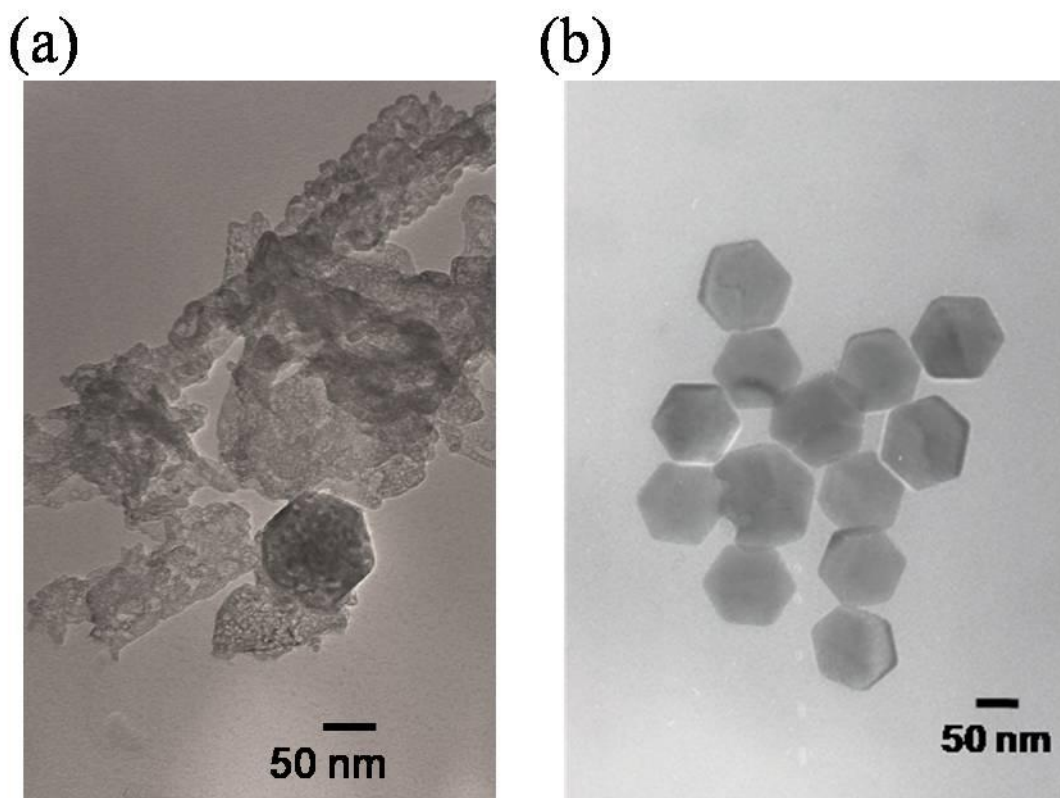


Fig. 4-6 TEM image of $\text{NaYF}_4: 20\% \text{Er}^{3+}$ NCs prepared under $\text{OA}/\text{ODE}=10/30$ at (a) 250 and (b) 310 °C.

It has been reported that the β -phase NaYF_4 was stable phase in higher temperature and the higher temperature was helpful to form the β -phase NaYF_4 compared with the α -phase [4-16]. In our case, pure β -phase NaErF_4 and NaYF_4 were separately obtained at 290 °C for 1 h and at 310 °C for 0.5 h following at 330 °C for 0.5 h. This different temperature for phase transition maybe stem from the different ionic radius of Er^{3+} and Y^{3+} [4-12], which results in different energy barrier from α - to β -phase transition. As mentioned above, the OA was used as ligand and/or termination of surface of NaYF_4 , and the OA had some effects on the crystal growth [4-13]. In various OA/OM ratios, the pure β -phase NaYF_4 were not obtained, in which OM was also used as ligand. In low OA concentration ($\text{OA}/\text{ODE}=10/30$), maybe a little OA bonding the NaReF_4 is beneficial to the growth of hexagonal nano-plate, which is the shape of β -phase NaReF_4 . In high OA concentration ($\text{OA}/\text{ODE}=30/10$), due to too much OA bonding the α -phase NaReF_4 , the growth rate is the same in all direction, resulting in difficult formation of hexagonal nano-plates. Therefore, the amount of OA should be minimum value which may be enough to terminate the surface dangling bonds. From these conditions, the optimum ratio of OA/ODE may be determined to be 10/30.

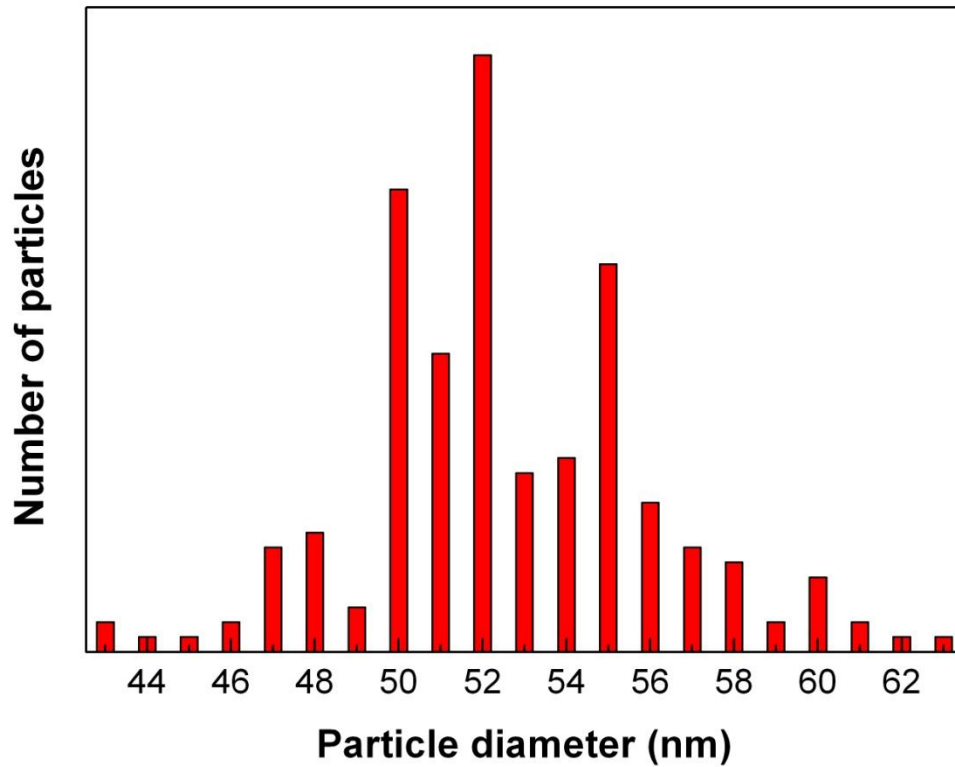


Fig. 4-7 Particle size distribution of pure β -phase $\text{NaYF}_4:20\%\text{Er}^{3+}$ obtained from 200 NCs in TEM image

4.3.3. Photoluminescence (PL) spectrum

Fig. 4-8 shows PL of cubic-phase (primary) and hexagonal-phase NaErF_4 excited at 532 nm (${}^4\text{I}_{15/2} \rightarrow {}^4\text{S}_{3/2}$) at room temperature. It was found that the PL of β -phase NaErF_4 had about 10 times enhancement of intensity compared to α -phase counterpart (primary). Fig. 4-9 shows PL of cubic-phase (primary), hexagonal-phase $\text{NaYF}_4:20\%\text{Er}^{3+}$ and hexagonal-phase NaErF_4 excited at 532 nm at room temperature. The results showed that the PL of β -phase $\text{NaYF}_4:20\%\text{Er}^{3+}$ demonstrated about 5 times enhancement compared to β -phase NaErF_4 and about 10 times enhancement compared to α -phase counterpart (primary). Thus, the highest PL intensity was β -phase $\text{NaYF}_4:20\%\text{Er}^{3+}$, compared to α -phase counterpart (primary), cubic-phase (primary) and hexagonal-phase NaErF_4 .

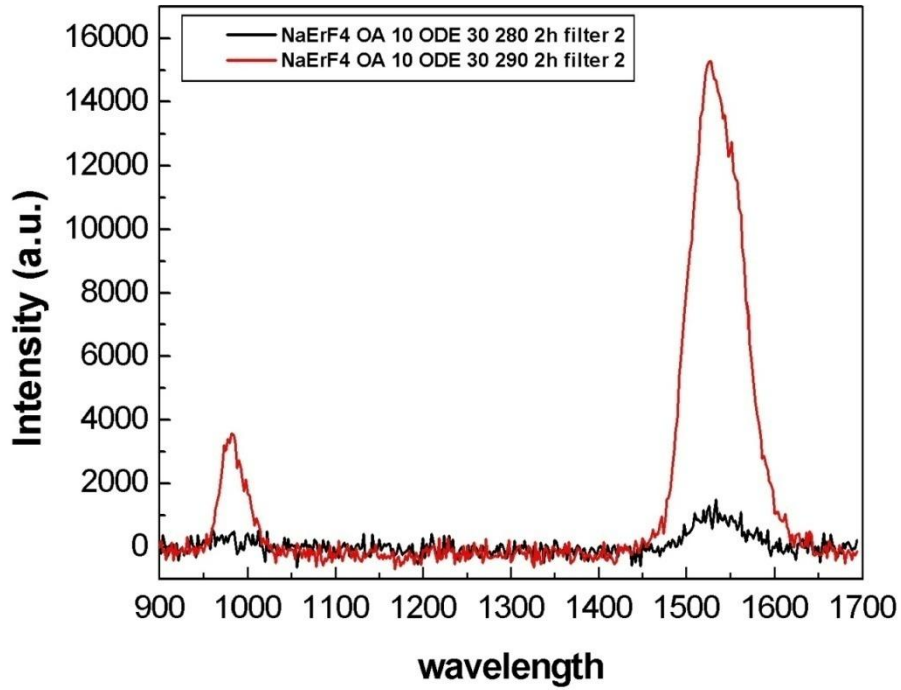


Fig. 4-8 PL of cubic-phase (primary) and hexagonal-phase NaErF₄ excited at 532 nm ($^4I_{15/2} \rightarrow ^4S_{3/2}$) at room temperature. (The absorption edge of the host NaYF₄ is about 155 nm.)

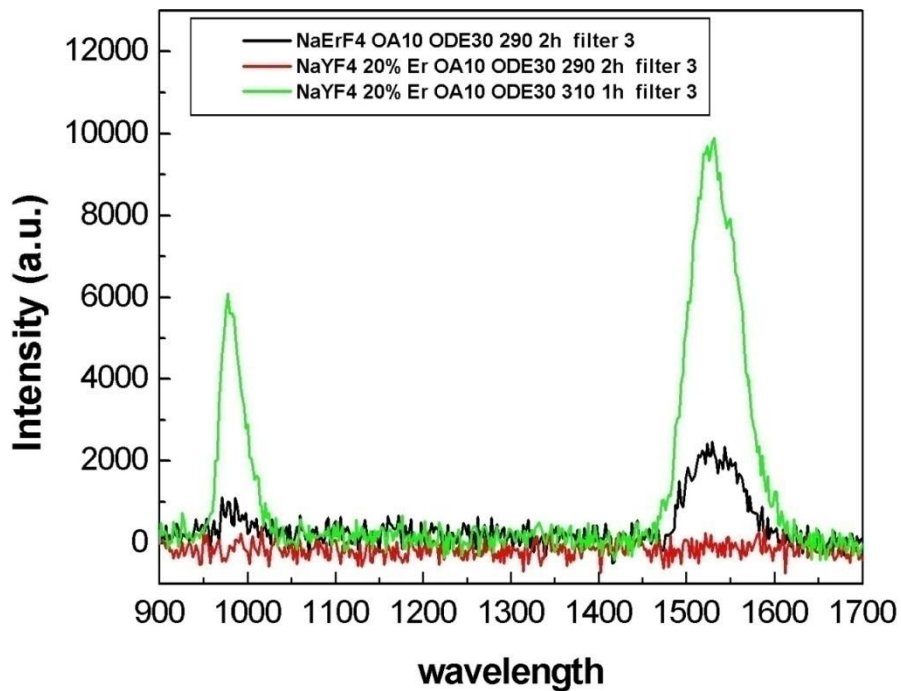


Fig. 4-9 PL of cubic-phase (primary), hexagonal-phase NaYF₄:20%Er³⁺ and hexagonal-phase NaErF₄ excited at 532 nm at room temperature.

4.3.4. UC emission spectrum

UC spectrum of α -phase (primary), β -phase NaYF₄: 20%Er³⁺ and β -phase NaErF₄ NCs, excited at 1550 nm, was dominated by four peaks at around 980 nm, 800 nm, 660 nm and 540 nm as shown in fig. 4-10. The pure β -phase NaYF₄: 20%Er³⁺ NCs had about one order of magnitude higher emission intensity than pure β -phase NaErF₄, which can be explained that in higher content of Er³⁺, the loss process, such as cross relaxation, may be increased [4-17]. Fig 4-11 shows the cross relaxation denoted as ${}^4I_{9/2} \rightarrow {}^4I_{13/2} \leftrightarrow {}^4I_{15/2} \rightarrow {}^4I_{13/2}$ [4-18]. Assuming that by an excitation at 980 nm, an electron can be excited to ${}^4I_{9/2}$. The excited electron in ${}^4I_{9/2}$ state could decay to ${}^4I_{13/2}$, and transfers this energy to the ground state, resulting in another electron excited to ${}^4I_{13/2}$ state through ${}^4I_{15/2} \rightarrow {}^4I_{13/2}$ transition. Thus, this cross relaxation leads to two electrons in ${}^4I_{13/2}$ state. At high doping levels, such cross relaxation will increase and the emission possibility corresponding to ${}^4I_{9/2} \rightarrow {}^4I_{15/2}$ transition in high excited state decreases. This cross relaxation process at high doping levels is denoted as concentration quenching.

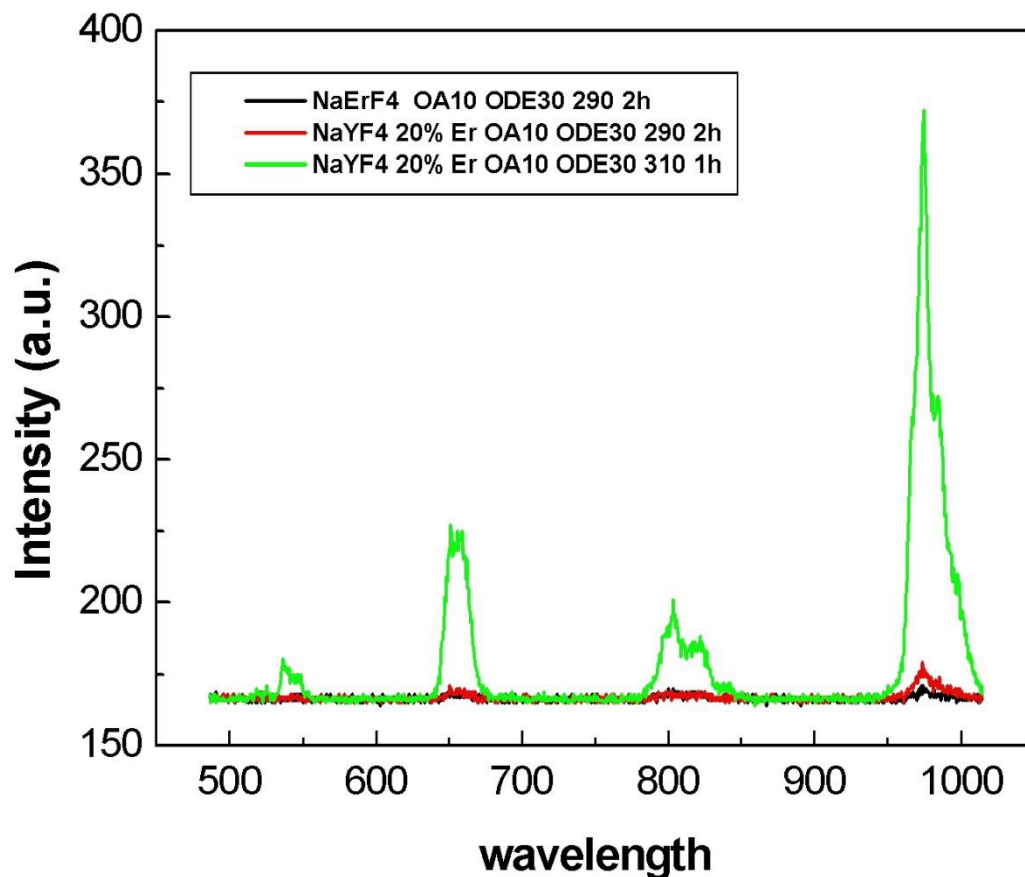


Fig. 4-10 UC spectrum of α -phase (primary), β -phase NaYF₄:20%Er³⁺ and β -phase NaErF₄ NCs, excited at 1550 nm.

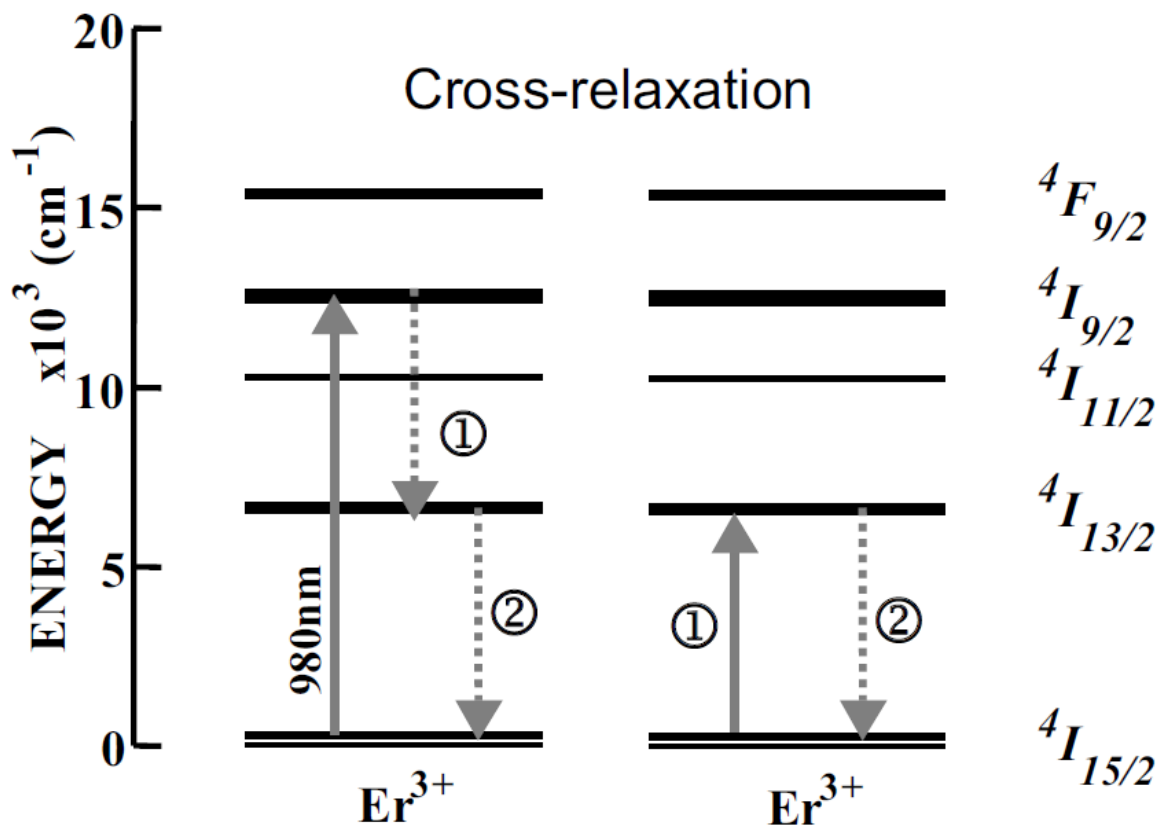


Fig. 4-11 The cross-relaxation process [4-18].

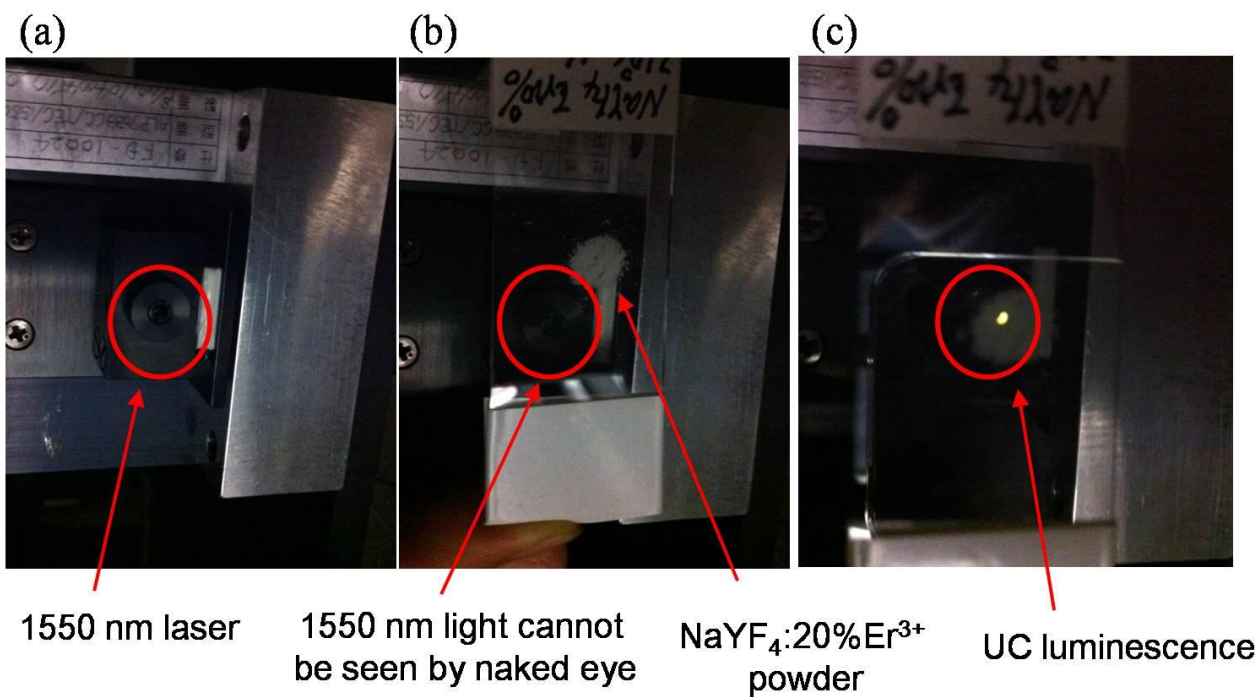


Fig. 4-12 Photography of the UC luminescence in hexagonal-phase NaYF₄:20%Er³⁺ excited at 1550 nm.

Fig. 4-12 shows photography of the UC luminescence in hexagonal-phase $\text{NaYF}_4:20\%\text{Er}^{3+}$ excited at 1550 nm. It was found that the color of UC emission was yellow, due to the visible UC emission peaks consisting of red (660 nm) and green (540 nm), as shown in fig. 4-10.

The excitation power dependence of the UC intensity for β -phase $\text{NaYF}_4:20\%\text{Er}^{3+}$, plotted by a double-logarithmic representation is illustrated in fig. 4-13. The slope n is the effective number of photons required to excite the UC related level. The slope n for 980 nm and 800 nm UC emissions were about 1.6 and 1.7, and for 660 nm and 540 nm emissions were about 2.3 and 2.2, respectively. Such n values indicated that the emission at 980 nm and 800 nm were generated by 2-step UC ($1 < n < 2$) and at 660 nm and 540 nm were 3-step UC ($2 < n < 3$).

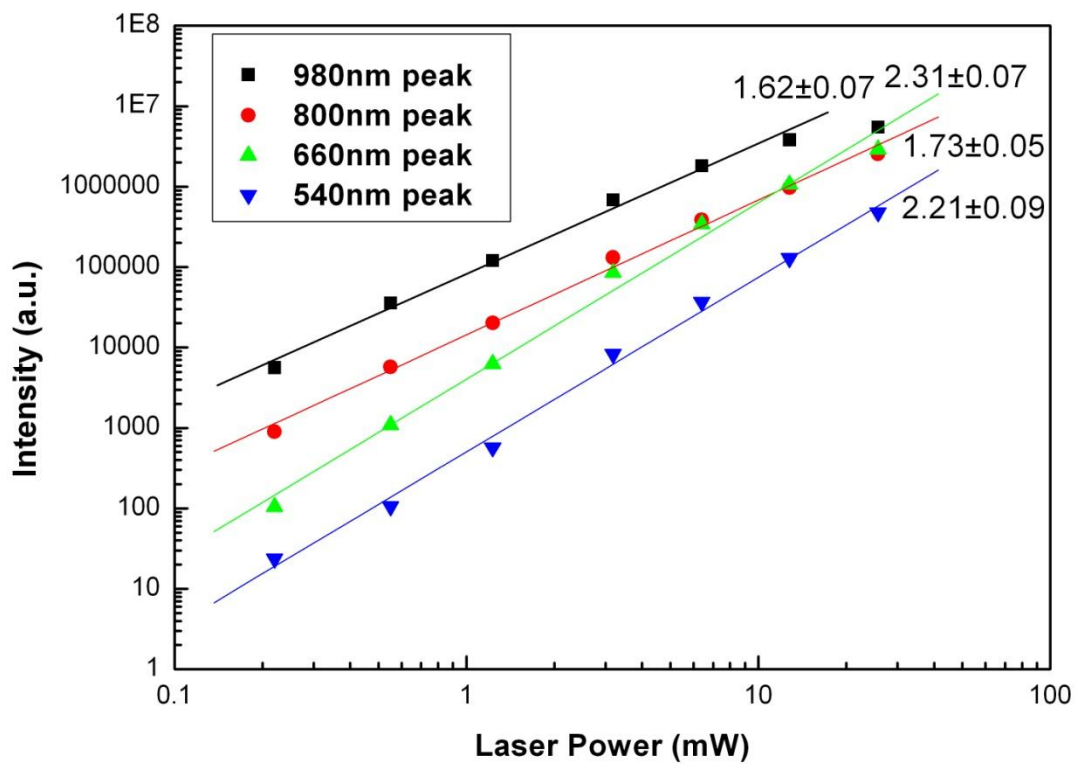


Fig. 4-13 Pump-power dependence for UC emission of pure β -phase $\text{NaYF}_4:20\%\text{Er}^{3+}$ prepared at 310 °C with OA/ODE=10/30.

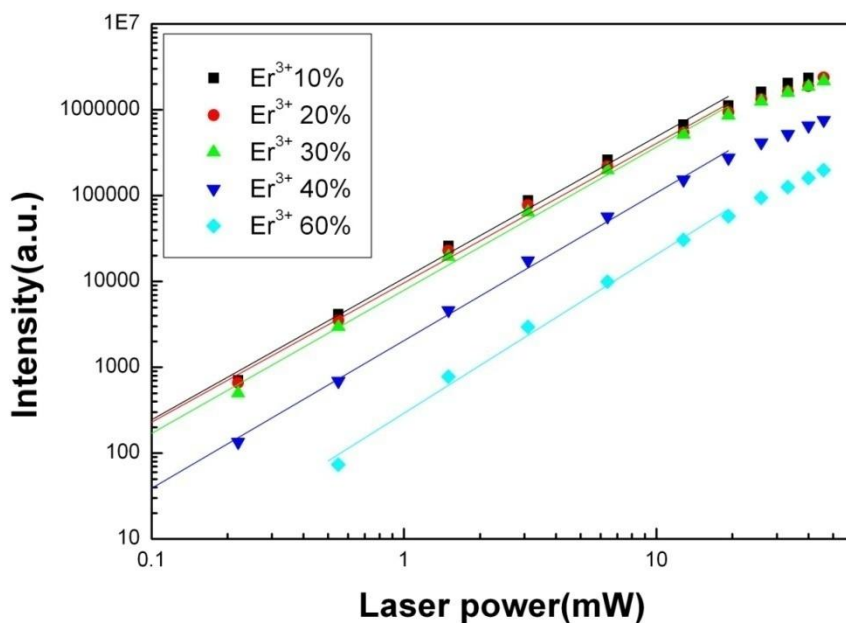


Fig. 4-14 Pump-power dependence for 980 nm UC emission of β -phase NaYF_4 :10%, 20%, 30%, 40%, 60% Er^{3+} NCs prepared at 310 °C for 0.5 h following 330 °C for 0.5 h with OA/ODE=10/30, excited at 1550 nm.

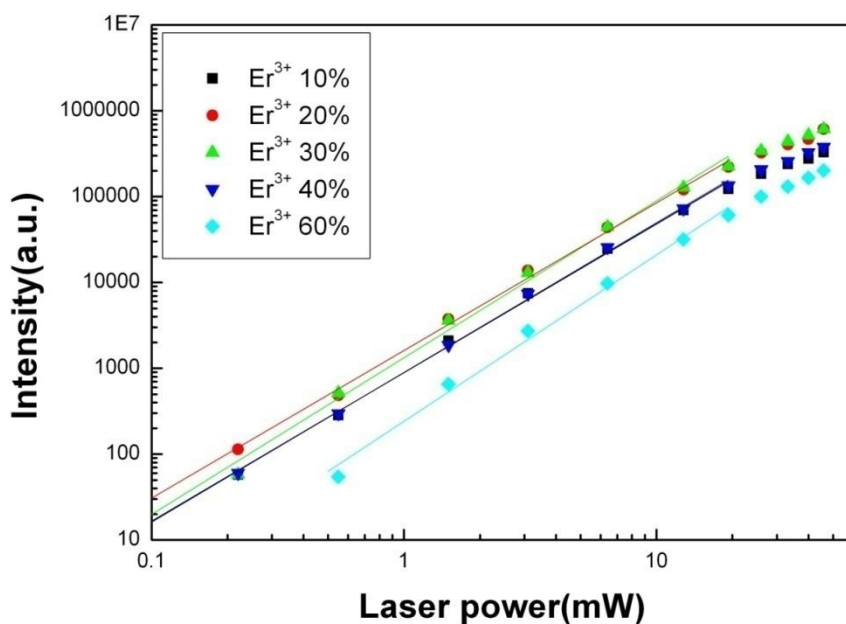


Fig. 4-15 Pump-power dependence for 800 nm UC emission of β -phase NaYF_4 :10%, 20%, 30%, 40%, 60% Er^{3+} NCs prepared at 310 °C for 0.5 h following 330 °C for 0.5 h with OA/ODE=10/30, excited at 1550 nm.

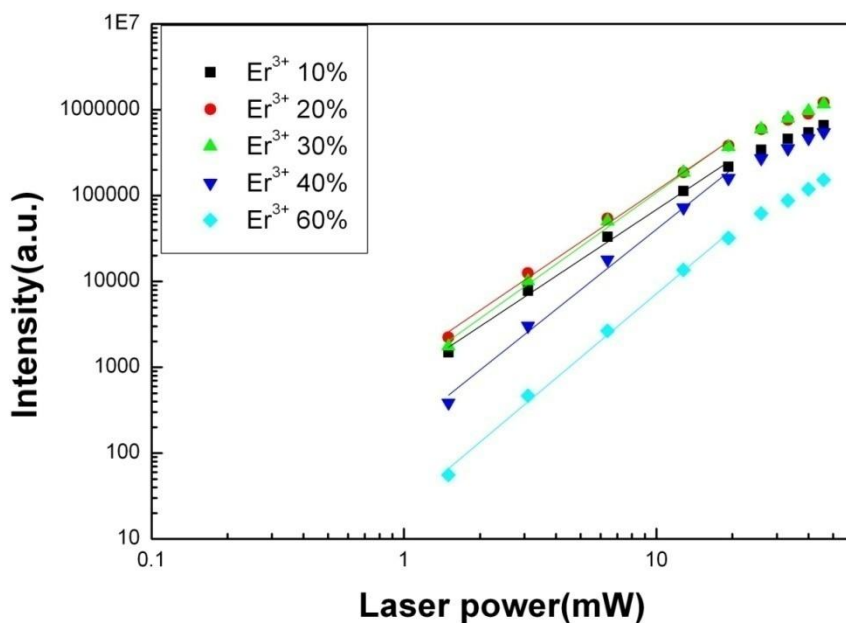


Fig. 4-16 Pump-power dependence for 660 nm UC emission of β -phase NaYF_4 :10%, 20%, 30%, 40%, 60% Er^{3+} NCs prepared at 310 °C for 0.5 h following 330 °C for 0.5 h with OA/ODE=10/30, excited at 1550 nm.

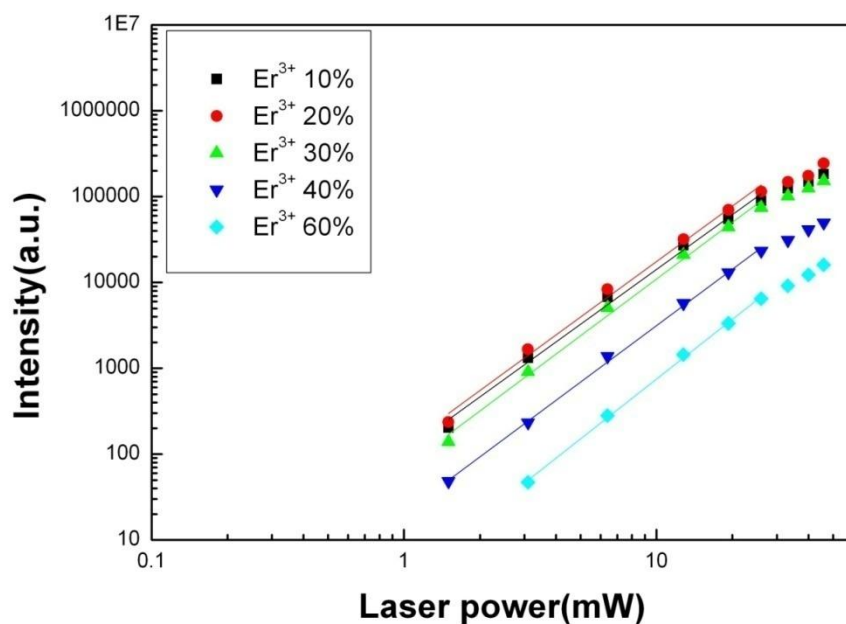


Fig. 4-17 Pump-power dependence for 540 nm UC emission of β -phase NaYF_4 :10%, 20%, 30%, 40%, 60% Er^{3+} NCs prepared at 310 °C for 0.5 h following 330 °C for 0.5 h with OA/ODE=10/30, excited at 1550 nm.

The excitation power dependence of UC emission at difference-peaks for β -phase NaYF₄:10%, 20%, 30%, 40%, 60% Er³⁺ NCs are illustrated in fig. 4-14, 4-15, 4-16, 4-17, plotted by a double-logarithmic representation. These figures showed linear power dependence in the region from 1.5 to 19.3mW for all four peaks. Slope n of all peaks decreased at high laser powers, which indicated a saturation effect in high excitation energy [4-19]. The NaYF₄ NCs with the Er³⁺ concentration of around 10~30% had relatively high intensity of UC emission for all four peaks. In higher doped Er³⁺ concentration, the loss process, such as cross relaxation, may be increased.

Table 4-1 shows the values of the slope n for 980 nm, 800 nm, 660 nm and 540 nm emissions of NaYF₄:10%, 20%, 30%, 40%, 60% Er³⁺ NCs. The n values for 980 nm and 800 nm emissions were about 1.7, and for 660 nm and 540 nm emissions were about 2.2, respectively. Such n values showed that the emission at 980 nm and 800 nm were generated by 2-step UC (n \approx 2) and at 660 nm and 540 nm were 3-step UC (n \approx 3). Compared to the n value of the 2-step UC and 3-step UC, it was found that higher excitation density preferred to increase 3-step UC rather than 2-step UC. Table 4-1 also demonstrates that the n value is strongly affected by the Er³⁺ concentration. The n value in higher Er³⁺ concentration was basically larger value than those in lower Er³⁺ concentration.

	980nm	800nm	660nm	540nm
10%Er³⁺	1.7	1.7	2.0	2.1
20%Er³⁺	1.6	1.7	2.0	2.1
30%Er³⁺	1.7	1.8	2.1	2.2
40%Er³⁺	1.7	1.7	2.3	2.2
60%Er³⁺	1.8	1.9	2.5	2.3

Table 4-1. The slope n for 980nm, 800nm, 660nm and 540nm emissions.

From the power dependence results combined with two major UC process models, those are, energy transfer up-conversion (ETU) and ground state absorption followed by excited state absorption (GSA/ESA), it may be possible to discuss the UC optical process. Energy level diagram and related transitions are demonstrated in Fig. 4-18. The optical process for the luminescence observed in fig. 4-10 may be considered as follows. By an excitation with the light wavelength of 1550nm, the ground state of Er³⁺ (⁴I_{15/2}) would be excited to ⁴I_{13/2}, and by the subsequent excitation, the transition from ⁴I_{13/2} to ⁴I_{9/2} would take place by ESA1 or ETU1 processes. Then the light emission with the wavelength of 800 nm originating from ⁴I_{9/2}→⁴I_{15/2} transition of Er³⁺ occurs. Some of electrons at ⁴I_{9/2} would be non-radiatively relaxed to ⁴I_{11/2} resulting in the generation of 980 nm emission which can be assigned as ⁴I_{11/2}→⁴I_{15/2} transition. The generation of the green emission at 540 nm (Er³⁺: ⁴S_{3/2}→⁴I_{15/2}) can be interpreted as another subsequent excitation of ⁴I_{9/2}→⁴S_{3/2} transition. The red emission at 660 nm (Er³⁺: ⁴F_{9/2}→⁴I_{15/2}) occurs through the ⁴S_{3/2}→⁴F_{9/2} relaxation or ⁴I_{11/2}→⁴F_{9/2} transition. Thus there are two optical passes to form ⁴F_{9/2} excited state.

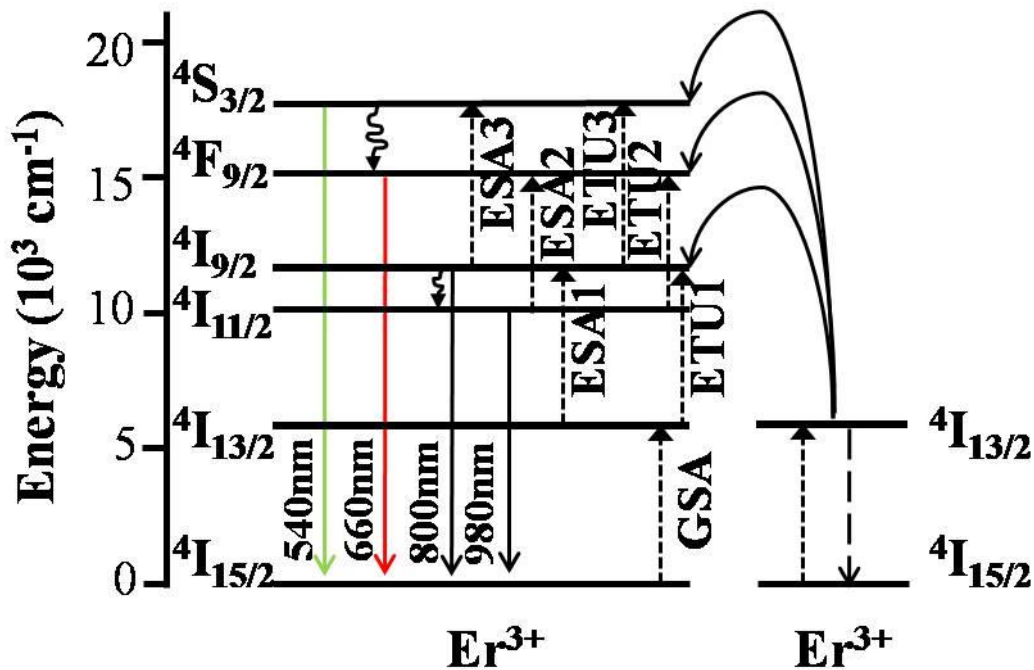


Fig. 4-18 Energy level diagram showing the optical process of up-conversion in $\text{NaYF}_4:\text{Er}^{3+}$. (Excitation photons, energy transfers, radiative and multiphonon processes are depicted in dotted, dashed, full and curly lines, respectively.)

These have been many reports on UC emission excited by the light wavelength about 980 nm [4-20]. In that case, the intensity of the green emission at 540 nm was stronger than that of the red emission at 660 nm for NaYF_4 doped Er^{3+} with low content, due to the 2-step process ${}^4\text{I}_{15/2} \rightarrow {}^4\text{I}_{11/2} \rightarrow {}^4\text{S}_{3/2}$. In our case, the UC emission demonstrated higher red than green emission. The result means that the non-radiative relaxation from ${}^4\text{S}_{3/2}$ to ${}^4\text{F}_{9/2}$ is not so significant, therefore, dominant excitation process to ${}^4\text{F}_{9/2}$ using the light wavelength of 1550 nm can be determined as not through the ${}^4\text{S}_{3/2}$ but from ${}^4\text{I}_{11/2}$.

4.3.5. Core/shell $\text{NaYF}_4:\text{Er}^{3+}/\text{NaYF}_4$ NCs

A TEM image of β -phase $\text{NaYF}_4:10\%\text{Er}^{3+}/\text{NaYF}_4$ NCs is shown in fig. 4-19. The NCs were seen to have a hexagonal shape with a diameter of around 65 nm, which was larger than the size of no shell NCs, shown in fig. 4-7.

Fig. 4-20 shows UC spectrum of β -phase $\text{NaYF}_4:10\%\text{Er}^{3+}$ and $\text{NaYF}_4:10\%\text{Er}^{3+}/\text{NaYF}_4$ core/shell NCs excited at 1550 nm. The UC enhancement of $\text{NaYF}_4:10\%\text{Er}^{3+}/\text{NaYF}_4$ core/shell NCs was 3-times compared to non-shell $\text{NaYF}_4:10\%\text{Er}^{3+}$ NCs. This enhancement may be ascribed to the NaYF_4 shell which can reduce the fluorescence quenching on NCs surface resulting from the organic surfactant [4-15].

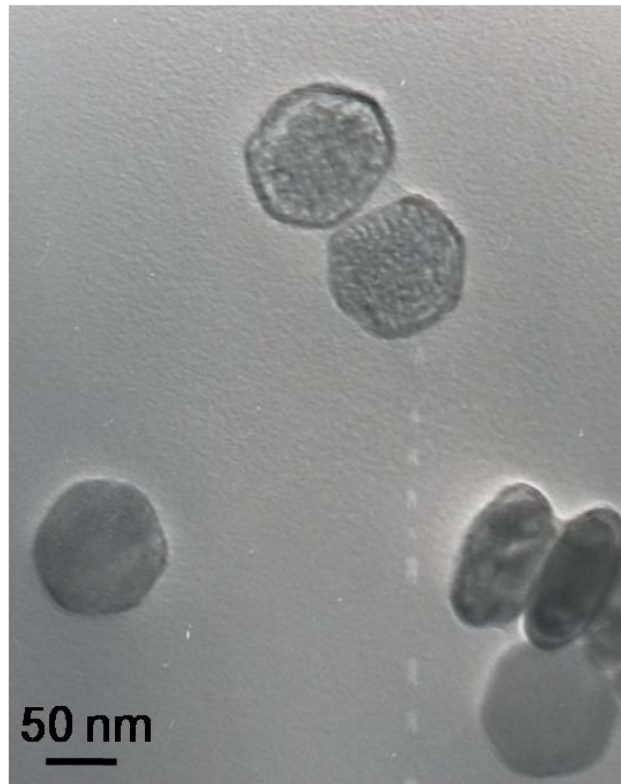


Fig. 4-19 TEM image of NaYF₄:10%Er³⁺/NaYF₄ NCs

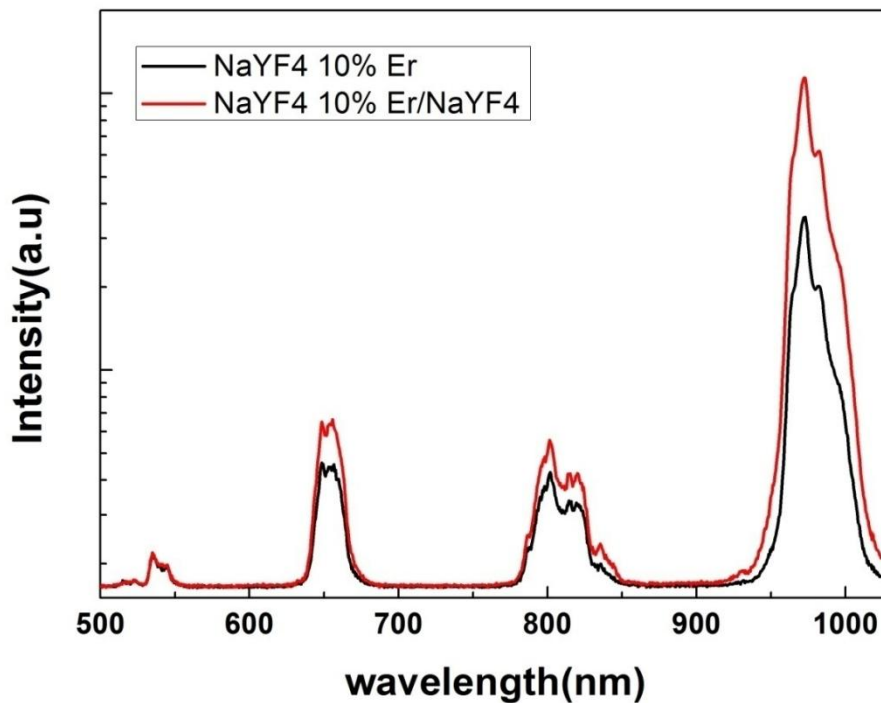


Fig. 4-20 UC spectrum of β -phase NaYF₄:10%Er³⁺ and NaYF₄:10%Er³⁺/NaYF₄ core/shell NCs excited at 1550 nm.

4.4. Summary

A user-friendly and facile synthesis method was developed for pure β -phase NaErF_4 , NaYF_4 , $\text{NaYF}_4:\text{Er}^{3+}$ and $\text{NaYF}_4:10\%\text{Er}^{3+}/\text{NaYF}_4$ core/shell NCs. These samples can be fabricated by controlling the temperature and the molar ratio of OA/ODE during synthesis. The UC emission spectra of β -phase NaErF_4 , $\text{NaYF}_4:\text{Er}^{3+}$ and core/shell NCs, excited at 1550 nm, showed four peaks at about 980 nm, 800 nm, 660 nm and 540 nm. 3 times UC enhancement was achieved by coating the core with NaYF_4 shell, compared to $\text{NaYF}_4:10\%\text{Er}^{3+}$ core NCs. The pure β -phase $\text{NaYF}_4:20\%\text{Er}^{3+}$ NCs had about one order of magnitude higher emission intensity than the pure β -phase NaErF_4 . The values of the slope n in pump-power dependence of UC emission intensity confirmed that 980 nm, 800 nm emission were 2-step UC, and 660 nm, 540 nm emission were 3-step UC. From the UC emission of all peaks, it was found the optimum Er^{3+} concentration for 2-step and 3-step UC was around 10~30%. It was also found that higher laser power preferred to increase 3-step UC. Main optical process for each UC was determined.

4.5. Chapter 4 references

- [4-1] C. Strumpel, M. McCann, G. Beaucarne, V. Arkhipov, A. Slaoui, V. Svrcek, C. del Canizo, I. Tobias, Modifying the solar spectrum to enhance silicon solar cell efficiency—An overview of available materials. *Solar Energy Materials and solar cells* 91 (2007) 238-249.
- [4-2] C. Atre Ashwin, A. Dionne Jennifer, Realistic upconverter-enhanced solar cells with non-ideal absorption and recombination efficiencies. *J. Appl. Phys.* 110 (2011) 034505.
- [4-3] J. C. G. Bunzli; S. V. Eliseeva, Lanthanide NIR luminescence for telecommunications, bioanalyses and solar energy conversion. *Journal of Rare Earths* 28 (2010) 824.
- [4-4] F. Wang and X. G. Liu, Recent advances in the chemistry of lanthanide-doped upconversion nanocrystals. *Chemical Society Reviews* 38 (2009) 976.
- [4-5] Z. Q. Li, Y. Zhang, S. Jiang, Multi-color core/shell-structured upconversion fluorescent nanoparticles. *Advanced Materials*, 20 (2008) 4765.
- [4-6] E. Downing, L. Hesselink, J. Ralston, R. Macfarlane, A three-color, solid-state, three-dimensional display. *Science* 273 (1996) 1185–1189.
- [4-7] F. Wang, Y. Han, C. S. Lim, Y. H. Lu, J. Wang, J. Xu, H. Y. Chen, C. Zhang, M. H. Hong, X. G. Liu, Simultaneous phase and size control of upconversion nanocrystals through lanthanide doping. *Nature*, 463 (2010) 1061.
- [4-8] F. Vetrone , R. Naccache , A. Zamarron , A. Juarranz de la Fuente , F. Sanz-Rodriguez , L. Martinez Maestro , E. Martin Rodriguez , D. Jaque , J. Garcia Sole , J. A. Capobianco , Temperature sensing using fluorescent nanothermometers. *ACS Nano* 4(6) (2010) 3254.
- [4-9] Quintanilla Marta, Cantelar Eugenio, Cusso Fernando, Villegas Marina Caballero Amador C, Temperature Sensing with Up-Converting Submicron-Sized $\text{LiNbO}_3:\text{Er}^{3+}/\text{Yb}^{3+}$ Particles. *Applied Physics Express*, 4 (2011) 022601.
- [4-10] X.P. Chen, W.J. Zhang, Q.Y. Zhang, *Physica B: Condensed Matter* 406 (2011) 1248.
- [4-11] H. Schafer, P. Ptacek, H. Eickmeier, M. Haase, *Adv. Funct. Mater.* 19 (2009) 3091.
- [4-12] H.X. Mai, Y.W. Zhang, R. Si, Z.G. Yan, L.D. Sun, L.P. You, C.H. Yan, *J. Am. Chem. Soc.* 128 (2006) 6426.
- [4-13] Z.Q. Li, Y. Zhang, *Nanotechnology* 19 (2008) 345606.
- [4-14] S. Liang, Y. Liu, Y. Tang, Y. Xie, H.Z. Sun, H. Zhang, B. Yang, *J. Nanomater.* 2011 (2011) 302364.
- [4-15] Y.G. Shun and G.M. Chow, *Chem. Mater.* 19 (3) (2007) 341–343.
- [4-16] F. Zhang, J. Li, J. Shan, L. Xu, D.Y. Zhao, *Chem. Eur. J.* 15 (2009) 11010.
- [4-17] T.M. Kozhan, V.V. Kuznetsova, I.I. Sergeev, Y.P. Timofeev, V.S. Khomenko, M. Chau, *J. Appl. Spectrosc.* 61 (1994) 500.
- [4-18] Avi Shalav, Thesis: Rare-earth Doped Up-converting Phosphors for an Enhanced Silicon Solar Cell Response, University of New South Wales, (2006).
- [4-19] M. Pollnau, D. R. Gamelin, S. R. Luthi, H. U. Gudel and M. P. Hehlen, *Physical Review B* 61 (2000) 3337.
- [4-20] J. F. Suyver, J. Grimm, M.K. Van Veen, D. Biner, K.W. Kramer, H.U. Gudel, *J. Lumin.* 117 (2006) 1.

Chapter 5. UC properties in β -phase $\text{NaYF}_4:\text{Er}^{3+}/\text{NaYF}_4$ NCs by off-resonant excitation

5.1. Introduction

There have been several reports regarding the UC properties of $\text{NaYF}_4:\text{Er}^{3+}$ for solar-cell applications, in which the excitation energy corresponds to the energy of the lowest f-f transition of Er^{3+} ($^4\text{I}_{15/2} \rightarrow ^4\text{I}_{13/2}$), that is, resonant excitation [5-1][5-2]. In order to effectively utilize the broad solar spectrum, however, the UC properties for off-resonant excitation should also be clarified [5-3]. It has recently been reported that higher UC efficiencies have been obtained under concentrated broad spectrum illumination, compared to those under resonant excitation, although the reason for this is as yet unknown [5-4]. To resolve this issue, it is necessary to form a clear understanding of the UC optical process during off-resonant excitation.

In this work, we studied the UC optical process in the hexagonal phase of $\text{NaYF}_4:10\%\text{Er}^{3+}/\text{NaYF}_4$ core/shell NCs using off-resonant excitation at 1620 nm. After absorption spectrum, Raman spectrum and the temperature and power dependence of the UC emission were measured, the UC optical process was determined.

5.2. Experimental

The hexagonal phase of $\text{NaYF}_4:10\%\text{Er}^{3+}/\text{NaYF}_4$ core/shell nanocrystals (NCs) were prepared by using the method mentioned at chapter 4. UC emission spectrum was measured using a Seki Technotron spectrometer at a laser wavelength at 1620 nm. Absorption spectrum was collected using a Jasco V-670 spectrometer. Raman spectrum and the power and temperature dependence of the UC emission were measured using a Nanofinder 30 microscopy system with 532, 1620 and 1550 nm excitation, respectively.

5.3. Results and discussions

5.3.1. UC emission spectrum

Fig. 5-1 shows a UC emission spectrum for $\text{NaYF}_4:10\%\text{Er}^{3+}/\text{NaYF}_4$ NCs produced by off-resonant excitation at 1620 nm. The spectrum could be seen to have five prominent peaks at around 1540, 980, 800, 660 and 540 nm, corresponding to transitions from the $^4\text{I}_{13/2}$, $^4\text{I}_{11/2}$, $^4\text{I}_{9/2}$, $^4\text{F}_{9/2}$ and $^4\text{S}_{3/2}$ states to the $^4\text{I}_{15/2}$ ground state of Er^{3+}

ions, respectively. The green emission around 540 nm could be seen by the naked eye. Thus, UC emission can be obtained even using off-resonant excitation at 1620 nm.

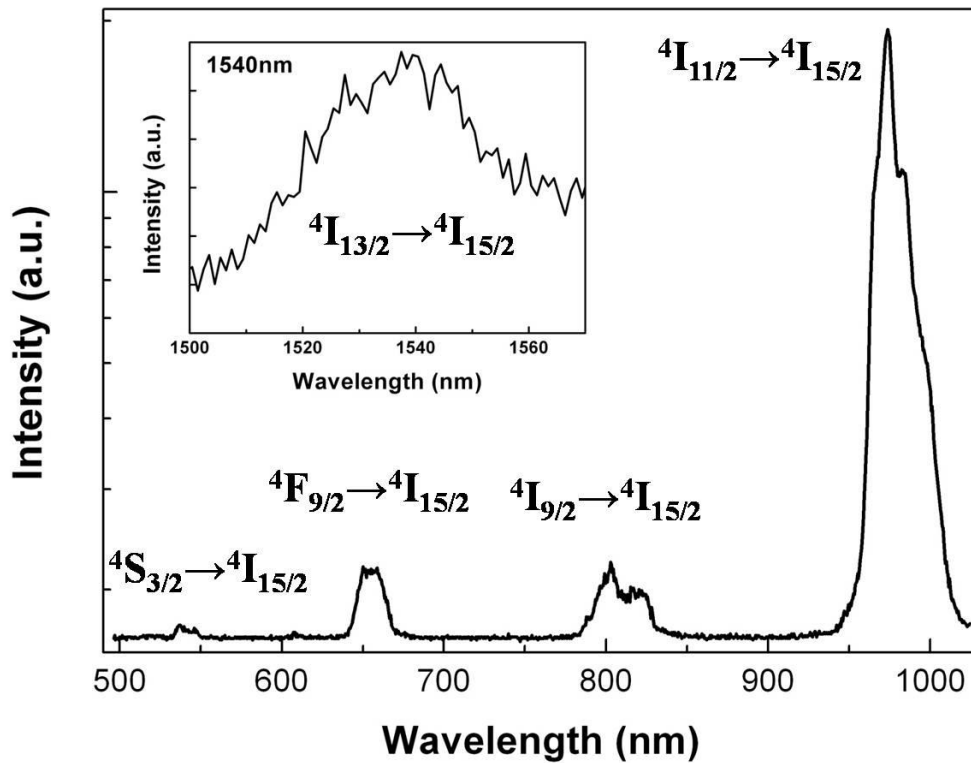


Fig. 5-1 UC spectrum for NaYF₄:10%Er³⁺/NaYF₄ NCs at room temperature under off-resonant excitation at 1620 nm.

5.3.2. Absorption and Raman spectrum

To investigate the cause of the off-resonant excitation, optical absorption and Raman spectra were measured. The optical absorption spectrum in the range 1450 to 1650 nm for NaYF₄:10%Er³⁺/NaYF₄ NCs is shown in fig. 5-2. Two absorption peaks can be observed at 1523 and 1599 nm, the former of which can be assigned to the $^4I_{15/2} \rightarrow ^4I_{13/2}$ transition of Er³⁺. The energy difference between the two peaks was about 315 cm⁻¹. The Raman spectrum for NaYF₄:10%Er³⁺/NaYF₄ NCs is shown in fig. 5-3. The peaks denoted as 1, 2, and 3 can be ascribed to vibrational modes of NaYF₄ [5-5]. As seen in fig. 5-3, the average energy of these vibrational modes for NaYF₄:10%Er³⁺/NaYF₄ NCs was around 300 cm⁻¹, which was roughly the same as the peak separation energy in the absorption spectrum shown in fig. 5-2. Therefore, the absorption peak at 1599 nm in fig. 5-2 can be considered to correspond to phonon-assisted absorption [5-11].

In the UC measurements, off-resonant and resonant excitations were carried out using excitation light wa-

wavelengths of 1620 and 1550 nm, respectively. The energy difference between these two excitation wavelengths is 280 cm^{-1} , which is almost the same as the vibrational energy of NaYF_4 , as shown in fig. 5-3. From these results, it can be concluded that the UC emission produced by off-resonant excitation shown in fig. 5-1 was the result of phonon-assisted excitation. According to the report by Shan et al., the peaks denoted as 4-6 in fig. 5-3 can be ascribed to the vibrational modes of organic surfactants [5-7].

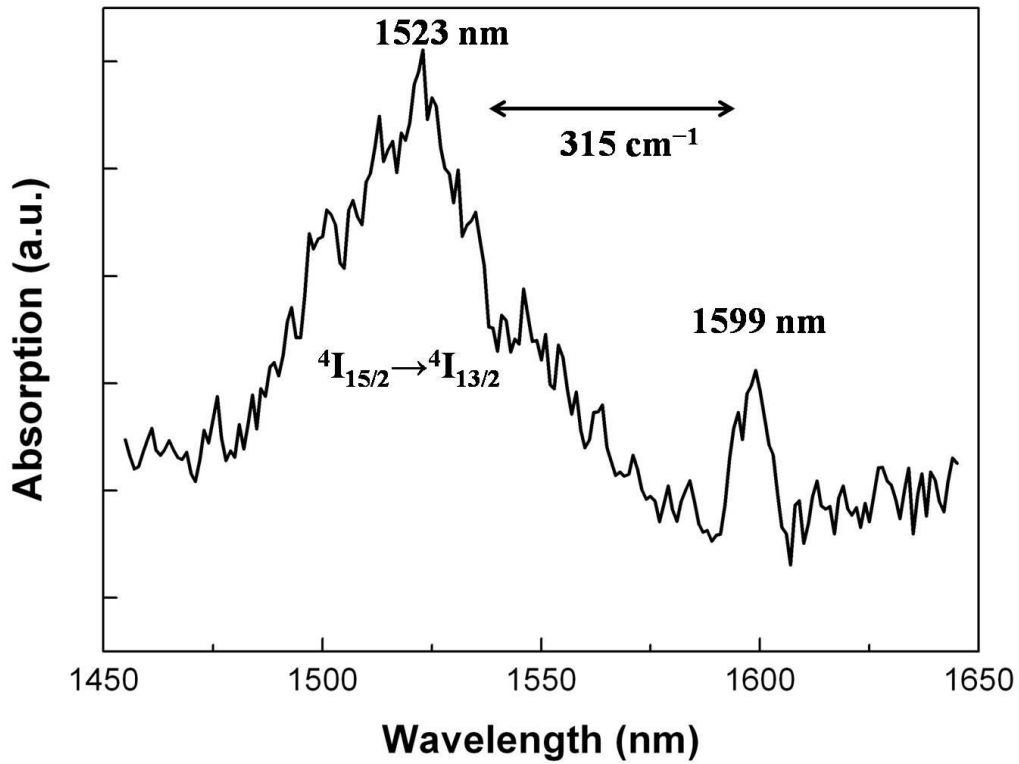


Fig. 5-2 Absorption spectrum for $\text{NaYF}_4:10\%\text{Er}^{3+}/\text{NaYF}_4$ NCs at room temperature in the infrared region.

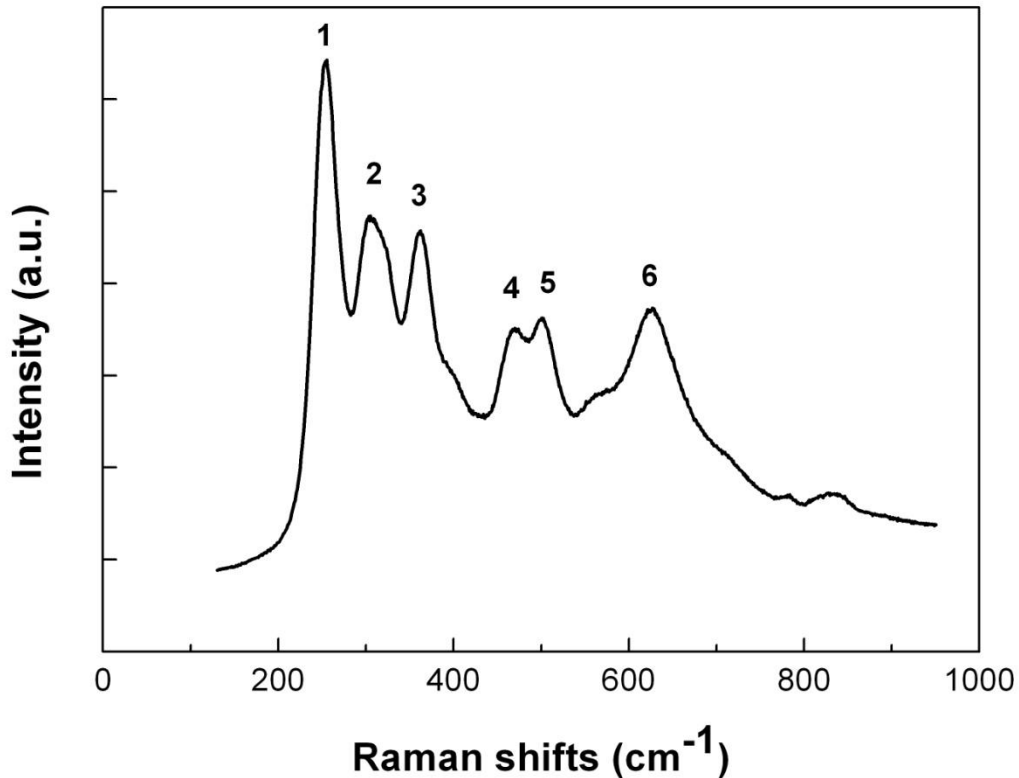


Fig. 5-3 Raman spectrum for NaYF₄:10%Er³⁺/NaYF₄ NCs at room temperature under 532 nm excitation.

5.3.3. UC Temperature dependence

The temperature dependence of the UC emission intensity under off-resonant excitation at 1620 nm is shown in fig. 5-4. The intensity at 980 nm was seen to increase by two orders of magnitude when the temperature was changed from 80 to 360 K. Such a strong temperature dependence is reasonable considering an optical process that involves phonon-assisted transitions. As far as we are aware, this is the highest UC enhancement obtained through thermal effects [5-8][5-9]. From fig. 5-4, it can also be seen that the emission intensity at 800 and 660 nm increased from 80 to 240 K and then decreased from 240 to 360 K. This can be interpreted by the competition between the thermally enhanced phonon-assisted absorption, which increases the UC efficiency by improving the possibility of the transition from ⁴I_{15/2} to ⁴I_{13/2} of Er³⁺, and temperature increased non-radiative decay rates, which decreases the radiative emission, such as ⁴F_{9/2} or ⁴I_{9/2} to ⁴I_{15/2} transition [5-8]. Thus, for the UC emission at 800 and 660 nm, the effect of thermally enhanced phonon-assisted absorption was dominant from 80 to 240 K, and the impact of temperature increased non-radiative decay rates became ascendant from 240 to 360 K. No obvious change in UC emission intensity at 980 nm from 240 to 360 K was observed, maybe since at low Er³⁺ ion doped host crystals, non-radiative decay rates decreased exponentially with the corresponding energy gap, ΔE, between the two energy levels of Er³⁺ and the ΔE from ⁴I_{11/2} to the next lower-lying state, that was 3710 cm⁻¹, was larger than that from ⁴F_{9/2} and ⁴I_{9/2} to the next lower-lying state

[5-10].

For comparison, the temperature dependence of the UC emission intensity under resonant excitation at 1550 nm was also examined. As shown in fig. 5-5, the intensity at 980 nm increased by only a factor of 4 in the temperature range 80 to 360 K. These results indicated that the UC intensity under off-resonant excitation at 1620 nm had a much stronger temperature dependence than that under resonant excitation at 1550 nm. This was consistent with the proposed model in which the off-resonant excitation involved phonon-assisted transitions.

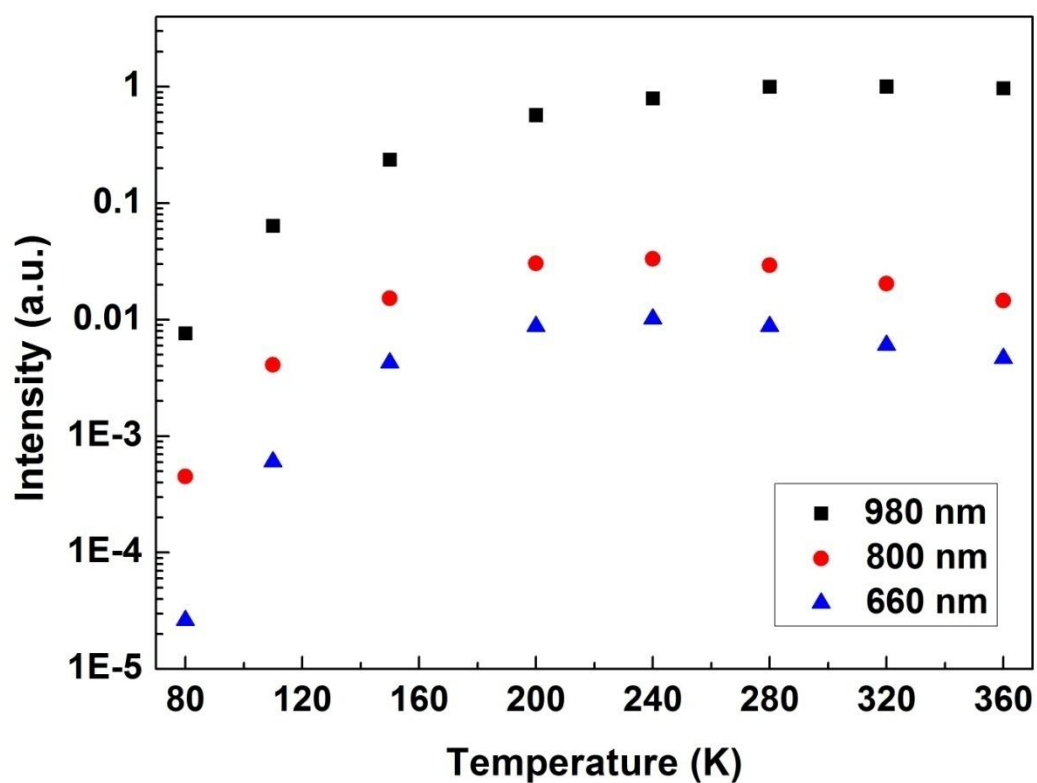


Fig. 5-4 Temperature dependence of UC emission intensity for NaYF₄:10%Er³⁺/NaYF₄ NCs excited at 1620 nm.

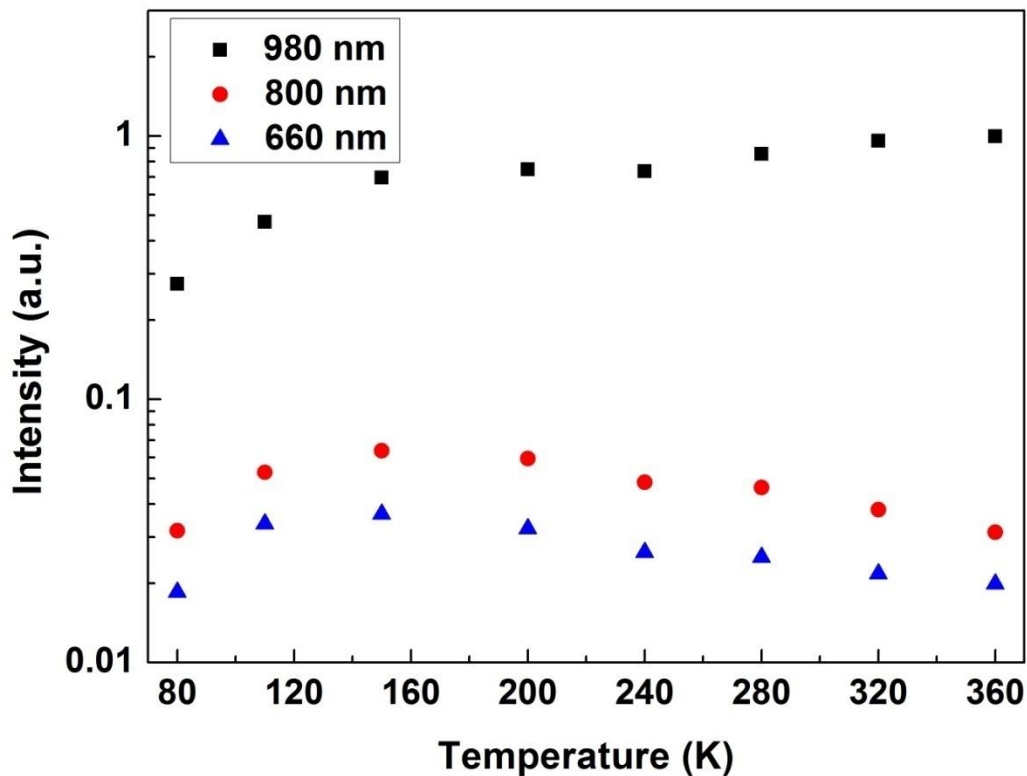


Fig. 5-5 Temperature dependence of UC emission intensity for NaYF₄:10%Er³⁺/NaYF₄ NCs excited at 1550 nm.

5.3.4. UC power dependence and optical process

The excitation power dependence of the UC intensity for NaYF₄:10%Er³⁺/NaYF₄ NCs under 1620-nm excitation is plotted in fig. 5-6 on a log-log scale. The slope n represents the effective number of photons required to produce one UC emission photon. The n values for the emissions at 1540, 980, 800 and 660 nm were determined to be about 0.71, 1.73, 1.83 and 2.36, respectively. This indicated that the emission at 1540 nm was generated by 1-photon absorption ($n < 1$), those at 980 and 800 nm by 2-step UC ($1 < n < 2$) and that at 660 nm by 3-step UC ($2 < n < 3$).

The above results, in combination with the two major UC process models, energy transfer upconversion, and ground state absorption followed by excited state absorption, allow the UC optical process to be discussed [5-11]. fig. 5-7 shows the energy level diagram and the relevant transitions. The optical process that gives rise to the UC emission spectrum in fig. 5-1 is considered to be the following. Due to excitation at 1620 nm together with phonon absorption, emission at 1540 nm (Er³⁺: $^4I_{13/2} \rightarrow ^4I_{15/2}$) occurs. Subsequent excitation causes a transition from $^4I_{13/2}$ to $^4I_{9/2}$ to take place. This leads to light emission at 800 and 980 nm, due to the $^4I_{9/2} \rightarrow ^4I_{15/2}$ and $^4I_{11/2} \rightarrow ^4I_{15/2}$ transitions, respectively. The green emission at 540 nm arises from further excita-

tion that induces the ${}^4I_{9/2} \rightarrow {}^4S_{3/2}$ transition, followed by the ${}^4S_{3/2} \rightarrow {}^4I_{15/2}$ transition. The red emission at 660 nm ($\text{Er}^{3+}: {}^4F_{9/2} \rightarrow {}^4I_{15/2}$) occurs through the ${}^4S_{3/2} \rightarrow {}^4F_{9/2}$ relaxation or ${}^4I_{11/2} \rightarrow {}^4F_{9/2}$ transition, which shows that there are two optical paths for producing the ${}^4F_{9/2}$ excited state.

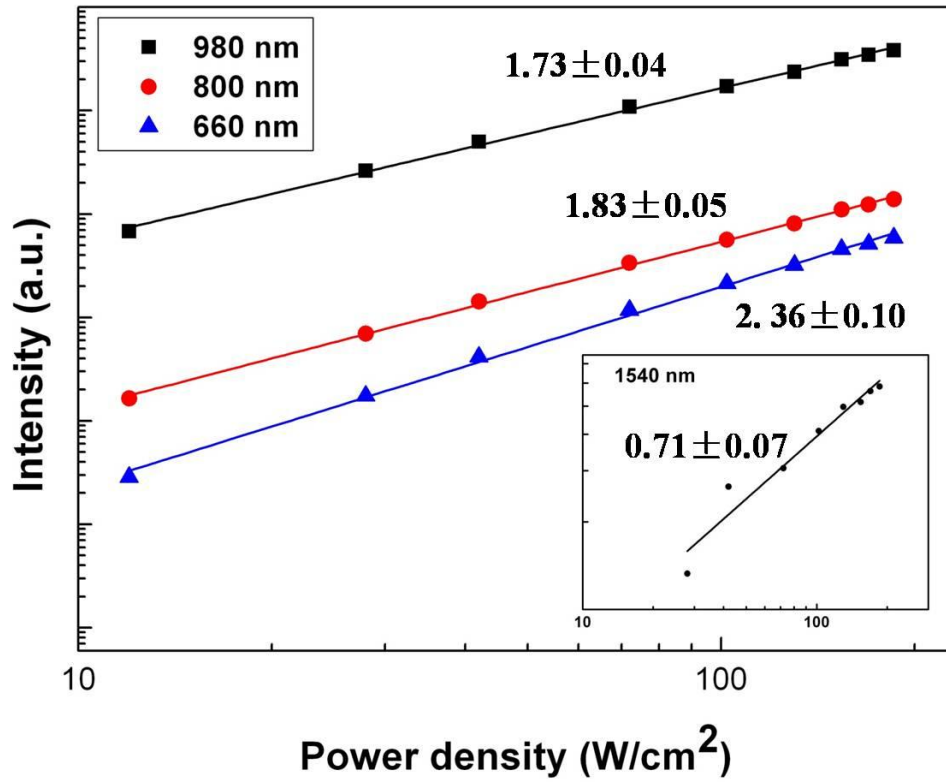


Fig. 5-6 Pump-power dependence of UC emission intensity for $\text{NaYF}_4:10\% \text{Er}^{3+}/\text{NaYF}_4$ NCs excited at 1620 nm.

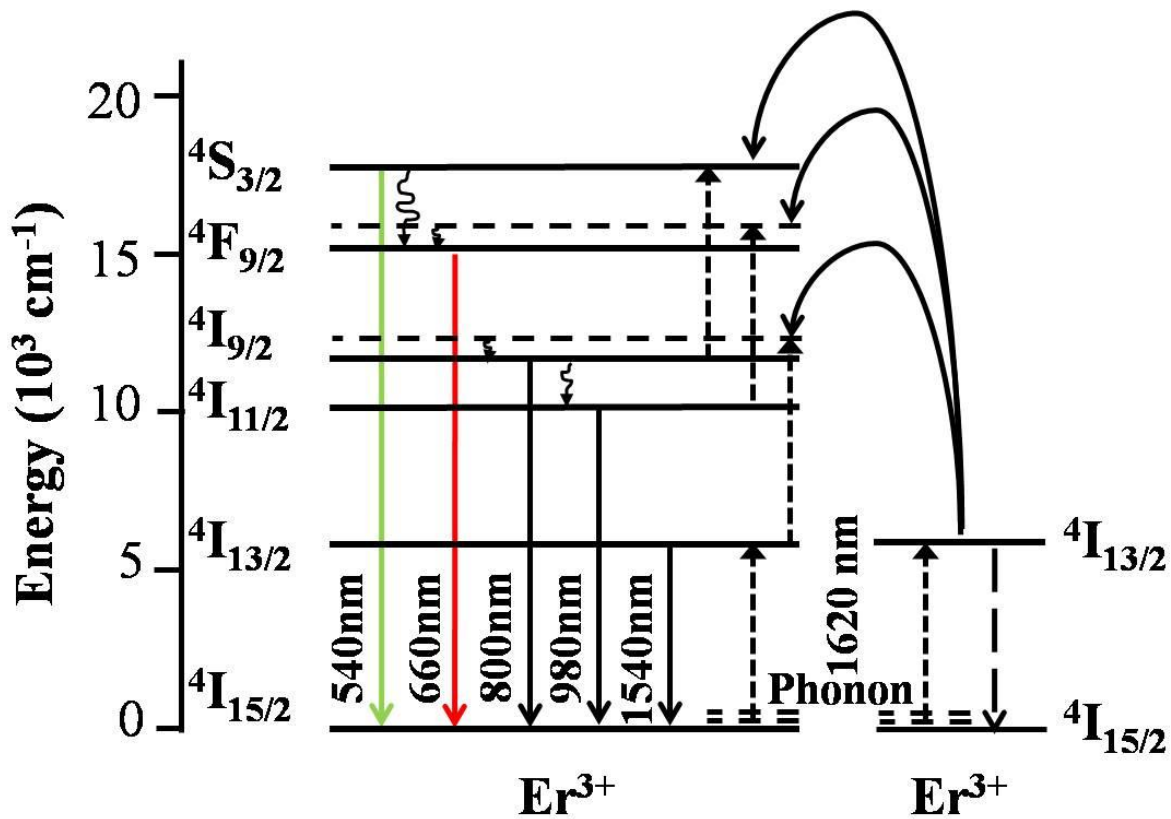


Fig. 5-7 Schematic energy diagram showing UC optical process under 1620 nm excitation. (Excitation photons, energy transfers, radiative and multiphonon processes are depicted in dotted, dashed, full and curly lines, respectively.)

5.4. Summary

The UC properties for hexagonal-phase $\text{NaYF}_4:10\%\text{Er}^{3+}/\text{NaYF}_4$ NCs under off-resonant excitation at 1620 nm were studied. Five UC emission peaks at around 1540, 980, 800, 660 and 540 nm were observed. The absorption and Raman spectra showed that the off-resonant absorption was phonon assisted. The UC emission intensity under off-resonant excitation was found to exhibit a much stronger temperature dependence than that under resonant excitation in the temperature range 80 to 360 K. This was consistent with the proposed model in which UC under off-resonant excitation involved phonon-assisted transitions. The power dependence of the UC intensity indicated that the emission at 1540 nm was generated by 1-phonon absorption ($n < 1$), those at 980 and 800 nm by 2-step UC ($1 < n < 2$) and that at 660 nm by 3-step UC ($2 < n < 3$).

5.5. Chapter 5 references

- [5-1] A. Shalav, B.S. Richards, T. Trupke, K.W. Kramer, H.U. Gudel, *Appl. Phys. Lett.* 86 (2005) 013505.
- [5-2] S. Fischer, J.C. Goldschmidt, P. Loper, G.H. Bauer, R. Brüggemann, K. Kramer, D. Biner, M. Hermle, S.W. Glunz, *J. Appl. Phys.* 108 (2010) 044912.
- [5-3] X.Y. Huang, S.Y. Han, W. Huang, X.G. Liu, *Chem. Soc. Rev.* 42 (2013) 173.
- [5-4] J.C. Goldschmidt, S. Fischer, P. Loper, K.W. Kramer, D. Biner, M. Hermle, S.W. Glunz, *Sol. Energy Mater. Sol. Cells.* 95 (2011) 1960.
- [5-5] J.F. Suyver, J. Grimm, M.K.V. Veen, D. Biner, K.W. Kramer, H.U. Gudel, *J. Lumin.* 117 (2006) 1.
- [5-6] F. Auzel, *Phys. Rev. B.* 13 (1976) 2809.
- [5-7] J.N. Shan, M. Uddi, N. Yao, Y.G. Ju, *Adv. Funct. Mater.* 20 (2010) 3530.
- [5-8] P.V.D. Santos, E.A. Gouveia, M.T.D. Araujo, A.S. Gouveia-Neto, A.S.B. Sombra, J.A.M. Neto, *Appl. Phys. Lett.* 74 (1999) 3607.
- [5-9] A.S. Oliveira, E.A. Gouveia, M.T.D. Araujo, A.S. Gouveia-Neto, B.D.A. Cid, Y. Messaddeq, *J. Appl. Phys.* 87 (2000) 4274.
- [5-10] J.M.F. van Dijk, M.F.H. Schuurmans, *J. Chem. Phys.* 78 (1983) 5317.
- [5-11] F. Auzel, *Chem. Rev.* 104 (2004) 139.

Chapter 6. UC properties under both off-resonant and resonant excitation

6.1. Introduction

UC materials should be applied to harvesting solar energy over a wide spectral range, so as to effectively utilize the solar spectrum [6-1]. Recently, the higher UC efficiencies have been reported under the broad spectrum illumination [6-2]. However, the mechanism of higher UC efficiencies is not clear. In order to better apply UC materials to improving the efficiency of solar cells under broad solar spectrum excitation, it is necessary to form a clear understanding of the UC optical process under both off-resonant and resonant excitation.

In this work, we have studied the UC mechanisms for $\text{NaYF}_4:10\%\text{Er}^{3+}@\text{NaYF}_4$ NCs under both off-resonant and resonant excitation simultaneously (1550 and 1620 nm), which are part of the AM1.5 spectrum and not absorbed by the silicon solar cells. This two-color excitation may be a simple model to examine the UC mechanism under the AM1.5 spectrum excitation.

6.2. Experimental

Since UC intensity under 1620 nm excitation strongly depended on the temperature, which has recently been mentioned in chapter 5, the mechanism of UC enhancement under two-color excitation have been studied through the temperature dependence.

The UC emission spectra were measured by using the Nanofinder 30 microscopy system, with 1620 nm and 1550 nm laser, respectively.

6.3. Results and discussions

6.3.1. UC emission under both off-resonant and resonant excitation at the same power

Fig. 6-1, 6-2 and 6-3 show the UC emission spectra of $\text{NaYF}_4:10\%\text{Er}^{3+}/\text{NaYF}_4$ NCs under 1550, 1620 nm and two-color excitation at 160 W/cm^2 at 80, 180 and 340 K separately, dominated by three peaks at around 980, 800, 660 nm corresponding to ${}^4\text{I}_{11/2}$, ${}^4\text{I}_{9/2}$, and ${}^4\text{F}_{9/2}$ transitions to the ${}^4\text{I}_{15/2}$ ground state. Since the detector can only measure the emission in the range from 650-1100 nm, the UC green emission (${}^4\text{S}_{3/2} \rightarrow {}^4\text{I}_{15/2}$) around 540 nm was not observed. But the green emission can be seen by naked eyes. No UC emission was observed under 1620 nm excitation at 80 K. However, about 114 % UC enhancement was obtained under two-color excitation at 80 K, compared to the UC intensity only under 1550 nm excitation. These results indicated that the UC response of 1620 nm only under its excitation was different from that under two-color excitation. They also suggested the difference of UC mechanism between only one laser excitation and broad spectrum illumination, such as concentrated solar spectrum. From fig. 6-2 and 6-3, it was found that about 104% and 105% UC enhancement were separately obtained under two-color excitation at 180 and 340 K, compared to the UC intensity only under 1550 nm excitation.

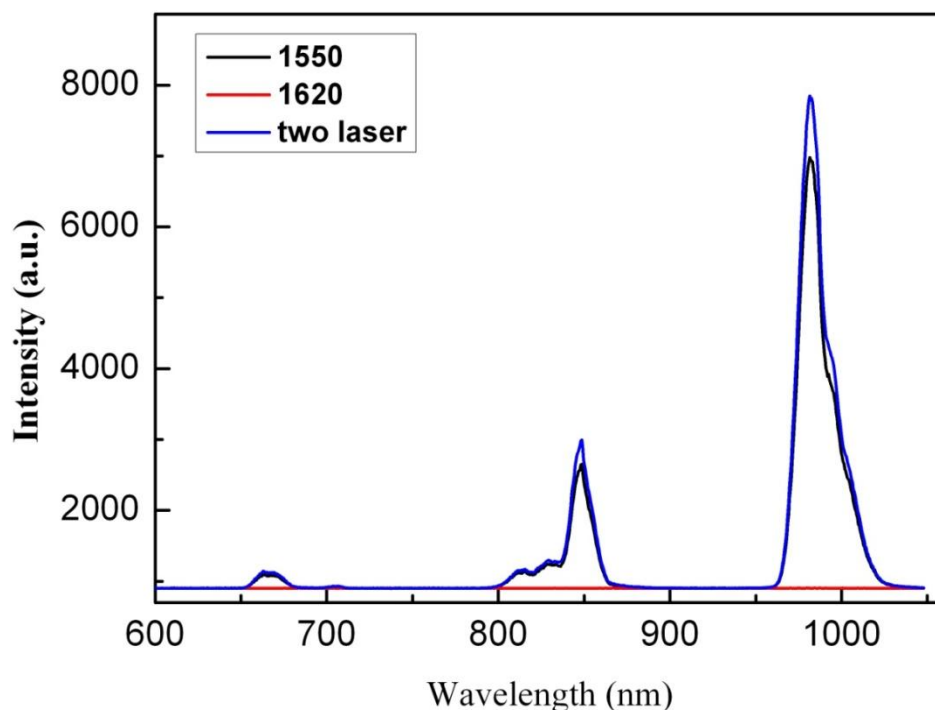


Fig. 6-1 The UC emission spectrum of $\text{NaYF}_4:10\%\text{Er}^{3+}/\text{NaYF}_4$ NCs under 1550, 1620 nm and two-color excitation at 160 W/cm^2 at 80 K.

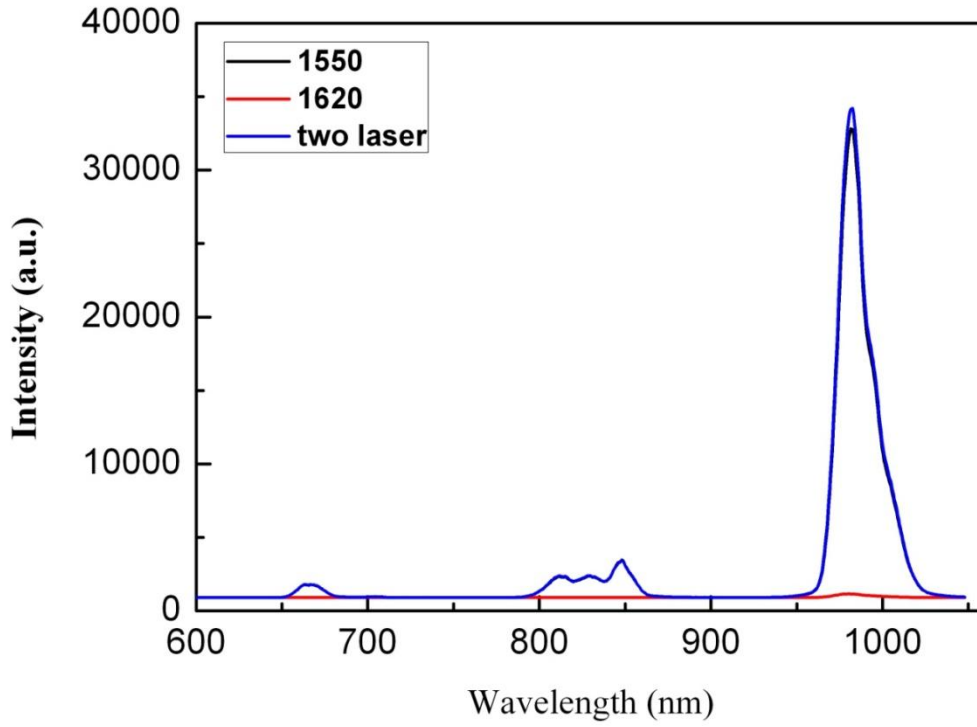


Fig. 6-2 The UC emission spectrum of NaYF₄:10%Er³⁺/NaYF₄ NCs under 1550, 1620 nm and two-color excitation at 160 W/cm² at 180 K.

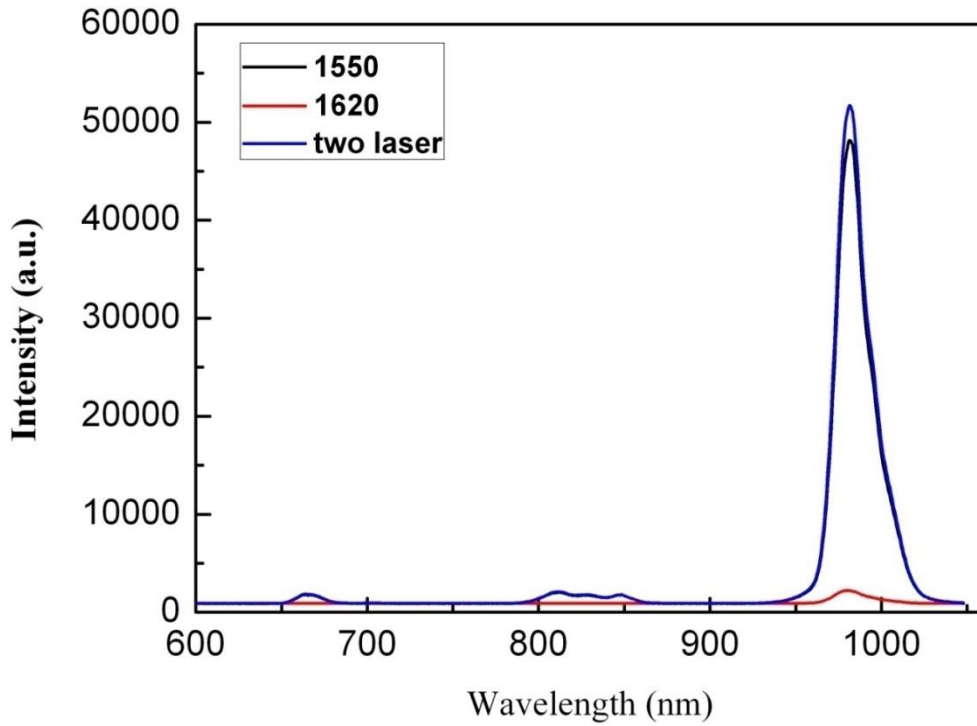


Fig. 6-3 The UC emission spectrum of NaYF₄:10%Er³⁺/NaYF₄ NCs under 1550, 1620 nm and two-color excitation at 160 W/cm² at 340 K.

The temperature dependence of UC intensity at 980 nm under 1550, 1620 nm, two-color excitation and UC enhancement ($\Delta = I_{\text{two-color}} - I_{1550\text{nm}} - I_{1620\text{nm}}$) are shown in fig. 6-4. The UC intensity increased around 1100 times under single laser excitation at 1620 nm, which was ascribed to temperature-dependent phonon-assisted excitation process, while that increase 9 times under single laser excitation at 1550 nm excitation. The UC enhancement (Δ) increase 3 times under two-color excitation from 80 to 340 K, which weakly depends on temperature, compared to UC increase under 1620 nm excitation.

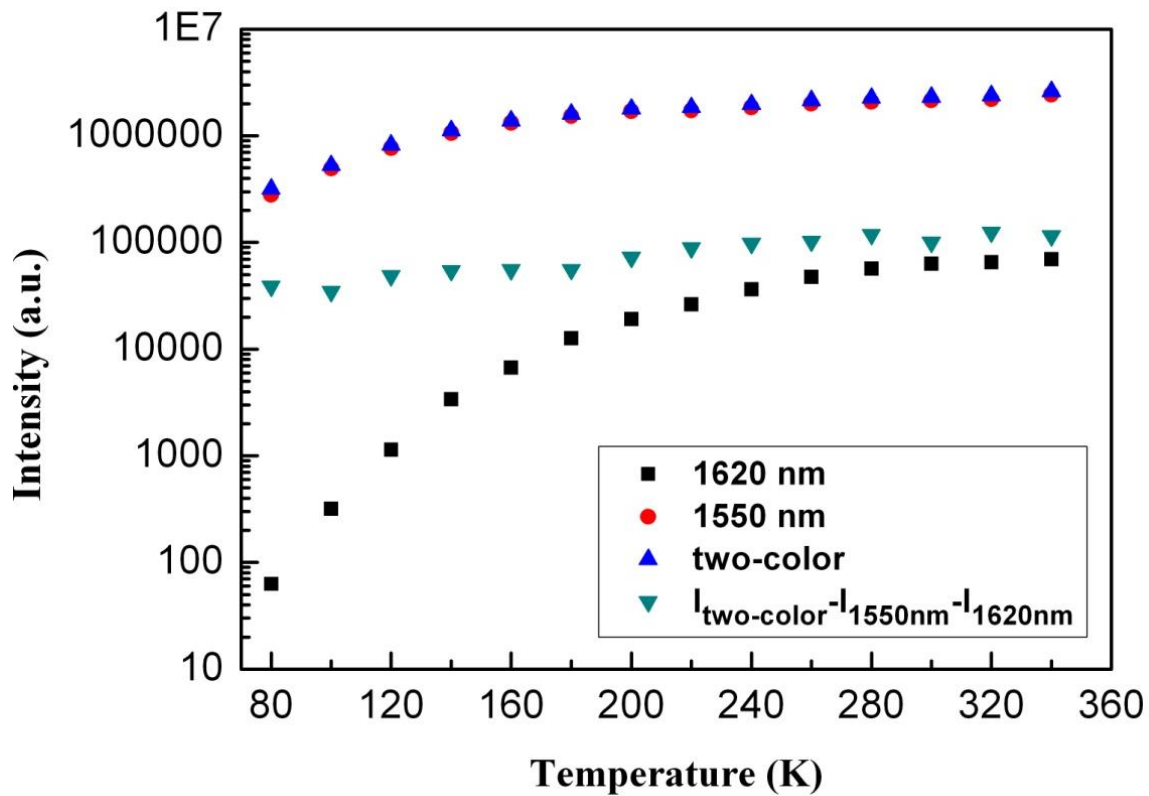


Fig. 6-4 The temperature dependence of UC intensity at 980 nm under 1550, 1620 nm, two-color excitation at 160 W/cm^2 and UC enhancement ($\Delta = I_{\text{two-color}} - I_{1550\text{nm}} - I_{1620\text{nm}}$).

Fig. 6-5 shows the temperature dependence of the ratio of UC intensity ($I_{1620\text{nm}}$) at 980 nm under 1620 nm excitation and UC enhancement (Δ) under two-color excitation to the UC intensity ($I_{1550\text{nm}}$) under 1550 nm excitation. The ratio of UC intensity under 1620 nm to 1550 nm excitation increased 134 times from 80 to 340 K, due to strongly temperature-dependent UC intensity under 1620 nm excitation and weakly temperature-dependent that under 1550 nm excitation. However, the ratio of $\Delta/I_{1550\text{nm}}$ did not depend on the temperature, which hardly vary from 0.04 to 0.07, except 0.14 in 80 k.

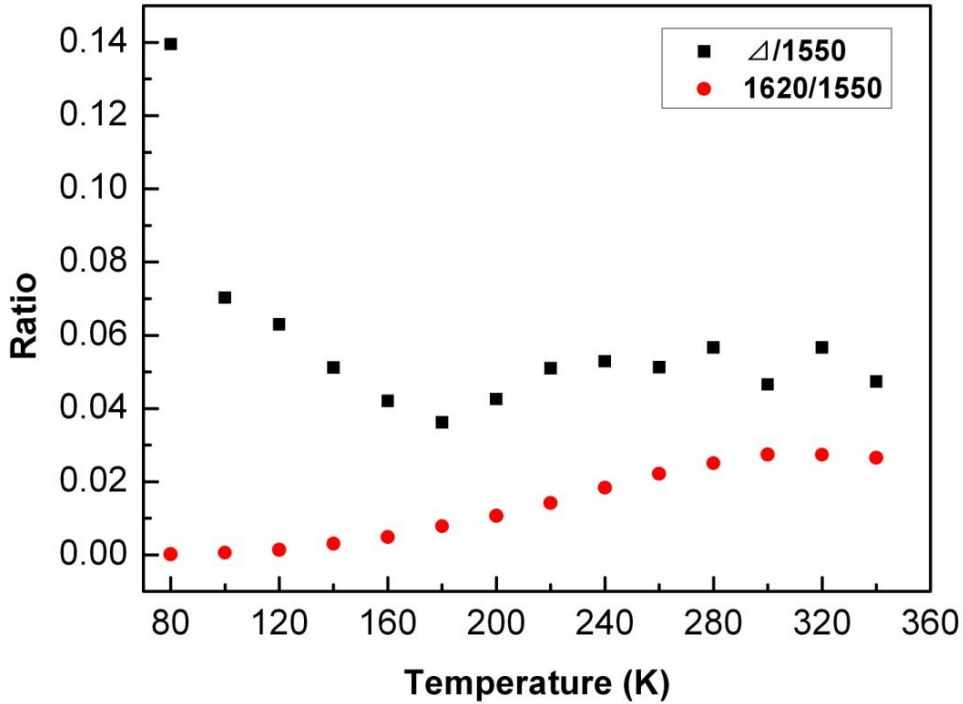


Fig. 6-5 The temperature dependence of the ratio of UC intensity ($I_{1620\text{nm}}$) at 980 nm under 1620 nm excitation and UC enhancement (Δ) under two-color excitation to the UC intensity ($I_{1550\text{nm}}$) under 1550 nm excitation at the same power 160 W/cm^2 .

From the above results, it may be possible to discuss the UC optical process. Fig. 6-6 shows the Energy level diagram and related transitions. The optical processes for the UC luminescence observed from fig. 6-1 to 6-4 may be considered as follows. By an excitation only at 1550 nm, the ground state of Er^{3+} ($^4I_{15/2}$) would be excited to $^4I_{13/2}$, through absorption of 1550 nm photon. By the subsequent excitation, the transition from $^4I_{13/2}$ to $^4I_{9/2}$ would take place by absorbing 1550 nm photon and then non-radiatively relaxation to $^4I_{9/2}$. The light emission at 800 nm occurs, originating from $^4I_{9/2} \rightarrow ^4I_{15/2}$ transition, and the 980 nm emission generates, corresponding to $^4I_{11/2} \rightarrow ^4I_{15/2}$ transition through non-radiatively relaxation to $^4I_{11/2}$ from $^4I_{9/2}$. Since the maximum ratio of $I_{1620\text{nm}}/I_{1550\text{nm}}$ is about 0.03 shown in fig. 6-5, it can leave the UC intensity only under 1620 nm excitation out of account. By two-color excitation, the UC enhancement Δ result from the ground state absorption of 1550 nm photon following excited state absorption of 1620 nm photon, not taking into account the electrons' population in excited state through absorption of 1620 nm photon, since the maximum ratio of $I_{1620\text{nm}}/I_{1550\text{nm}}$ is about 0.03. As the UC intensity under 1550 nm excitation and UC increase Δ under two-color excitation both stem from the ground state absorption of 1550 nm photon, the ratio of $\Delta/I_{1550\text{nm}}$ does not rely on temperature, which agrees with the result shown in fig. 6-5.

This optical process of UC enhancement under two-color excitation could explain the reason of higher UC efficiency under broad spectrum illumination, as shown in table 1-3. The UC enhancement under two-color excitation originates from the ground state absorption of 1550 nm photon following excited state absorption of 1620 nm photon, while the UC response only under off-resonant (1620 nm) excitation is very weak and can

be ignored, compared to the UC intensity only under resonant excitation (1550 nm). In addition, AM 1.5G spectrum shows that the spectral power between 1150 to 2500 nm is 164 Wm^{-2} , as shown in fig. 1-2 [6-3]. Shalav et al. have reported that the spectral power between 1500 and 1580nm is about 20 Wm^{-2} [6-4]. Thus, the power of off-resonant spectrum is about 140 Wm^{-2} , which is 7 times the power of resonant spectrum. Based on the mention above, it is reasonable that the UC enhancement under broad spectrum illumination could be larger than 114%, which was observed under off-resonant and resonant excitation. Table 1-3 shows that the ratios of UC enhancement under broad spectrum illumination to UC intensity under 1523 nm excitation with the same power corresponding to sum irradiance from 1460 to 1600 are $0.81/0.47=1.7$ at 458 suns and $1.07/0.71=1.5$ at 732 suns.

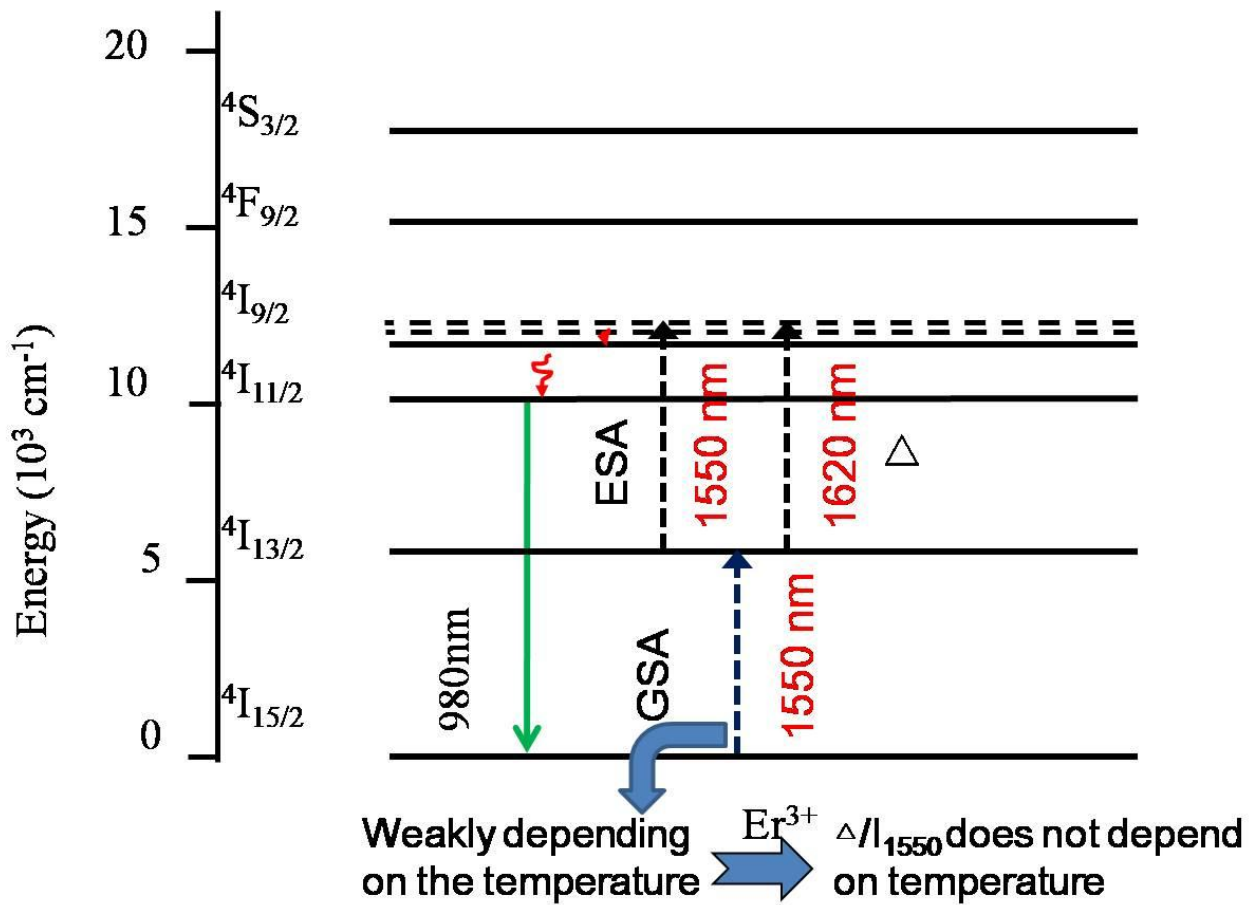


Fig. 6-6 Energy level diagram showing the optical processes of up-conversion under 1550 and 1620 nm excitation at 160 W/cm^2 . (Excitation photons, radiative and multiphonon relaxation processes are depicted in dotted, full and curly lines, respectively.)

6.3.2. UC emission under both off-resonant and resonant excitation at different power

Fig.6-7, 6-8, 6-9 show the UC emission spectra under 1550 nm excitation at 8 W/cm^2 , 1620 nm excitation at 160 W/cm^2 and two-color excitation separately at 80, 220 and 340 K. Compared to UC intensity under 1550 nm excitation, no obvious UC emission was observed under 1620 nm excitation at 80 K, while this UC intensity increased to close to and higher than that under 1550 nm excitation at 220 and 340 K. About 1.2, 2.0 and 2.8 times UC enhancement were separately obtained under two-color excitation at 80, 220 and 340 K compared to the UC intensity only under 1550 nm excitation.

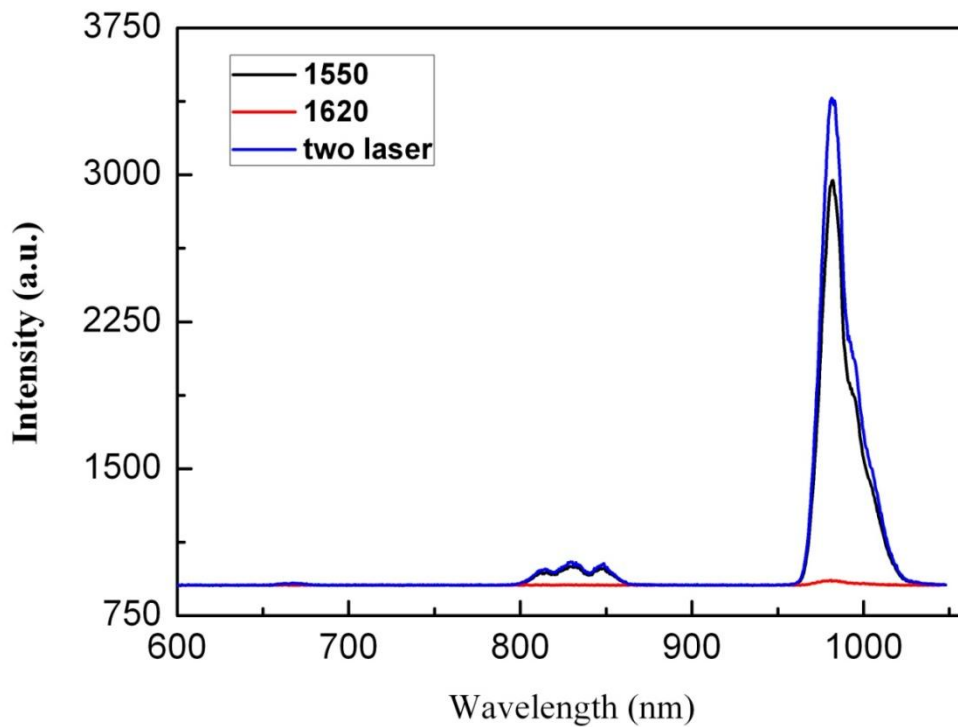


Fig. 6-7 The UC emission spectrum under 1550 nm excitation at 8 W/cm^2 , 1620 nm excitation at 160 W/cm^2 and two-color excitation separately at 80 K.

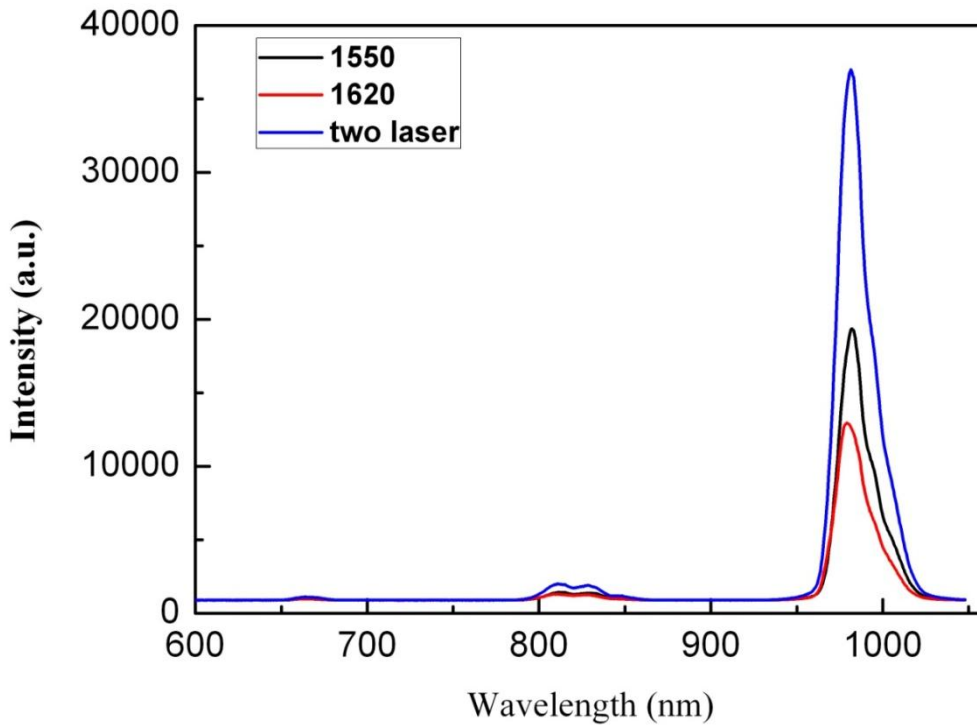


Fig. 6-8 The UC emission spectrum under 1550 nm excitation at 8 W/cm^2 , 1620 nm excitation at 160 W/cm^2 and two-color excitation separately at 220 K.

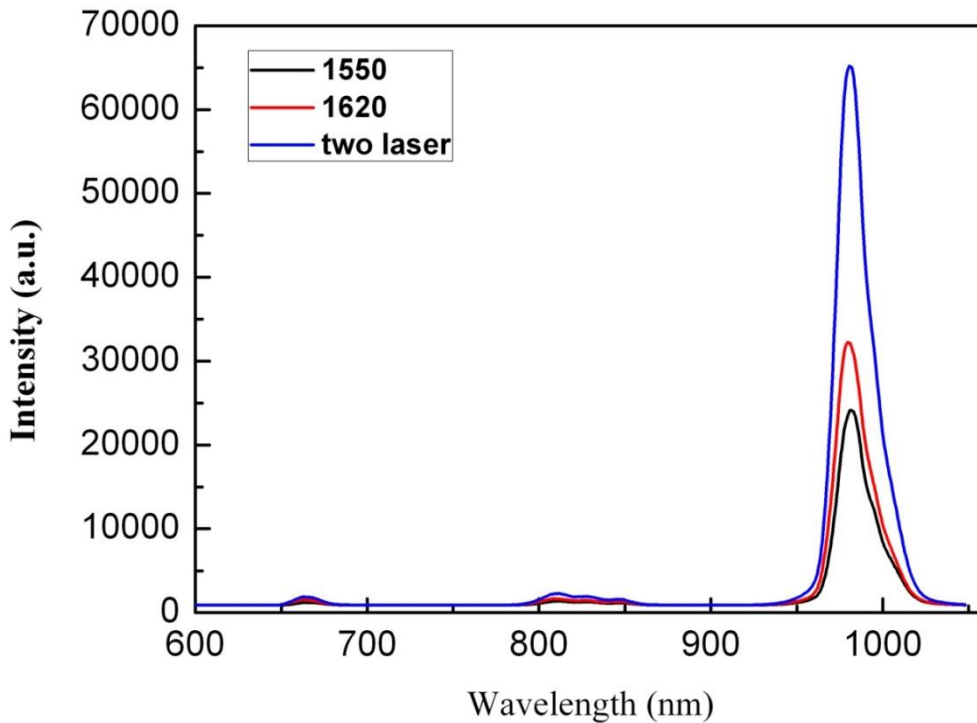


Fig. 6-9 The UC emission spectrum under 1550 nm excitation at 8 W/cm^2 , 1620 nm excitation at 160 W/cm^2 and two-color excitation separately at 340 K.

The temperature dependence of UC intensity at 980 nm under 1550 nm excitation at 8 W/cm², 1620 nm excitation at 160 W/cm², two-color excitation and UC enhancement (Δ) are shown in fig. 6-10. The UC intensity increased around 1500 times under 1620 nm excitation, that increased 13 times under 1550 nm excitation and UC enhancement (Δ) increased 28 times from 80 k to 340 k. This UC enhancement depends on temperature, which is different from the weakly temperature-dependent UC enhancement under two-color excitation at the same power.

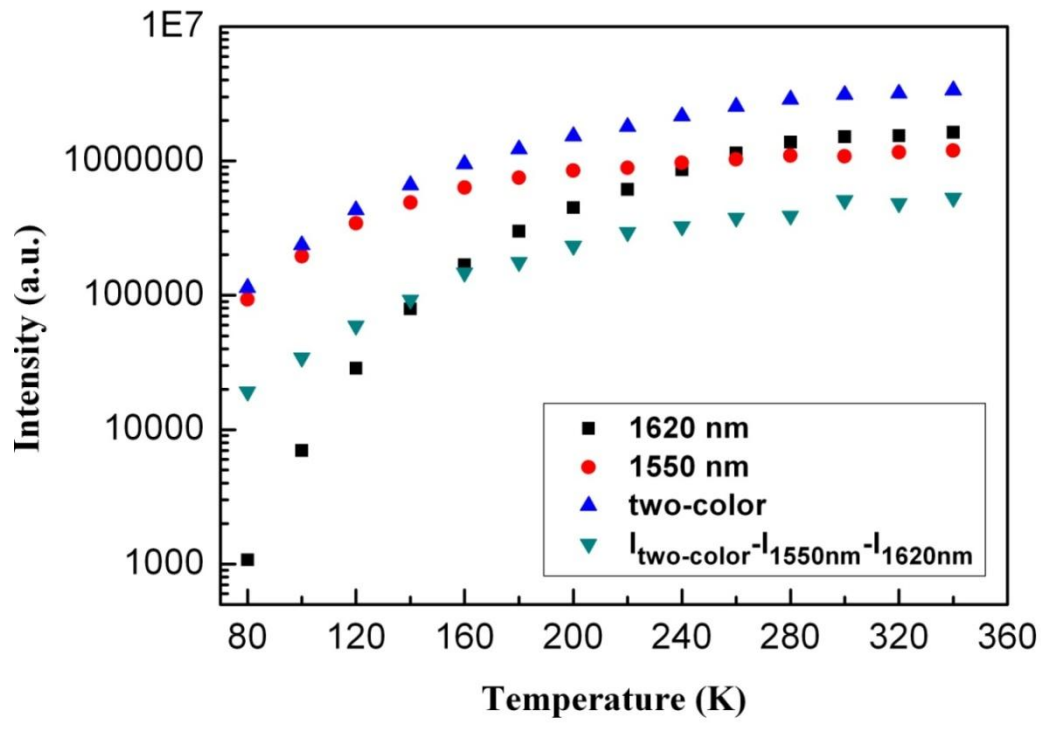


Fig. 6-10 The temperature dependence of UC intensity at 980 nm under 1550 nm excitation at 8 W/cm², 1620 nm excitation at 160 W/cm², two-color excitation and UC enhancement (Δ) under two-color excitation.

Fig.6-11 indicates the temperature dependence of the ratio of UC intensity ($I_{1620\text{nm}}$) to the UC intensity ($I_{1550\text{nm}}$) at 980 nm, which increases 119 times from 80 to 340 K. Fig. 6-12 demonstrates an increase of the ratio $\Delta/I_{1550\text{nm}}$ from 0.20 to 0.47 at temperature from 80 to 300 K and no obvious change from 300 to 340 K. It was found that this $\Delta/I_{1550\text{nm}}$ depended on the temperature and was different from the results shown in fig. 6-5. It suggested that the different mechanism of UC enhancement under both off-resonant and resonant excitation between at the same power and at different power. This different mechanism is attributed to the ratio of I_{1620}/I_{1550} , which is close to and higher than 1, shown in fig. 6-11.

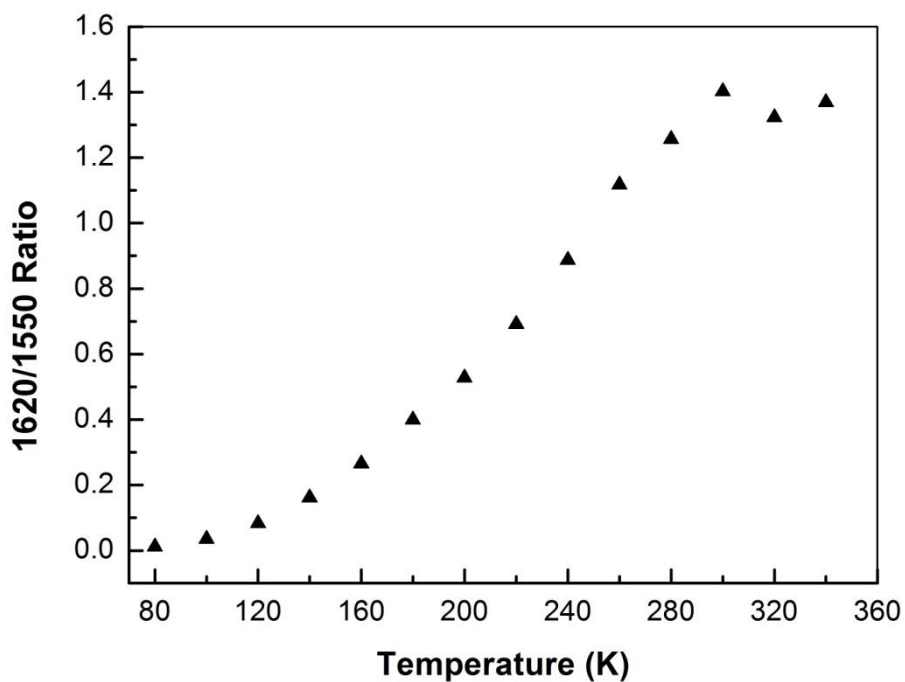


Fig. 6-11 The temperature dependence of the ratio of UC intensity ($I_{1620\text{nm}}$) at 980 nm under 1620 nm excitation at 160 W/cm^2 and UC increase (Δ) to the UC intensity ($I_{1550\text{nm}}$) under 1550 nm excitation at 8 W/cm^2 .

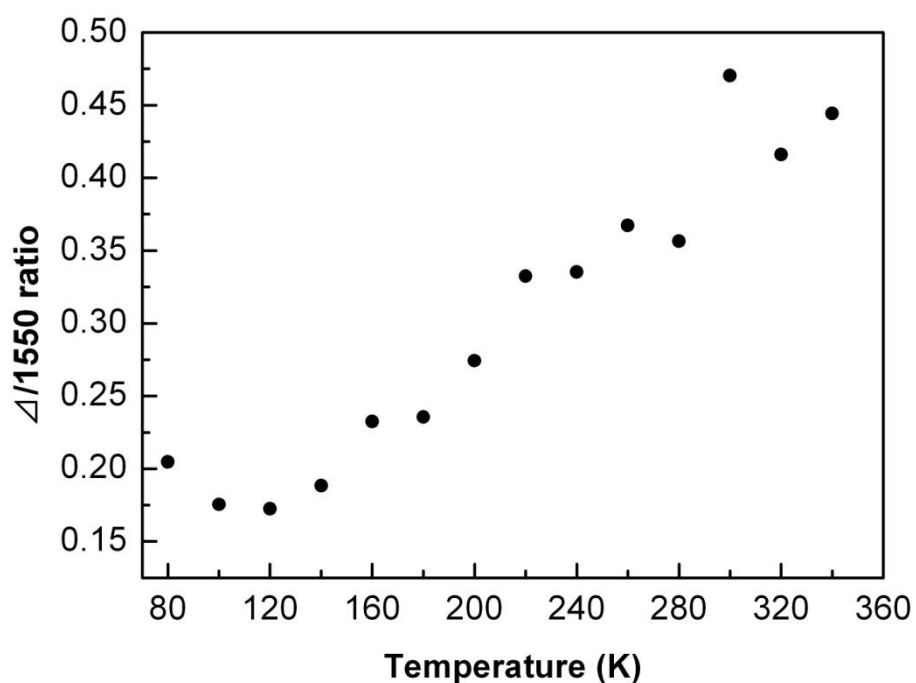


Fig. 6-12 The temperature dependence of the ratio $\Delta / I_{1550\text{nm}}$ under 1620 nm excitation at 160 W/cm^2 and 1550 nm excitation at 8 W/cm^2

Fig. 6-13 shows the temperature dependence of the ratio of UC enhancement (Δ) to the sum of UC intensity (I_{1620}) under 1620 nm excitation and I_{1550} under 1550 nm excitation. The ratio of $\Delta / (I_{1550} + I_{1620})$ does not depend on the temperature. It varies from 0.16 to 0.20 (maximum enhancement).

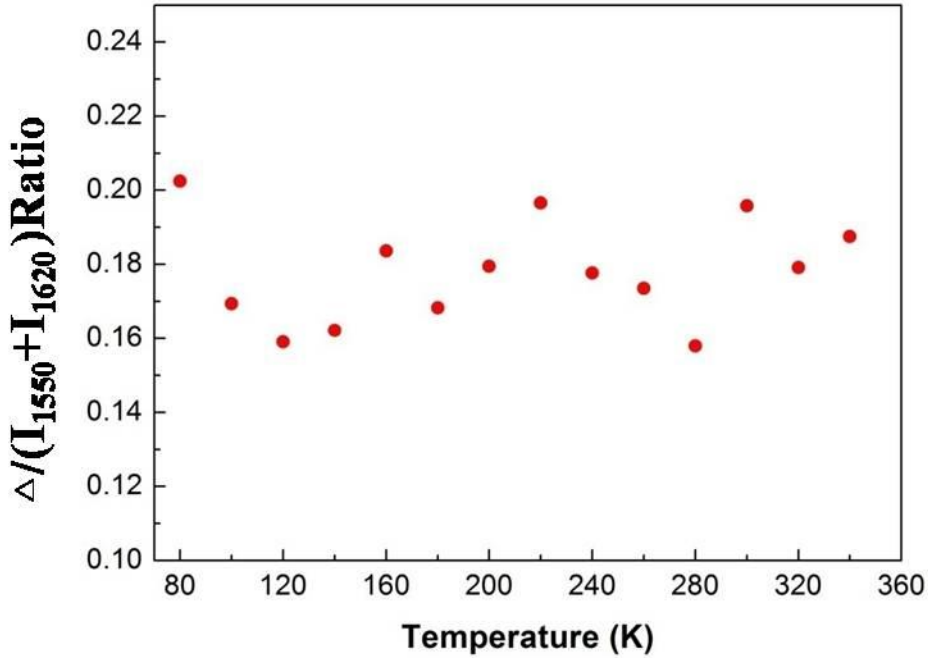


Fig. 6-13 The temperature dependence of the ratio of UC enhancement (Δ) to the sum of UC intensity (I_{1620}) under 1620 nm excitation at 160 W/cm² and I_{1550} under 1550 nm excitation at 8 W/cm².

Based on the above results, it may be possible to discuss the UC optical process. Fig. 6-14 shows the Energy level diagram and related transitions. At low temperature such as 80 K, the ratio of $I_{1620\text{nm}}/I_{1550\text{nm}}$ is about 0.01, therefore the UC enhancement Δ results from the ground state absorption of 1550 nm photon following excited state absorption of 1620 nm photon, not considering the ground state absorption of 1620 nm (denoted as ② in fig. 6-14). The ratio of $I_{1620\text{nm}}/I_{1550\text{nm}}$ increases from 0.01 to 1.40, when the temperature is changed from 80 to 300 K. In the case of 300 K, the ions in $^4I_{13/2}$ state should take into account the ground state absorption of 1620 nm. Thus, the UC enhancement Δ includes the other optical process, the ground state absorption of 1620 nm photon and following $^4I_{13/2} \rightarrow ^4I_{9/2}$ transition through absorption of 1550 nm photon (denoted as ③ in fig. 6-14). Due to temperature-dependent phonon-assisted ground state absorption of 1620 nm photon, the ratio of $\Delta / I_{1550\text{nm}}$ depends on the temperature, which coincides with the results shown in fig. 6-12. This result suggests that when the ratio of $I_{1620\text{nm}}/I_{1550\text{nm}}$ is close to 1, there are two optical processes for UC increase Δ . One is the ground state absorption of 1550 nm photon following $^4I_{13/2} \rightarrow ^4I_{9/2}$ transition through absorption of 1620 nm photon and the other is the ground state absorption of 1620 nm photon and following $^4I_{13/2} \rightarrow ^4I_{9/2}$ transition through absorption of 1550 nm photon. At 80 K, the UC enhancement Δ only originates from the ground state absorption of 1550 nm photon following excited state absorption of 1550 nm photon, while at 300 K, the UC enhancement Δ results from two optical processes. The 2.9 times enhancement of UC was observed at 300 K under 1550 nm excitation at 8 W/cm² and 1620 nm excitation at 160 W/cm², compared

to the UC intensity only under 1550 nm excitation.

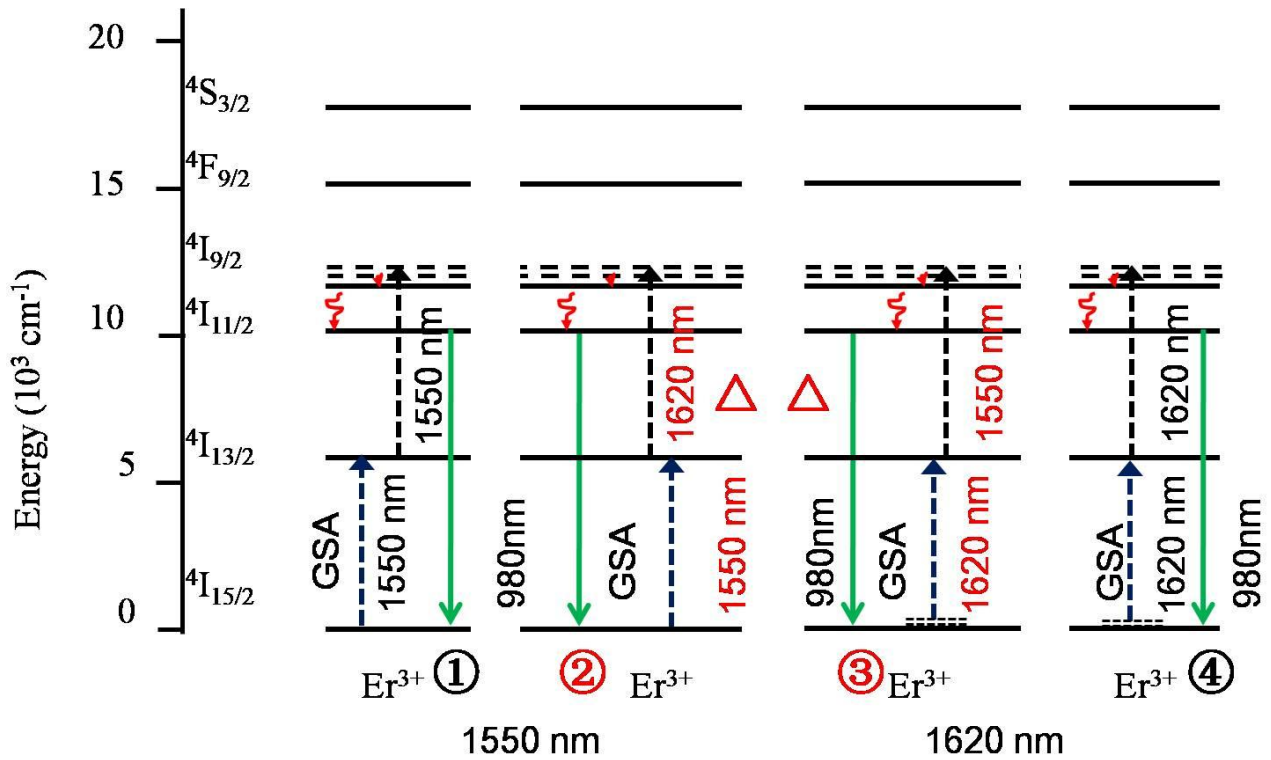


Fig. 6-14 Energy level diagram showing the optical processes of up-conversion under 1550 nm excitation at 8 W/cm^2 and 1620 nm excitation at 160 W/cm^2 . (Excitation photons, radiative and multiphonon relaxation processes are depicted in dotted, full and curly lines, respectively.)

6.4. Summary

The results show two dominant optical processes for UC enhancement under both off-resonant and resonant excitation. When the ratio of $I_{1620\text{nm}}/I_{1550\text{nm}}$ is low, such as 0.03 at the same power excitation, the process of UC enhancement is the ground state absorption of 1550 nm photon following excited state absorption of 1620 nm photon. In this case, the maximum UC enhancement is 114% at 80 K, while no UC emission have been observed only under 1620 nm excitation. This result can explain why the higher UC efficiencies have been obtained under the broad spectrum illumination, compared to that under 1523 nm excitation at comparable irradiance. When the ratio of $I_{1620\text{nm}}/I_{1550\text{nm}}$ is close to 1, the other optical process for UC enhancement also occurs. It is the ground state absorption of 1620 nm photon and following $4I_{13/2} \rightarrow 4I_{9/2}$ transition through absorption of 1550 nm photon, which depends on the temperature. The 2.9 times UC enhancement have been observed when two optical processes occur.

6.5. Chapter 6 references

- [6-1] X.Y. Huang, S.Y. Han, W. Huang, X.G. Liu, *Chem. Soc. Rev.* 42 (2013) 173.
- [6-2] J.C. Goldschmidt, S. Fischer, P. Loper, K.W. Kramer, D. Biner, M. Hermle, S.W. Glunz, *Sol. Energy Mater. Sol. Cells.* 95 (2011) 1960.
- [6-3] B. S. Richards, *Sol. Energy Mater. Sol. Cells.* 90 (2006) 2329–2337.
- [6-4] A. Shalav, B. S. Richards, T. Trupke, K. W. Kramer, H. U. Gudel, Application of NaYF₄:Er up-converting phosphors for enhanced near-infrared silicon solar cell response. *Applied Physics Letters* 86 (2005) 013505.

Chapter 7. Final conclusions

In this thesis, a simple and less toxic synthesis method was developed for pure β -phase NaErF_4 , NaYF_4 , $\text{NaYF}_4:\text{Er}^{3+}$ and $\text{NaYF}_4:10\%\text{Er}^{3+}/\text{NaYF}_4$ core/shell NCs. The XRD results showed that the molar ratio of OA/ODE=10/30 and the high temperature (330°C) were key factors for β -phase NaReF_4 (RE:Y and Er) NCs. The UC emission spectra were obtained with the emission wavelength at about 980 nm ($^4\text{I}_{11/2} \rightarrow ^4\text{I}_{15/2}$), 800 nm ($^4\text{I}_{9/2} \rightarrow ^4\text{I}_{15/2}$), 660 nm ($^4\text{F}_{9/2} \rightarrow ^4\text{I}_{15/2}$) and 540 nm ($^4\text{S}_{3/2} \rightarrow ^4\text{I}_{15/2}$) excited at 1550 nm. 3 times UC enhancement was achieved by coating the core with NaYF_4 shell, compared to $\text{NaYF}_4:10\%\text{Er}^{3+}$ core NCs. The pure β -phase $\text{NaYF}_4:20\%\text{Er}^{3+}$ NCs had about one order of magnitude higher emission intensity than the pure β -phase NaErF_4 . The slope values, n , in the pump-power dependence, showed that the emission at 980 nm and 800 nm were generated by 2-step UC and at 660 nm and 540 nm were 3-step UC. From the UC emission of all peaks, the optimum Er^{3+} concentration was around 10~30%. It was found that higher laser power preferred to increase 3-step UC.

The UC properties for hexagonal-phase $\text{NaYF}_4:10\%\text{Er}^{3+}/\text{NaYF}_4$ core/shell NCs were studied under off-resonant excitation at 1620 nm, whose energy was smaller than that corresponding to the lowest f-f transition of Er^{3+} ($^4\text{I}_{15/2} \rightarrow ^4\text{I}_{13/2}$). The UC emission spectrum consisted of five main peaks at around 1540, 980, 800, 660 and 540 nm. The infrared absorption spectrum showed a weak peak at around 1600 nm which was separated from the $^4\text{I}_{15/2} \rightarrow ^4\text{I}_{13/2}$ absorption peak by 315 cm^{-1} , and phonon bands of NaYF_4 was observed at about 300 cm^{-1} in the Raman spectrum. From these results, the UC emission was interpreted to involve a phonon-assisted excitation process. The UC emission intensity under off-resonant excitation at 1620 nm exhibited a much stronger temperature dependence than that under resonant excitation at 1550 nm, which was consistent with the phonon-assisted interpretation. The power dependence of the UC intensity indicated that the emission at 1540 nm was generated by 1-phonon absorption ($n < 1$), those at 980 and 800 nm by 2-step UC ($1 < n < 2$) and that at 660 nm by 3-step UC ($2 < n < 3$).

The UC properties for hexagonal-phase $\text{NaYF}_4:10\%\text{Er}^{3+}/\text{NaYF}_4$ core/shell NCs were also investigated under both off-resonant and resonant excitation. The temperature dependence was selected to study the mechanism of UC enhancement under two-color excitation, due to strongly temperature dependence of UC intensity under 1620 nm excitation. The results showed two dominant optical processes for UC enhancement under both off-resonant and resonant excitation. On one hand, the ratio of UC enhancement under two-color excitation at the same power (160 W/cm^2) to the UC intensity under 1550 nm excitation did not depend on the temperature. This result indicates that the process of UC enhancement is the ground state absorption of 1550 nm photon following excited state absorption of 1620 nm photon. In this case, the maximum UC enhancement was 114% at 80 K, while no UC emission was observed only under 1620 nm excitation. This result can explain that the higher UC efficiencies were obtained under the broad spectrum illumination, compared to that under 1523 nm excitation at comparable irradiance. On the other hand, the ratio of UC enhancement under 1550 nm excitation at 8 W/cm^2 and 1620 nm excitation at 160 W/cm^2 simultaneously, to the UC intensity under 1550 nm excitation depended on the temperature. This result showed including another optical process for UC enhancement, ground state absorption of 1620 nm photon and following $^4\text{I}_{13/2} \rightarrow ^4\text{I}_{9/2}$ transition through absorption of 1550 nm photon. The 2.9 times UC enhancement was observed under two-color excitation at different power.

Acknowledgements

Foremost, I would like to thank my supervisor, Professor Katsuhiro Akimoto, in Applied Physics, University of Tsukuba, Japan, for his guidance and support I have received throughout my research in University of Tsukuba. I greatly appreciate his guiding me to be independent researcher. Thanks to Dr. Takeaki Sakurai for the support in my research.

I wish to thank all the members of Akimoto and Sakurai Laboratory in Applied Physics, University of Tsukuba. It has been a pleasure to work with them.

I would also like to thank my parents, brothers and sisters who have constantly encourage me over these years.

Finally, I greatly thank the financial support by Ministry of Education, Sports and Culture, Government of Japan.

Publication list

- [1] Effect of Er^{3+} Concentration on Upconversion in Hexagonal-Phase $\text{NaYF}_4:\text{Er}^{3+}$ Nanocrystals, Journal of Physics: Conference Series, in press.
- [2] A novel synthesis method and up-conversion properties of hexagonal-phase $\text{NaYF}_4:\text{Er}^{3+}$ nano-crystals, Journal of Rare Earths, in press.
- [3] Upconversion properties in hexagonal-phase $\text{NaYF}_4:\text{Er}^{3+}/\text{NaYF}_4$ nanocrystals by off-resonant excitation, Applied Surface Science, in press.